A new diplodocine sauropod
from the Morrison Formation, Wyoming, USA

**Tom T.P. van der Linden, Emanuel Tschopp, Roland B. Sookias,
Jonathan J.W. Wallaard, Femke M. Holwerda, and Anne S. Schulp**

ABSTRACT

The Morrison Formation of the western United States is well-known for its high diversity of sauropod dinosaurs. The Howe-Stephens Quarry in northern Wyoming is one of several quarries which has yielded several associated to completely articulated dinosaur specimens, among which a semi-articulated diplodocid specimen, MAB011899, which was excavated in 1993. This diplodocid specimen is represented by posterior cervical, dorsal, sacral, and anterior caudal vertebrae, multiple thoracic ribs, two chevrons, a left coracoid, a left ilium, both pubes and ischia, a left femur, a left tibia, and a left fibula. Through comparative anatomy, we interpret this specimen as a new species of diplodocine sauropod, *Ardetosaurus viator* gen. et sp. nov. Unambiguous autapomorphies include paired accessory laminae in the spinoprezygapophyseal fossae of posterior cervical and anterior dorsal vertebrae, bifurcating anterior centrodiapophyseal laminae in the anterior dorsal vertebrae, fossae present in the centropostzygapophyseal laminae of the second dorsal vertebra, a low vertebral height/centrum length ratio of the posterior dorsal vertebrae and reduced to absent centroprezygapophyseal laminae in the anterior caudal vertebrae. Local autapomorphic features include single centroprezygapophyseal laminae in the posterior cervical vertebrae and a highly elliptical cross-section of the femoral midshaft. *Ardetosaurus viator* is the first skeletally mature sauropod specimen described from the Howe-Stephens Quarry. This specimen provides insight into serial variation of vertebral laminae and laminar transitions. Finally, the peculiar morphology of the -often not preserved- first chevron is described in detail, and its possible use in studying sexual dimorphism in sauropods is discussed.

Tom T.P. van der Linden. Oertijdmuseum, Bosscheweg 80, 5283 WB Boxtel, The Netherlands.
(Corresponding author) tppaleo@gmail.com
Emanuel Tschopp. Department of Animal Biodiversity, Universität Hamburg, Martin-Luther-King-Platz 3,

20146 Hamburg, Germany and Division of Paleontology, American Museum of Natural History, Central Park West @ 79th Street, New York 10024, USA and GeoBioTec, NOVA School of Science and Technology, NOVA University Lisbon, Quinta da Torre, 2829-516 Caparica, Portugal. emanuel.tschopp@uni-hamburg.de
Roland B. Sookias. Evolution and Diversity Dynamics Lab, Department of Geology, University of Liège, Liège, Belgium. r.sookias@gmail.com
Jonathan J.W. Wallaard. Oertijdmuseum, Bosscheweg 80, 5283 WB Boxtel, The Netherlands. curator@oertijdmuseum.nl
Femke M. Holwerda. Royal Tyrrell Museum of Palaeontology, Drumheller, AB T0J 0Y0, Canada and Department of Earth Sciences, Utrecht University, P.O. Box 80115, 3508 TC, Utrecht, The Netherlands. f.m.holwerda@uu.nl
Anne S. Schulp. Department of Earth Sciences, Utrecht University, P.O. Box 80115, 3508 TC, Utrecht, The Netherlands and Naturalis Biodiversity Center, Darwinweg 2, 2333CR, Leiden, The Netherlands. a.s.schulp@uu.nl

INTRODUCTION

Sauropods are among the best studied dinosaurs (Kanayama and Iwasa, 2021) and include the largest terrestrial vertebrates throughout most of the Mesozoic (Upchurch et al., 2004a). They are best recognized by their long necks (Damke et al., 2022; Moore et al., 2023) and long tails (Baron, 2021), and their success can be attributed to their extreme size (Rauhut et al., 2011), an intricate bird-like air sac system (Wedel, 2003; Taylor and Wedel, 2005; Taylor and Wedel, 2021), as well as their unique feeding and digestive strategies (Christiansen, 2000; Hummel et al., 2008; D'Emic et al., 2013) and oviparous reproduction (Mikhailov, 1997). Sauropod remains have been found on every continent, including Antarctica (Cerda et al., 2012).

One of the most recognizable sauropod families is Diplodocidae, erected by Marsh (1884), and currently defined as "all diplodocoids closer to *Diplodocus* than to *Dicraeosaurus*" (Sereno, 1998, p. 63). These sauropods are generally characterized by their extremely long necks and even longer tails (Hatcher, 1901; Gilmore, 1936; Taylor and Wedel, 2013). Diplodocid paleontology is a vibrant field of study, with many recent contributions on morphology (Tschopp and Mateus, 2017; Woodruff et al., 2017, 2018; Tschopp et al., 2018; Gallagher et al., 2021; Mannion et al., 2021; Taylor and Wedel, 2021), histology (Moretti et al., 2018; Waskow, 2019; Rothschild and Witzmann, 2021; Price and Whitlock, 2022), biomechanics (Woodruff, 2017; Klinkhamer et al., 2018; Vidal Calés, 2019;

Conti et al., 2022; Peterson et al., 2022), pathologies (Hone and Chure, 2018; Woodruff et al., 2022), and ecology (McHugh, 2018; Woodruff, 2019). Moreover, considerable progress has been made in diplodocid phylogeny since the beginning of the twenty-first century (Wilson, 2002; Upchurch et al., 2004b; Harris, 2006; Lovelace et al., 2007; Whitlock, 2011; Mannion et al., 2012; Tschopp and Mateus, 2013; Tschopp et al., 2015a; Tschopp and Mateus, 2017; Whitlock and Wilson Mantilla, 2020; Mannion et al., 2021). Currently, 17 diplodocid genera are considered valid (Tschopp and Mateus 2017; Mannion et al. 2021), with only three species outside of the Morrison Formation, *Tornieria* (Fraas, 1908), *'Dinheirosaurus'* Bonaparte and Mateus, 1999 (*Supersaurus* sensu Tschopp et al., 2015a), and *Leinkupal* Gallina et al., 2014, all three of which are part of Diplodocinae, a clade defined as all taxa more closely related to *Diplodocus* than to *Apatosaurus* (Taylor and Naish, 2005).

Diplodocids are known from North and South America, Europe, and Africa, and have a temporal range from the Oxfordian to possibly the early Valanginian (Foster, 2003; Remes, 2006; Mannion et al., 2012; Gallina et al., 2014). They became highly abundant and taxonomically diverse in the Upper Jurassic Morrison Formation of the western United States (e.g., Hatcher, 1901; Gilmore, 1936; Foster, 2003; Taylor and Wedel, 2013b; Mannion et al., 2021) during the Kimmeridgian and Tithonian (Maidment and Muxworthy, 2019). The entirety of the Morrison Formation was originally interpreted as a semi-arid environment with fluvial components (e.g., Foster, 2003; Parrish et al., 2004), but more

recent studies (Whitlock et al., 2018; Maidment and Muxworthy, 2019) indicate a more dynamic, more spatially varied and temporally changing environment. The entire formation encompasses at least eight million years (Maidment and Muxworthy, 2019), this long time of deposition being one of several factors, apart from, e.g., sauropod distribution and niche partitioning (Button et al., 2014; Woodruff, 2019; Mannion et al., 2021), which likely account for the large diversity of sauropods in the Morrison Formation. Our understanding of the diversity of sauropods, as well as their spatial and temporal distribution within the Morrison Formation, is still limited, but recent studies suggest that the diversity is currently rather underestimated (Tschopp and Mateus, 2017; Mannion et al., 2021). However, ontogeny (a number of species are known from immature material, possibly representing different ontogenetic stages) and stratigraphy, which may indicate an anagenetic lineage between, e.g., *Kaatedocus* Tschopp and Mateus, 2013 and *Diplodocus* Marsh, 1878, might affect these higher diversity estimates (Woodruff, 2019).

Here, we provide a detailed description of MAB011899, formerly cataloged as SMA 0013, an articulated diplodocid specimen from the Howe-Stephens Quarry, Howe Ranch, Wyoming. Comparisons with all other diplodocines reveals numerous morphological differences between MAB011899 and other diplodocine specimens, which warrants the erection of a new genus and species: *Ardetosaurus viator* gen. et sp. nov.

THE HISTORY OF THE HOWE-STEPHENS QUARRY AND THE DISCOVERY OF MAB011899

The Howe Ranch in the northern Bighorn Basin of Wyoming has become famous for its highly productive Morrison Formation outcrops (Brown, 1935; Bird, 1985; Ayer, 2000; Siber and Möckli, 2009; Tschopp and Mateus, 2013; Tschopp et al., 2015b; Tschopp and Mateus, 2017; Tschopp et al., 2020). Multiple quarries are located at the ranch, which have yielded numerous dinosaur taxa (Brown, 1935; Schwarz et al., 2007; Christiansen and Tschopp, 2010; Carballido et al., 2012a; Tschopp and Mateus, 2013, 2017; Foth et al., 2015; see Figures 1C and 2). The most famous of these quarries is the Howe Quarry (Tschopp et al.,
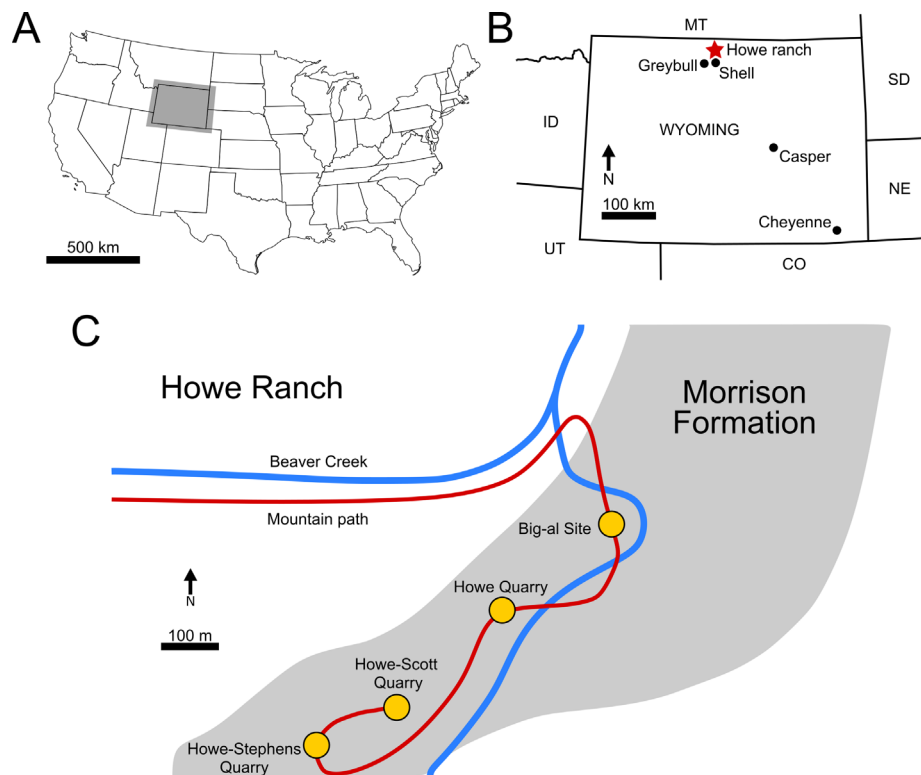
FIGURE 1. Locality of the Howe-Stephens Quarry. A) Map of the United States. Grey box outlines Wyoming, in which the Howe Ranch is located. B) Position of the Howe Ranch in Wyoming, just north of Shell, is indicated by the red star. C) The Howe Ranch, and the positions of the quarries on the site exposing the Morrison Formation. Figure 1B is based on Tschopp et al. (2015b) and information from the SMA, and 1C is based on Siber and Möckli (2009).

2020). Excavations of the Howe Quarry started on the 6th of June, 1934, and were led by AMNH fossil reptile curator Barnum Brown (Bird, 1985; Ayer, 2000; Tschopp et al., 2020). Barnum Brown and his team revealed a bonebed which yielded about three thousand bones (Tschopp et al., 2020). Unfortunately, a great part of this collection was lost due to neglect (Ayer, 2000; Tschopp et al., 2020). The site was also abandoned after 1934 until Hans-Jakob Siber, director of the SMA, and his team from the SMA in Switzerland reopened the Howe Quarry in 1989. In 1992, this team discovered a second fossil-rich site on the Howe Ranch, which was later named Howe-Stephens Quarry (Ayer, 2000; Tschopp et al., 2020). This site, shown in Figure 2, yielded multiple diplodocids, an almost complete skeleton of a camarasaurid, and other non-sauropod dinosaurs (Ayer, 2000; Christiansen and Tschopp, 2010; Tschopp et al., 2015b; Wiersma-Weyand et al., 2021). In 1993 and 1994, a partial, articulated skeleton of a diplodocid (MAB011899) was found, excavated, and given the nickname Brösmeli (meaning 'Crumbly' in Swiss German; see Figure 2). This individual has later been acquired by the Oertijdmuseum, Boxtel, The Netherlands, where it is now accessioned. Ayer (2000) suggested that during the Upper Jurassic the Howe-Stephens Quarry was formed through the simultaneous burial of the dinosaurs seen in Figure 2. Sedimentological and taphonomic interpretations by Ayer (2000) suggest that the animals were dead before burial when they were all simultaneously transported by a flooding event. Subsequent burial of the carcasses occurred rapidly when their further transportation was obstructed by a large tree trunk lying across the river (see top of Figure 2). Most of the animals are exceptionally well preserved, including skin and other integumentary impressions (Christiansen and Tschopp, 2010; Tschopp et al., 2015b), and only minor evidence of scavenging has been found, further implying a rapid burial process in which the animals were largely buried.

MATERIAL

Locality

The Howe-Stephens Quarry, where the specimen was found, is located on the Howe Ranch (see Figure 1; 44°39′N, 107°49′W), north of Shell, Wyoming, USA. The Howe-Stephens Quarry exposes continental sandstones and marls, with sporadic layers of carbonate. The Howe-Stephens Quarry has been interpreted as a fluvial system,

representing an oxbow lake (Ayer, 2000; Foster, 2003; Tschopp et al., 2015b). Figure 3 shows the overall stratigraphy of the Morrison Formation on the Howe Ranch, with the Howe-Stephens Quarry located ~30 m above the marine Sundance Formation and ~30 m below the terrestrial Cloverly Formation. The Howe-Stephens Quarry is stratigraphically located slightly above the Howe Quarry, but all quarries on the Howe Ranch are stratigraphically overlain by the 'clay change', which has been used in the past for long distance correlation in the Morrison Formation (Schwarz et al., 2007, figure 3a; Tschopp et al., 2015b). However, this change is considered to be too variable between localities and can therefore not be used for temporal correlation within the Morrison basin (Maidment and Muxworthy, 2019). A bentonite layer beneath the quarry layers near the base of the Morrison Formation, which was dated at 151.5 ± 4.0 Ma, was used to determine the approximate age of the Howe-Stephens Quarry at 147 Ma (Kvale et al., 2001). However, more recent analyses place the Howe-Stephens Quarry within Systems Tract five of Maidment and Muxworthy (2019; Maidment, personal commun., 2022), which has a maximum age of 150.44 Ma and a minimum age of 149.21 Ma.

Specimen History

The specimen known as Brösmeli (MAB011899) was excavated in episodes from summer 1993 until fall 1994. It was discovered during the excavations of the camarasaurid 'E.T.' (SMA 0002/NMZ 1000002) where the sacrum and caudal vertebrae became exposed during the uncovering of the neck and head of SMA 0002/NMZ 1000002 (Gross, 1993). From there, the remaining bones were excavated, found mostly fully articulated, working from the sacrum anteriorly. Excavations halted when a gap was reached after exposing a sixth cervical vertebrae, and no other cervical vertebrae or skull material was found. After the excavations of 1994, the material was brought to Switzerland. It is unclear when, but before October of 2003, a selection of bones from MAB011899 was brought to the Dinosaurier Freilichtmuseum in Münchehagen (DFMMh/FV), Germany, to be prepared. In the night of the 4th to the 5th of October, through malicious arson, the laboratory and exhibition hall were burnt down, destroying 15% of the prepared bones at that time (Knötschke et al., 2014). There are no clear records of which bones were brought there, but, based on burn scars and incompleteness of bones
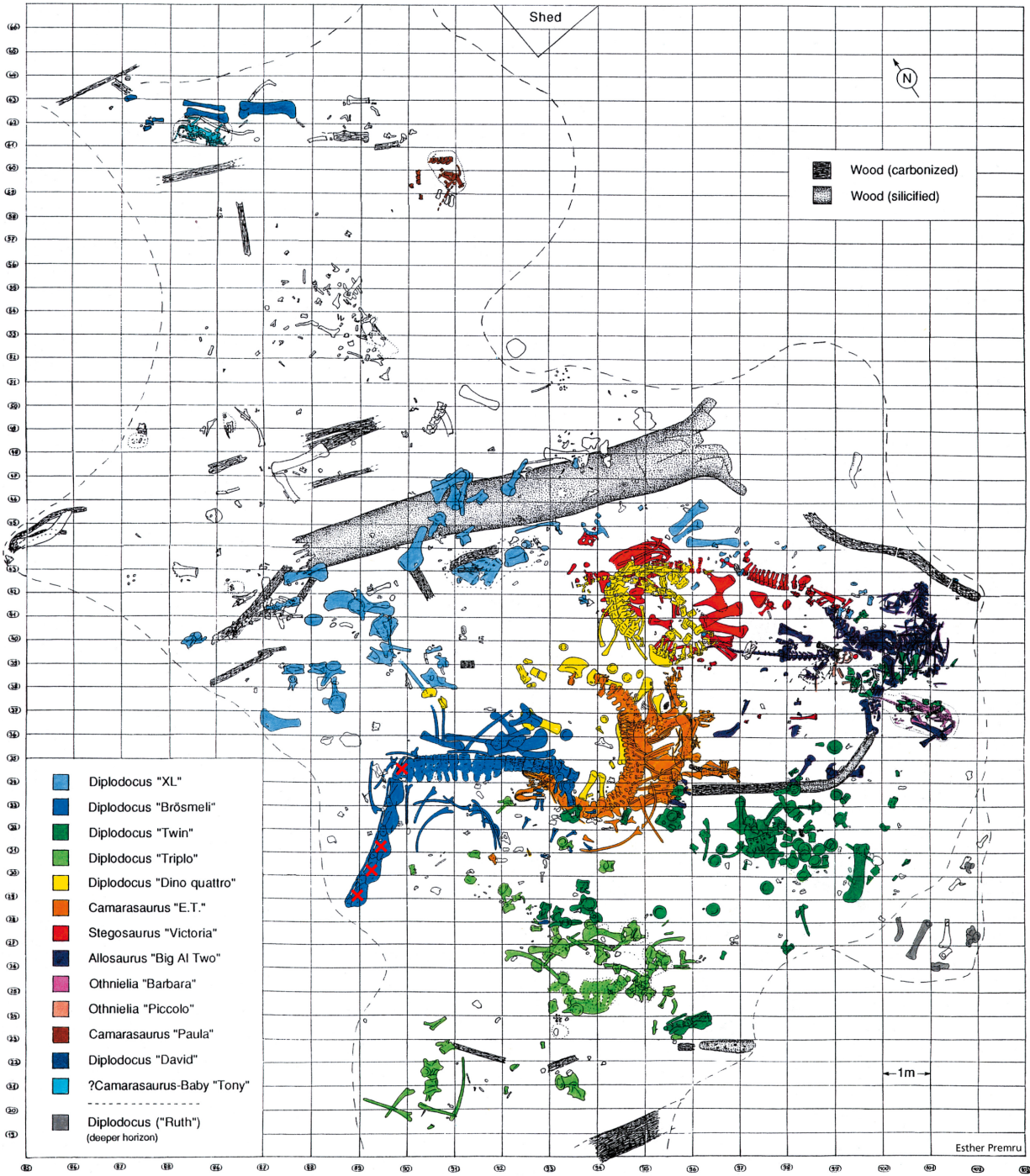
FIGURE 2. Quarry map of *Ardetosaurus viator* MAB011899. Excavation map of the Howe-Stephens Quarry, indicating the major finds from 1992-2000. Individual dinosaurs are color coded, and MAB011899 is coded with dark blue, and named *'Diplodocus* Brösmeli' herein. The red crosses indicate the missing/lost cervical vertebrae. Note the relatively similar color for 'Brösmeli' and 'David' (SMA 0086), but their significant separation in the quarry. Figure is courtesy of the SMA. Quarry sections equal 1 by 0.5 m.
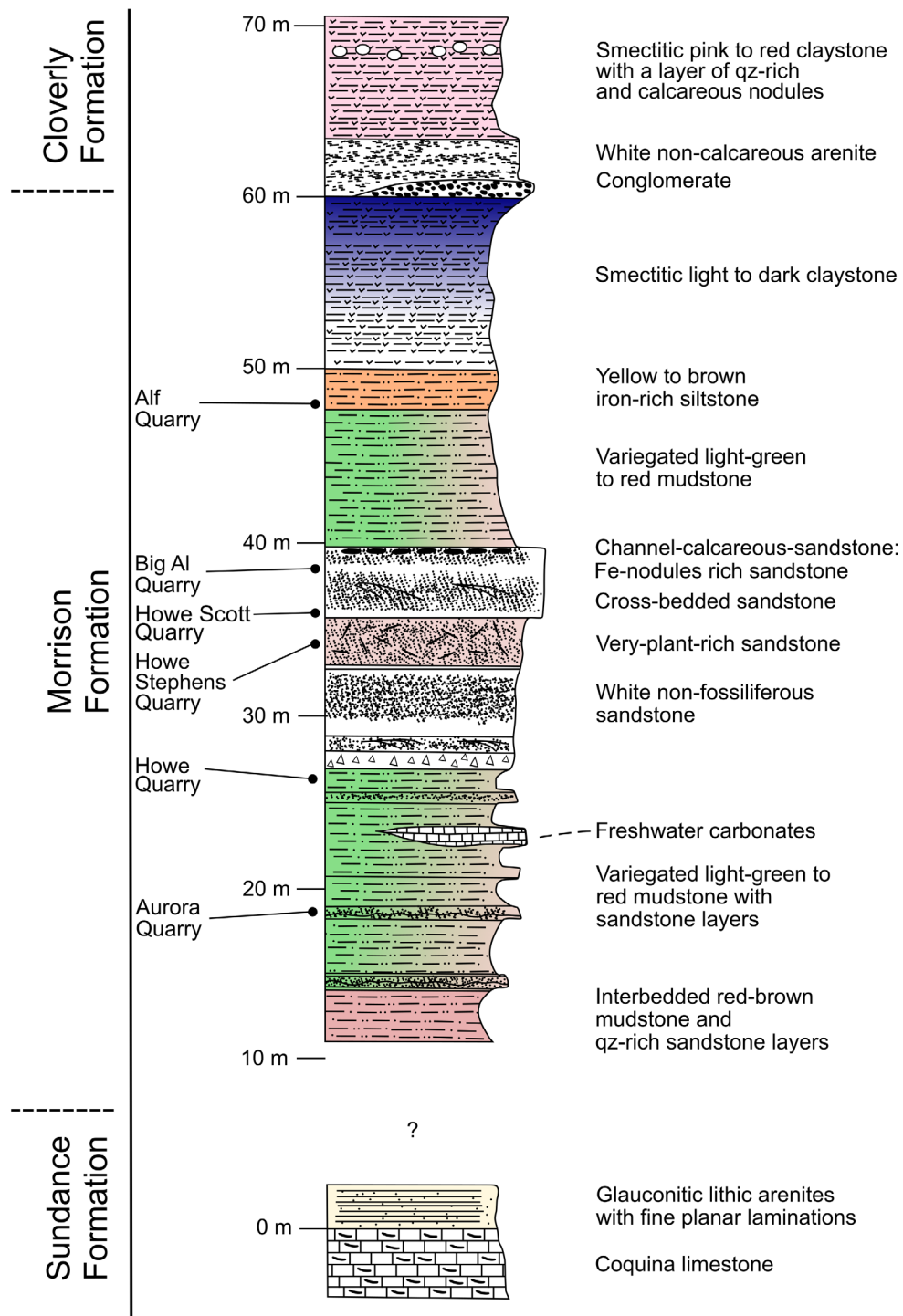
FIGURE 3. Stratigraphic positions of the quarries located on the Howe Ranch. Figure is based on the stratigraphy log made by the SMA in 2003.

which were complete before, it would have included the anterior three cervical vertebrae, the tibia, possibly the fibula, and the complete femur, but it also likely included the field jackets of the dorsal vertebrae. The fire destroyed most of the cervical vertebrae of MAB011899 that were being prepared at the time. Pieces of at least two of the three missing cervical vertebrae were found in the debris of the fire, but were too damaged to be restored or analyzed. The femur was recovered in

three pieces, missing a portion of the proximal shaft. The tibia and fibula were also present. The tibia still shows some burn marks, whereas the proximal part of the fibula is currently missing, of which there is no mention in the SMA records of the 1993-94 excavations (Siber, 1994). In 2018 and 2019, the Oertijdmuseum bought the skeleton of MAB011899, as well as those of the individuals 'Twin', 'Triplo', 'XL' (formerly SMA 0007), and 'Aurora' (formerly SMA 0008). From 2018 onwards, the bones of MAB011899 were further prepared, as were the bones from 'Twin' and 'Triplo'. The bones of these three individuals together form a relatively complete composite diplodocid mount, which was finished on March 1, 2022. The following material can be assigned to MAB011899 with certainty, based on coordinates, field notes, pictures, and other notes: two posterior cervical vertebrae (CV), which very likely represent cervical vertebrae 13 and 14, 10 dorsal vertebrae (DV), which very likely represent DV1-DV10, multiple thoracic ribs, a partial sacrum including a left ilium, five anterior-most caudal vertebrae, two anterior chevrons, a left coracoid, both pubes and ischia, an incomplete left femur, a left tibia, and a partial left fibula (Figure 4). More chevrons are visible on the excavation map, but most did not receive a coordinate or note on the bone surface, which renders assignment of further chevrons to MAB011899 now impossible, with caudal vertebrae from the other individuals having been found in the close vicinity.

Ontogeny

MAB011899 was determined to be an adult diplodocine (Waskow, 2019). A dorsal rib cross section of right rib ?6, sectioned just below the rib head, displays 19 well developed cycles, with a distinct decrease after the tenth countable cycle, indicating that MAB011899 became sexually mature around the age of 13. The total growth time of MAB011899 can be estimated to be 22 years. The additional three years which are added to the age of MAB011899 are related to their loss by the growth of the medullary cavity, which are achieved through retrocalculation. Skeletal maturity was reached at approximately 17 years of age, based on a developed external fundamental system (EFS) of five closely spaced lines of arrested growth (LAGs). An EFS develops only in skeletally mature animals (Sander et al., 2011; Waskow, 2019).

METHODS

Preparation and Reconstruction

Preparation was performed using air scribes, dental tools, and sandblasting with sodium bicarbonate. The bones are reinforced using cyanoacrylate glues, a water-based acrylate dispersion, whereas larger openings are filled and missing pieces are reconstructed using acrylic resin.

Phylogenetic Analysis

We refrain from providing a detailed phylogenetic analysis, as this description is part of a collaborative project investigating the systematics of Diplodocoidea. Currently, multiple diplodocoid specimens are being described by various researchers. They would end up using either updated versions of the matrices of Tschopp et al. (2015a) or Whitlock and Wilson Mantilla (2020), only minorly changing the character and operational taxonomic unit composition. Instead, this collaborative study will combine the score and character data of all these newly described specimens and investigate their systematics as a whole.
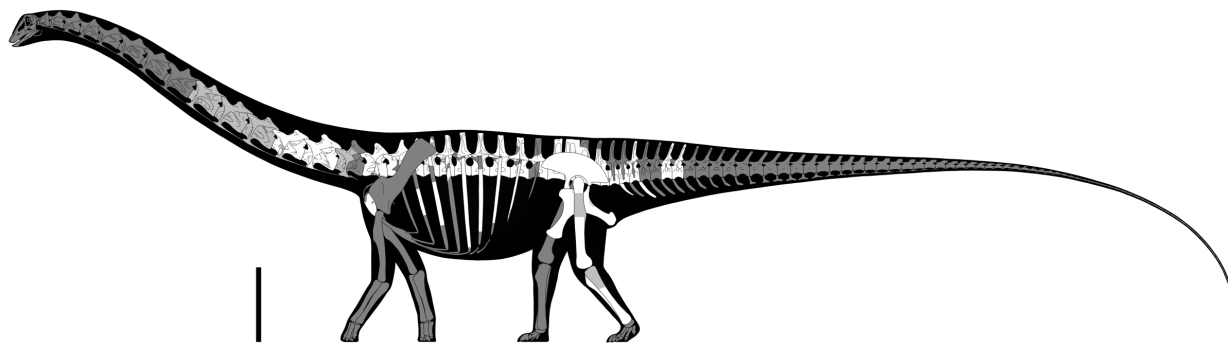

FIGURE 4. Skeletal reconstruction of *Ardetosaurus viator* MAB011899. Skeletal reconstruction indicating preserved bones (white), excavated bones but subsequently lost (light gray) and not preserved (dark gray). Unknown elements are based on other diplodocines. Scale bar equals 1 m. Reconstruction by Ole Zant.

Institutional Abbreviations

AMNH FARB, American Museum of Natural History, New York City, New York, USA. Fossil Amphibian, Reptile, and Bird Collections; **BYU,** Brigham Young, Museum of Paleontology, Provo, Utah, USA; **CM,** Carnegie Museum of Natural History, Pittsburgh, Pennsylvania, USA; **DFMMh/FV,** Dinosaurier-Freilichtmuseum Münchehagen/Verein zur Förderung der Niedersächsischen Paläontologie e.V., Rehburg-Loccum, OT Münchehagen, Germany; **DMNS,** Denver Museum of Nature and Science, Denver, Colorado, USA; **HMNS,** Houston Museum of Nature and Science, Houston, Texas, USA; **LCM,** Leicester City Museums, Leicester, United Kingdom; **MAB,** Oertijdmuseum, Boxtel, The Netherlands; **MB.R.,** Museum für Naturkunde, Berlin, Germany; **MDS,** Museo de Dinosaurios de Salas de los Infantes, Salas de los Infantes, Burgos, Spain; **ML,** Museu da Lourinhã, Lourinhã, Portugal; **MMCh-Pv,** Museo Municipal "Ernesto Bachmann", Villa El Chocón, Neuquén, Argentina; **NMMNH,** New Mexico Museum of Natural History and Science, Albuquerque, New Mexico, USA; **NMZ,** Natural History Museum, University of Zurich, Zurich, Switzerland; **NSMT,** National Museum of Nature and Science, Tokyo, Japan; **SMA,** Sauriermuseum Aathal, Aathal, Switzerland; **SMF,** Senckenberg Museum Frankfurt, Frankfurt, Germany; **SMNS,** Staatliches Museum für Naturkunde, Stuttgart, Germany; **Tate,** Tate Geological Museum, Casper College, Casper, Wyoming, USA; **UW,** University of Wyoming Geological Museum, Laramie, Wyoming, USA; **WDC,** Wyoming Dinosaur Center, Thermopolis, Wyoming, USA; **YPM,** Yale Peabody Museum, New Haven, Connecticut, USA.

Anatomical Abbreviations

ACDL, anterior centrodiapophyseal lamina; **ACPL,** anterior centroparapophyseal lamina; **ap,** anterior process; **cc,** cnemial crest; **Cd,** caudal vertebra; **cof,** coracoid foramen; **CPOF,** centropostzygapophyseal fossa; **CPOL,** centropostzygapophyseal lamina; **CPOL-f,** centropostzygapophyseal lamina fossa; **CPRL,** centroprezygapophyseal lamina; **CV,** cervical vertebra; **DV,** dorsal vertebra; **EFS,** external fundamental system; **fbtr,** fibular trochanter; **fic,** fibular condyle; **gl,** glenoid; **hc,** haemal canal; **hyp,** hyposphene; **LAG,** lines of arrested growth; **lCPOL,** lateral centropostzygapophyseal lamina; **mCPOL,** medial centropostzygapophyseal lamina; **PACDF,** parapophyseal centrodiapophyseal fossa; **pap,** parapophysis; **PCDL,** posterior centrodiapophyseal lamina; **PCPL,** posterior centropara-

pophyseal lamina; **pl,** pleurocoel; **POCDF,** postzygapophyseal centrodiapophyseal fossa; **PODL,** postzygodiapophyseal lamina; **POSL,** postspinal lamina; **poz,** postzygapophysis; **pp,** pubic peduncle; **PPDL,** paradiapophyseal lamina; **PRCDF,** prezygapophyseal centrodiapophyseal fossa fossa; **PRDL,** prezygodiapophyseal lamina; **PRPADF,** prezygapophyseal paradiapophyseal fossa; **PRPL,** prezygoparapophyseal lamina; **PRSDF,** prezygapophyseal spinodiapophyseal fossa; **PRSL,** prespinal lamina; **prz,** prezygapophysis; **pvf,** posteroventral flange; **SDF,** spinodiapophyseal fossa; **SPDL,** spinodiapophyseal lamina; **SPOF,** spinopostzygapophyseal fossa; **SPOL,** spinopostzygapophyseal lamina; **SPRF,** spinoprezygapophyseal fossa; **SPRL,** spinoprezygapophyseal lamina; **sTPOL,** single interpostzygapophyseal lamina; **SV,** sacral vertebra; **tap,** triangular aliform process; **tic,** tibial condyle; **tilf,** *M. iliofibularis* trochanter; **TPOL,** interpostzygapophyseal lamina; **TPRL,** interprezygapophyseal lamina.

SYSTEMATIC PALEONTOLOGY

DINOSAURIA Owen, 1842
SAUROPODA Marsh, 1878
EUSAUROPODA Upchurch, 1995
NEOSAUROPODA Bonaparte, 1986
DIPLODOCOIDEA Marsh, 1884
FLAGELLICAUDATA Harris and Dodson, 2004
DIPLODOCIDAE Marsh, 1884
DIPLODOCINAE Marsh, 1884
Ardetosaurus viator gen. et sp. nov.

Holotype. MAB011899: two cervical vertebrae, 10 dorsal vertebrae, sacrum, five caudal vertebrae, eight dorsal ribs, two chevrons, a left coracoid, a left ilium, both pubes, both ischia, a left femur, a left tibia, and a partial left fibula.

Diagnosis. *Ardetosaurus viator* is diagnosed by the combination of the following autapomorphies: 1) the presence of distinct, paired accessory laminae in the spinoprezygapophyseal fossae (SPRF) in the posterior cervical and anterior dorsal vertebrae, 2) anteroventrally bifurcating anterior centrodiapophyseal laminae (ACDLs) in the anterior dorsal vertebrae, 3) the presence of centropostzygapophyseal lamina fossae (CPOL-f) in the second dorsal vertebra, 4) a vertebral height/centrum length ratio of <2.5 of the posterior dorsal vertebrae, and 5) reduced or absent centroprezygapophyseal laminae (CPRLs) in the anterior-most caudal vertebrae. *Ardetosaurus viator* differs from all other diplodocines by having unbifurcated

CPRLs in the posterior cervical vertebrae and a highly elliptical femoral cross-section. *Ardetosaurus viator* differs from *Amphicoelias* Cope, 1878, in lacking the rounded, lateral projections of the neural spine tip and the thin neural spine base in the dorsal vertebrae; from *Barosaurus* Marsh, 1890, by having tall cervical neural spines, single midline keels, narrower prezygapophyseal rami in the cervical vertebrae, ten dorsal vertebrae, the presence of infradiapophyseal foramina in the dorsal vertebrae, unbifurcated caudal neural spines and a posterodorsally expanded distal end of the ischia; from *Diplodocus* by having more elongated posterior cervical vertebrae, postzygapophyses that terminate in front of the cotyle edge, the presence of a prespinal lamina (PRSL) and laterally inclined spinoprezygapophyseal laminae (SPRLs) in the posterior cervical vertebrae, the absence of the midline cleft in the dorsal vertebrae and the presence of lateral projections on caudal neural spines tips; from *Galeamopus* Tschopp et al., 2015a, by having posteriorly projecting interpostzygapophyseal laminae (TPOL) in the posterior cervical vertebrae, strongly opisthocoelous anterior dorsal vertebrae, and the absence of a second cnemial crest in the tibia; from *Kaatedocus* in lacking the rugose tuberosities and transverse sulci posterior to the prezygapophyses, by having a wider gap between the metapophyses, and postzygapophyses which terminate in front of the rim of the cotyle of the cervical vertebrae; from *Leinkupal* in having procoelous-distoplatyan caudal vertebrae without distinct pleurocoels and with less developed transverse processes; from *Tornieria* in lacking strongly procoelous anterior caudal vertebrae, having a mildly concave ischial acetabular surface, having elongate lateral fossae on the ischial shaft and a more transversely expanded distal end of the ischia; and from *Supersaurus* Jensen, 1985 by being much smaller *(S. vivianae),* the presence of bifurcated neural spines in the cervical vertebrae *(S. lourinhanensis),* the absence of distinct grooves posterolateral to the parapophyses, and paired fossae lateral to the midline keel in the cervical vertebrae, anteriorly inclined neural spines, horizontal transverse processes, and less persistent bifurcation along the series in the dorsal vertebrae, as well as lacking pneumatic foramina and oblique ridges on the thoracic rib heads (both species).

Etymology. 'Ardeto' is an inflection of Latin ārdēre, meaning 'to burn.' It refers to the history of some of the elements, which were either fully destroyed in a fire, or still show burn scars from the fire. 'saurus,' Latinized form of the Greek σαῦρος (saúros),

meaning lizard or reptile. 'viator' is Latin for traveler, referring to the journey of the specimen from the USA, via Switzerland and Germany, to the Netherlands.

Locality and horizon. *Ardetosaurus viator* comes from the Howe-Stephens Quarry of northern Wyoming, USA. The quarry is dated, based on magnetostratigraphy and correlation with other sections in the Morrison basin (Maidment and Muxworthy, 2019; Maidment, personal communication, 2022) at 150.44 to 149.21 million years old, placing it in the Kimmeridgian Stage of the Upper Jurassic.

DESCRIPTION OF MAB011899

Terminology

Terminology from Wilson (1999) and Wilson (2012) is used for the vertebral laminae, Wilson et al. (2011) for the vertebral fossae, and Wilson (2011) for the sacrum. For the definitions of the positional terms for the vertebrae, table 3 from Tschopp et al. (2015a) is followed. Following Tschopp et al., (2015a), Wilson (2002), and Upchurch (1998) and many other authors, 'anterior' and 'posterior' is preferred over 'cranial' and 'caudal'. As suggested by Tschopp and Mateus (2013), interpre- and interpostzygapophyseal lamina is here preferred over the terms intrapre- and intrapostzygapophyseal lamina of Wilson (1999), as both laminae are positioned in between their respective zygapophyses. Cervical ribs are fused to their respective vertebrae, whereby the tuberculum fuses with the diapophysis and the capitulum fuses with the parapophysis. This creates a structure known as the ansa costotransversaria in birds, but in non-avian dinosaurs, such as sauropods, it is referred to simply as the 'cervical rib loop' (Taylor and Wedel, 2013).

AXIAL SKELETON

The Cervico-Dorsal Transition and Presacral Neural Spine Bifurcation Patterns

Identifying the first dorsal vertebra is important, because the precise location of the cervico-dorsal transition (Tschopp and Mateus, 2017) or junction (Taylor, 2022) has implications for the biomechanics of the animal, as well as for phylogenetic analyses and morphological comparisons. Tschopp and Mateus (2017) discuss several characteristics that could be informative regarding the transition in diplodocids, whereas Taylor (2022) broadened the discussion towards all sauropods.

In MAB011899, 16 presacral vertebrae were recorded in the quarry map, which were articulated with the sacrum. Twelve of these vertebrae are still preserved today. The elongation of the anterior-most, preserved presacral vertebrae and the presence of cervical ribs clearly demonstrate that they are cervical vertebrae (Figure 5). Based on photographs taken during preparation (Figure 5C and 5D), the two cervical vertebrae and the 10 other, articulated presacral vertebrae, were separated from each other by one additional vertebra, which also bore cervical ribs. The anterior-most element of the 10 articulated presacral vertebrae is identified as the first dorsal vertebra based on a combination of the following characteristics: 1) the assumed general vertebral count for diplodocids (n=25, 15 CV, 10 DV; Hatcher, 1901; Huene, 1929; see Tschopp and Mateus, 2017; Taylor, 2022), thus the position within the axial column as seen in Figure 2; 2) the lack of a fused rib, whereas more anterior elements clearly have fused cervical ribs; 3) the location of the parapophysis ventral to the pleurocoel, which follows a similar, gradual transition as in *Diplodocus carnegii* (Hatcher, 1901); and 4) the distinct shortening from DV2 to DV3 as also

occurs in *Diplodocus* and *Barosaurus* (Hatcher, 1901; McIntosh, 2005). Hence, assuming a total of 25 presacral vertebrae, we interpret the preserved presacral vertebrae to represent CV13 and 14, and subsequently DV1 to DV10.

Although CV15 is currently missing, neural spine bifurcation is relatively clear for all vertebrae. Following the terminology of Wedel and Taylor (2013), the neural spines of CV13 through DV4 (including CV15) are all deeply bifid, with bifurcation deeper than half of the neural spine length. Shallowing of this bifurcation occurs rapidly, as DV5 is shallowly bifid, DV6 is notched/unsplit (see description of DV6), and DV7-9 and all sacral vertebrae are unsplit, and do no longer show evidence of dorsal midline indentation (no neural spine tip is preserved in DV10). From the cervical to the anterior dorsal vertebrae, the transverse distance increases between the metapophyses, but is never as short as in *Suuwassea* (Harris and Dodson, 2004).

Cervical Vertebrae (Figures 5–7, Table 1)

Preservation and orientation. The cervico-dorsal transitional vertebra is missing, as well as the three
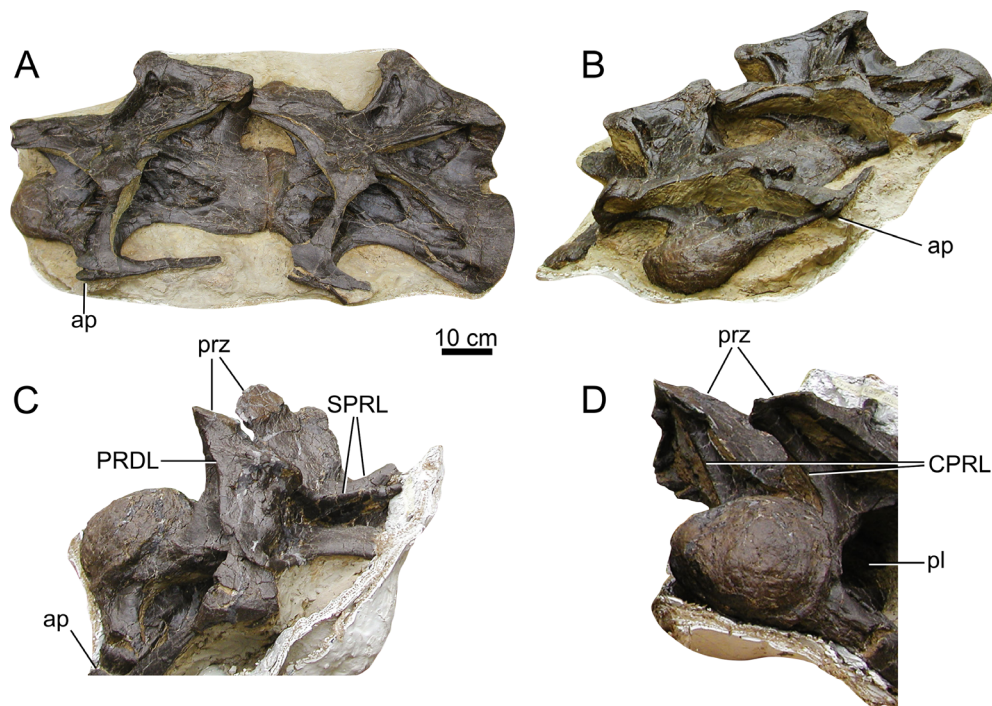
FIGURE 5. Cervical vertebrae 13, 14 and 15 of *Ardetosaurus viator* MAB011899, as photographed by the SMA. Cervical vertebrae 13 and 14 in A) left lateral and B) anterolateral view, with the preserved cervical ribs still present. Cervical vertebra 15 is shown in C) posterolateral and D) anterolateral view. Photographs are courtesy of the SMA. Scale bar is only applicable for figures A and B, as there is no measurable reference for CV15 due to the oblique views. Abbreviations: ap, anterior process; CPRL, centroprezygapophyseal lamina; pl, pleurocoel; PRDL, prezygodiapophyseal lamina; prz, prezygapophysis; SPRL, spinoprezygapophyseal lamina.

FIGURE 6. Cervical vertebra 13 of *Ardetosaurus viator* MAB011899. CV13 is shown in A) ventral, B) dorsal, C) left lateral, D) right lateral, E) posterior, and F) anterior view. A close up of the white box in F is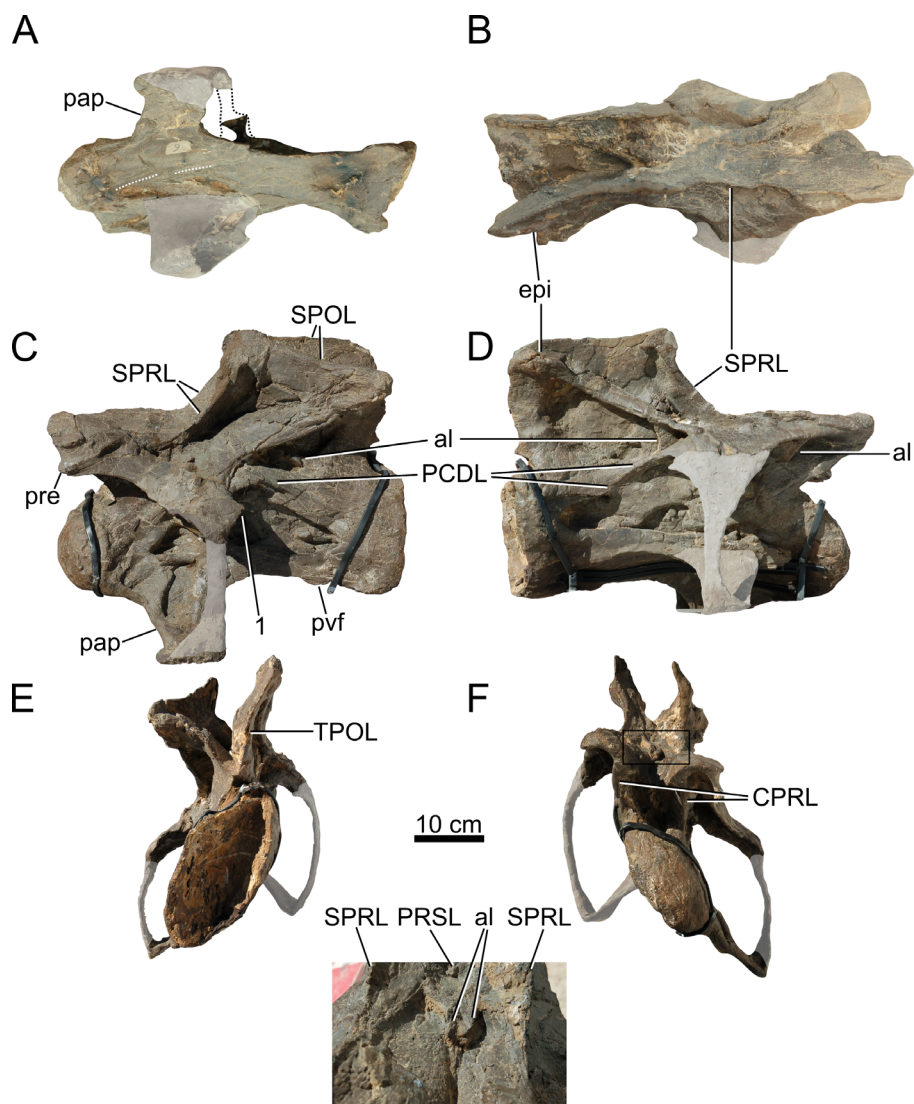 provided of the accessory laminae in the SPRF, shown in anterodorsal view. White shaded areas indicate reconstructed parts. The left cervical rib loop was obscured in ventral view for support and therefore roughly outlined here. White dotted lines in A indicate the remnants of the ventral keel. 1 indicates the triangular projections on the diapophysis. Abbreviations: al, accessory lamina; CPRL, centroprezygapophyseal lamina; epi, epipophysis; pap, parapophysis; PCDL, posterior centrodiapophyseal lamina; pre, pre-epipophysis; PRSL, prespinal lamina; pvf, posteroventral flange; SPOL, spinopostzygapophyseal lamina; SPRL, spinoprezygapophyseal lamina; TPOL, interpostzygapophyseal lamina.

vertebrae anterior to CV13. There are photographs of CV15; this vertebra will be briefly described based on those photographs. Both CV13 and CV14 are well-preserved, although both vertebrae were subject to transverse compression and shearing, especially the centra. Additionally, all cervical rib loops are now missing from both vertebrae, including the accompanying cervical ribs. However, left lateral photographs (see Figure 5) exist that show the vertebrae with preserved ribs; these have

been used to describe and score these parts of the vertebrae. The vertebrae are described with the long axis of the centra parallel to the horizontal.

Centrum morphology. Both cervical vertebral centra are strongly opisthocoelous. In posterior view, the articular facet has an oval shape, which is higher than wide. Foramina present in the pleurocoels indicate that pneumatic diverticula along the neck invaded the vertebral centra. Because of compression and shear, the condyle and the cotyle
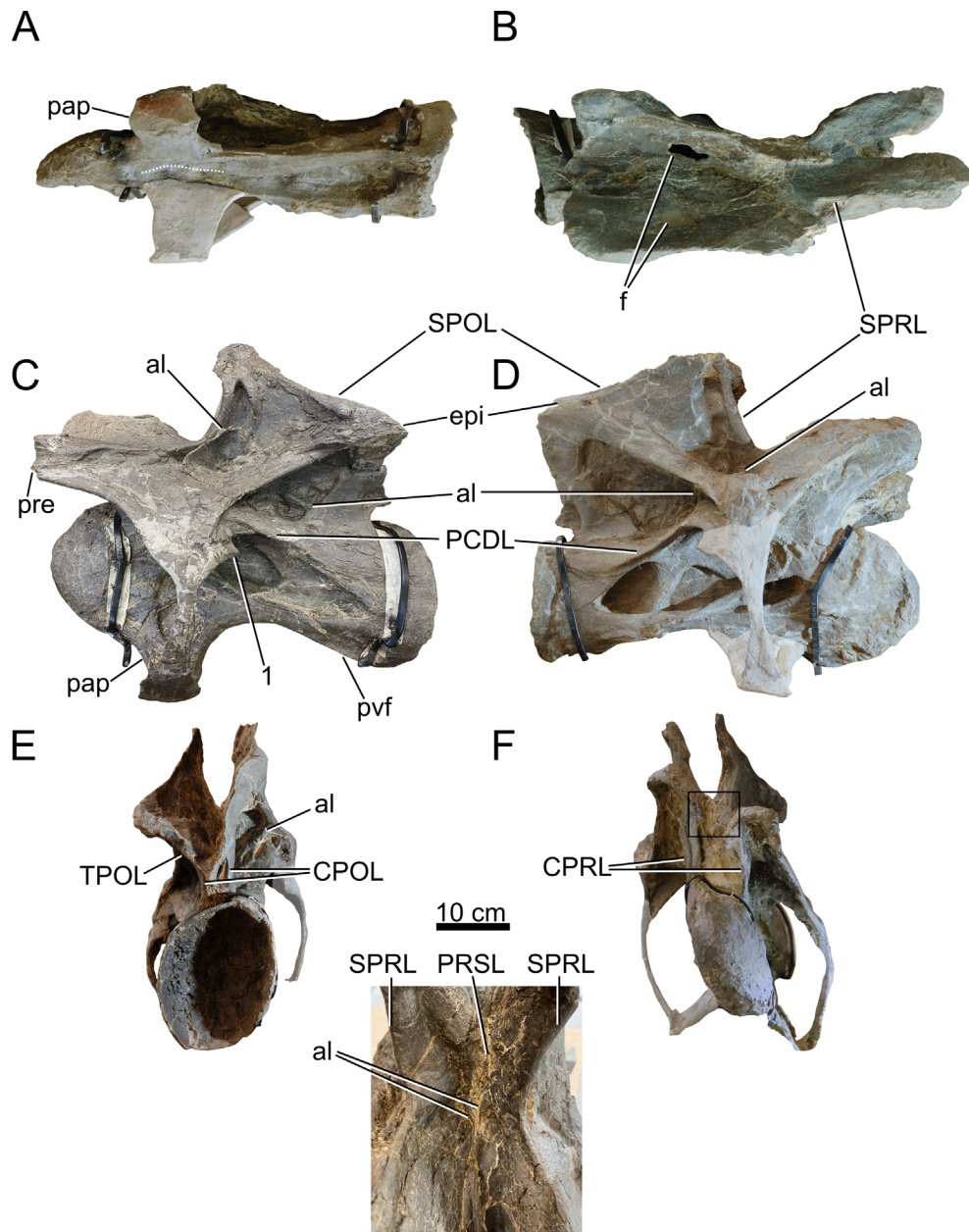
11

FIGURE 7. Cervical vertebra 14 of *Ardetosaurus viator* MAB011899. CV14 is shown in A) ventral, B) dorsal, C) left lateral, D) right lateral, E) posterior, and F) anterior view. A close up of the white box in F is provided of the accessory laminae in the SPRF, shown in anterodorsal view. Note the transition of these laminae to a more posterior position in the SPRF. White shaded areas indicate reconstructed parts. White dotted line indicates the remnant of the ventral keel. 1 indicates the triangular projections on the diapophysis. Abbreviations: al, accessory lamina; CPOL, centropostzygapophyseal lamina; CPRL, centroprezygapophyseal lamina; epi, epipophysis; pap, parapophysis; PCDL, posterior centrodiapophyseal lamina; pre, pre-epipophysis; PRSL, prespinal lamina; pvf, posteroventral flange; SPOL, spinopostzygapophyseal lamina; SPRL, spinoprezygapophyseal lamina; TPOL, interpostzygapophyseal lamina.

of CV13 have a flattened oval shape, but they were probably subcircular in outline originally, as in *Diplodocus, Kaatedocus* and *Galeamopus* (Hatcher, 1901; Tschopp and Mateus, 2013, 2017). The condyle is pronounced, rugose, and bordered by a ridge, which is preserved on the left lateral

and dorsal sides of the condyle. The lateral sides of the centra are strongly pneumatized. In CV13, a large pleurocoel, with multiple subfossae, is present on the left lateral surface, extending from the anterior border of the parapophysis to the beginning of the last quarter of the centrum. The pleuro-

TABLE 1. Measurements of the cervical vertebrae of *Ardetosaurus viator* MAB011899 (in mm).

Dimension	13	14
Anteroposterior length	507*	545*
Greatest height (left/right)	316*/342*	416*/369*
Centrum length	484*	541*
Centrum minimum width	76	74
Width across diapophyses	250*	250*
Width across prezygapophyses	165	176*
Width across postzygapophyses	154	181*
Pleurocoel length (left/right)	262/285	302/295
Pleurocoel height (left/right)	63/51	73/69
Cotyle width	119	152
Cotyle height	136	186
Condyle width	85*	91*
Condyle height	136*	144*
Neural spine height	190*	248*
Centrum length minus condyle length	418	441
Neural arch height	146*	148*

Notes: Asterisks indicate estimates. Measurements are influenced by shear and transverse compression. Centrum length includes condyle length. Neural arch height is measured from the dorsal margin of the cotyle rim vertically to an horizontal line joining both posterior margins of the postzygapophyses. Neural spine height is measured vertically from the dorsal margin of the cotyle rim to the neural spine tip.

coel is oval, longer anteroposteriorly than dorsoventrally. The anterior-most subfossa is sub-triangular and contains two smaller subfossae. The lamina dividing the first and second subfossae is angled anterodorsally-posteroventrally. The second subfossa is sub-oval and located just ventral to the diapophysis. The posterior-most subfossa is larger than the preceding subfossa. The subfossa is subtriangular, is longer than high, and deepens posteriorly. The right lateral surface, on the other hand, is marked by three fossae, which are well separated from each other, and not enclosed within a single, well-delimited pleurocoel. However, the posterior two subfossae possess a joint ventral rim, which fades anteriorly, indicating the original presence of a larger fossa. Transverse compression most likely has caused the dorsal border and part of the ventral border of the pleurocoel to fade, causing the pleurocoel as present on the left lateral side to no longer be present on the right lateral side. The anterior-most of these subfossae is located just dorsal to where the parapophysis would be (if preserved), and is oval in shape, anteroposteriorly longer than dorsoventrally tall. The second fossa is located dorsal to the posterior end of the reconstructed parapophysis and has a subtriangular 'shark-fin'-like outline. The posterior-most fossa is located just posterior to the second

fossa, and is a posteriorly deepening, oval depression, ending just anterior to the anterolateral border of the cotyle. The left parapophysis is located in the first half of the centrum and possesses a mediolaterally elongated fossa on the dorsal side, starting just ventral to the anterior border of the large lateral pleurocoel. The right lateral side does not preserve the cervical rib loop, and most of the parapophysis and the diapophysis are also missing; they were reconstructed symmetrically for mounting purposes. Therefore, it cannot be confidently concluded if a dorsal pneumatization was present on the right parapophysis of CV13.

In left lateral view, CV14 also shows a fossa on the dorsal part of the parapophysis. The fossa is egg-shaped, with the pointed end directed lateroventrally. Dorsal to this fossa, the lateral surface of the centrum is marked by a small 'half-moon'-shaped fossa, with the convex edge pointing dorsally. Posterior and posterodorsal to this small fossa is a large, sub-oval fossa, which extends until just anterior to the cotyle rim. Within this larger fossa, a smaller, oval subfossa is present in the anterior part. As in CV13, the right parapophysis and diapophysis of CV14 are partly missing, and reconstructed with the cervical rib loop for mounting purposes. Three distinct, smooth, relatively deep fossae are present on the right lateral sur-

face. The first fossa is located dorsal to the proximal part of the parapophysis. The fossa is teardrop-shaped, with the long axis of the fossa oriented nearly parallel to the long axis of the centrum. The pointed end of the fossa faces posteriorly. The second fossa, located posterior to the first, is subtriangular with rounded corners. The posterior-most fossa is similar to that in CV13 on the same side: a posteriorly deepening, roughly teardrop-shaped fossa, with the pointed end oriented posteriorly. Two small, shallow depressions are present dorsal to the first two fossae, in between the anterior centrodiapophyseal lamina (ACDL) and posterior centrodiapophyseal lamina (PCDL), obscured by the diapophyses in lateral view. Both vertebrae contain small, oval fossae on the posteroventral corners of the lateral surfaces of the centra, which are more pronounced on the left sides, with CV14 lacking such a fossa entirely on the right side.

The deformation of the centra of CV13 and CV14 results in a somewhat flattened ventral surface, especially in CV13. Posteroventral flanges are present and are most distinct on the left lateral sides of both centra. Ventral keels are present at the anterior part of the centra, but are difficult to discern due to the deformation and shear of the vertebrae, which is especially true for CV13. Only CV14 preserves a distinct keel, whereas CV13 only preserves severely flattened remnants of the keel. Deformation shifted the posterior end of the ventral keel in CV14 laterally to the left. The surface is transversely concave, although in CV13, the surface is close to flat due to compression. A sulcus is present, most distinct in CV14.

Neural arch morphology. The prezygapophyses of both vertebrae are strongly convex transversely, with the medial part of the rami bending ventrally. Pre-epipophyses are present laterally on the prezygapophyseal rami of both vertebrae, projecting anterodorsally as short, rugose projections. They are more developed on the left lateral side of each vertebra. As the prezygapophyses overhang the condyles in both vertebrae, the CPRLs of both vertebrae extend anterodorsally from the centra. Both CV13 and CV14 contain single CPRLs with no medial or lateral branches, as those present in e.g., *Diplodocus carnegii* (Hatcher, 1901, plate V) or *Kaatedocus* (Tschopp and Mateus, 2013, p. 873). In both CV13 and 14, the paired TPRL connects to the posteromedial sides of the prezygapophyseal articular facets. Posteriorly, the paired TPRL meets dorsal to the neural canal in an acute angle. The left and right prezygapophyseal centrodiapophy-

seal fossae (PRCDFs) of CV13 contain a single, dorsoventrally oriented lamina, which divides both PRCDFs into two cavities. The right lamina is more prominent and less damaged compared to the left lamina. Within the PRCDF of CV14 on the right side, two small bony protrusions are visible which would have formed two dorsoventrally oriented accessory laminae, with the flat side of the laminae facing laterally. The dorsal end of these laminae connects to the ventral side of the PRDL and is positioned more anteriorly compared to the ventral part of the laminae, creating a diagonal outline in lateral view. The more anterior of these two laminae is well exposed, but the posterior lamina is almost fully destroyed, leaving only a small vestige of this lamina. Similarly, on the left lateral side, two small bony protrusions are visible which would have formed these double laminae, subdividing the PRCDF into multiple cavities.

The left diapophysis of CV13, due to the shear, is pushed slightly posteroventrally, whereas the right diapophysis – although largely lost – is seemingly in a more laterally oriented plane. Both diapophyses dip ventrally towards their lateral end. The left diapophysis has a posteriorly oriented, triangular projection, as also seen in *Kaatedocus*, but it is wider at its base and protrude further posteriorly in CV13 of MAB011899 compared to the holotype of *Kaatedocus siberi* (Tschopp and Mateus, 2013). The diapophyses of CV14 are different, as the right diapophysis is not oriented horizontally, but more obliquely, with the anterior margin located more dorsally than the posterior margin, such that the diapophysis slopes posteroventrally in posterior direction. This is, however, a result of poor preservation of the diapophysis, as well as shear of the vertebra. The diapophysis would have been oriented more horizontally in vivo. The left diapophysis is oriented horizontally, and projects lateroventrally, with a complete cervical rib loop preserved. This diapophysis also has the triangular, posteriorly oriented projection. ACDLs are present on the ventral sides of the diapophyses of CV13 and CV14, and fuse with the centrum at their anteroventral end. On the right side of both vertebrae, however, the ACDLs are more posteriorly restricted; this is not a result of the obvious transverse compression. PCDLs are present in both vertebrae, extending posteriorly onto the centrum. The anterior-most part of the left PCDL of CV13 meets the medial end of the triangular projection of the diapophysis. The right PCDL bifurcates anteriorly, with a short fading branch projecting ventrally close to the diapophysis. This bifurcation is also present in *Barosaurus*

lentus (Lull, 1919; see Tschopp et al., 2015a), but it is not nearly as prominent in MAB11899 as that seen in, e.g., YPM VP.000429. In CV14, the anterior end of the left PCDL does not meet at the medial base of the triangular projection, but instead proceeds slightly onto the dorsal surface of the diapophysis, meeting the posteroventral side of the postzygodiapophyseal lamina (PODL). The right PCDL is similar in morphology as the right PCDL of CV13. The PRDLs of both CV13 and CV14 are similar. The left PRDLs of CV13 and CV14 are oriented posteroventrally at their anterior end, and subsequently bend lateroventrally to reach the diapophyses. The right PRDLs are slightly different in the two vertebrae. The right PRDL of CV13 is oriented nearly horizontal, only dipping ventrally just anterior to the diapophysis. In CV14, the right prezygapophysis is raised further dorsally, resulting in a diagonal trajectory of the PRDL, as the diapophysis is located further ventrally. However, the dorsal displacement of the prezygapophysis in CV14 is caused by the shear of the vertebra. The anterior half of all PRDLs is roughened laterally but this is most prominent on the left sides of both vertebrae. The PODLs of CV13 are similar in orientation, with their anteroventral ends extending onto the dorsomedial surface of the diapophyses. The edges of the anteroventral halves face laterally, with the posterodorsal halves facing ventrally. This transition occurs earlier in the left PODL of CV13, wherein most of the edge faces ventrally, likely a result of the transverse compression. Both PODLs connect to the anteroventral sides of the postzygapophyses. In CV14, the PODLs are similar in morphology as to those in CV13, except for the posterodorsal half of the left PODL. Although the PODL connects to the postzygapophysis on the anteroventral side of the postzygapophysis, the posterodorsal end of the PODL is overlain by an accessory lamina, which is connected posteriorly to the epipophysis, and anteromedially fades into the SDF.

The metapophyses of both vertebrae are nearly vertical to posteriorly inclined in lateral view. The SPRLs are oriented anteroventrally from the neural spine apices towards the prezygapophyses in lateral view in both vertebrae. Only the anterodorsal tip of the left SPRL in CV14 preserves an anterior projection, which is not as prominent as seen in, e.g., *Diplodocus carnegii* (Hatcher, 1901) or *Kaatedocus siberi* (Tschopp and Mateus, 2013). The dorsal tip of the left SPRL in CV13 is deflected medially in anterior view, because of deformation. The SPRLs are inclined laterally proximal to the

prezygapophyses, but no fossae are present ventral to the inclined laminae, posterior to the prezygapophyseal facets. Each SPOL has a somewhat different trajectory, due to shear, but both meet their respective neural spine apices at the same height. A median tubercle occurs between the metapophyses, with a faint, rugose PRSL extending along the anterior side of the tubercle. Anterior to the median tubercles of CV13 through DV2 (except for CV15, where it is unknown due to the angle of the photographs, see below), within the spinoprezygapophyseal fossa (SPRF), accessory laminae are present, most prominently in CV13. In CV13, these accessory laminae are positioned anterior to the tubercle and just posterior to the midpoint of the interprezygapophyseal lamina (TPRL). They project anterodorsally, forming a bony protrusion, and extend posteriorly towards the metapophyses, but fade early at the base of the median tubercle. The right accessory lamina is slightly pushed into the left, and both are dorsally rugose. In CV14, these laminae have moved posteriorly, project anterodorsally, are more lamina-like, and are located lateral to the PRSL and the tubercle, and posteromedial to both SPRLs. Both laminae fade dorsally just ventral to the dorsal-most edge of the tubercle. Figures 6 and 7 show close-ups of the morphology of these accessory laminae in CV13 and CV14. Similar laminae are present in DV1 and DV2. Therefore, these accessory laminae possibly play a role in laminar capture sensu Wilson (2012, p. 103-105), a process whereby vertebral landmarks 'capture' laminae, such as the creation of the spinodiapophyseal lamina (SPDL) through the capture of the SPRL (Wilson, 2012, figure 10). Posterior to the SPRLs, a dorsoventral coel pierces the lateral side of the metapophyses of both vertebrae, forming a well-delimited, small subfossa within the spinodiapophyseal fossa (SDF). All coels are ventrally open, and the right coels are more pronounced compared to the left, likely a result of compression. An accessory, semi-horizontal lamina is present in the center of the right SDF of CV14, medial to the diapophyses and ventral within the fossa, similar to *Barosaurus lentus* (Lull, 1919). This lamina does not touch the PODL, or the SPRL, but is oriented with the anterior end facing perpendicular to the SPRL, and the posterior end facing roughly perpendicular to the PODL. The left SDF of CV14 contains an unusual sheet of bone, which appears to be an accessory lamina. The dorsal part of this lamina is connected to the ventral-most part of the lateral coel. The lamina is oriented obliquely, with

its ventral portion located more anteriorly, roughly parallel to the SPRL. The middle part of the lamina is pushed against the adjacent SPRL. The lamina ends laterally close to the adjacent SPRL, approximately medial to the diapophysis. Although MAB011899 lacks the complex laminae in the SDF seen in *Diplodocus carnegii* (Hatcher, 1901, plate III), the accessory lamina is probably best identified as one of the accessory laminae seen in the SDF of *D. carnegii*, whereby the lamina is partially broken and pushed against the left SPRL.

Within the SPOF of CV14, there are two suboval foramina, which pierce the SPOLs and connect to the dorsal part of the postzygapophyseal centrodiapophyseal fossae (POCDFs). Contrary to *Galeamopus pabsti* (Tschopp and Mateus, 2017), these foramina are not visible in lateral view in MAB011899, as the foramina are smaller, and located in the dorsal part of the POCDFs, which is obscured by the PODLs in lateral view. In CV13, these foramina might have been present, but the right POCDF was poorly preserved, and thus infilled with acrylic resin. The left POCDF is better preserved, but at the place where the foramina are located in CV14, acrylic resin has been added. In dorsal view, acrylic resin is visible in the SPOFs, which thus likely obscures the presence of the foramina. CV14 also possesses a ridge on the medial side of the right metapophysis, extending from the middle of the SPOL to the middle of the SPRL, although not directly connected to either lamina. The POCDFs of both vertebrae have different morphologies. The left POCDF of CV13 contains a well-delimited subfossa. Within the subfossa, an accessory lamina projects laterally and is oriented roughly anteroposteriorly, fusing posteriorly with the border of the subfossa. Additionally, a short, thin, dorsoventrally oriented accessory lamina is present ventral to the anteroventral part of the PODL, connecting medially to the anterodorsal part of the PCDL. A similar morphology is found in CV14, although the subfossa is larger, and the accessory lamina fades anteriorly into the fossa, and the additional, dorsoventrally oriented lamina is partially reconstructed (the ventral part). The right fossae of both vertebrae are also similar but have posteriorly projecting accessory laminae. In CV13, a similar, vertical accessory lamina is present in the POCDF on the left side. An additional, dorsoventrally shorter, but similarly oriented accessory lamina is present, just posteromedial to the other lamina in the POCDF. In CV14, within the right POCDF, an accessory lamina is located in a similar position as the first accessory lamina within the right POCDF of CV13, but this lamina bifurcates in CV14, forming two accessory laminae, and is oriented obliquely, not vertical. The bifurcation of this particular lamina occurs roughly halfway of the total length of the lamina, whereby the thicker, dorsal part forms two thin laminae, which constitute the ventral half of the structure. The medial lamina extends further posteroventrally than the lateral branch, with the lateral branch retaining the same trajectory as the initial dorsal part of the lamina. An additional posteriorly-projecting lamina is present posteromedial to the bifurcating laminae in this POCDF.

Due to the shear of both vertebrae, the left postzygapophyses are ventrally displaced compared to the right postzygapophyses. Epiphyses are present on both sides of both vertebrae, but are not as prominent as seen in e.g., *Patagosaurus* (Holwerda et al., 2021) or *Kaatedocus* (Tschopp and Mateus, 2013). On the right side of CV13, the epipophysis is located dorsolateral to the postzygapophysis, and is pneumatized, showing a small, oval depression, which is infilled by sediment. The epipophyses are compressed asymmetrically between the left and right sides of both vertebrae. This bilateral asymmetry of the posterodorsal side of cervical vertebrae is also observed for the entire posterodorsal region of the vertebrae in *Diplodocus carnegii* (Hatcher, 1901), although some of the observed variation in *D. carnegii* may be deformation. In MAB011899, the left epipophysis of CV13, which is pneumatized from the inside via a small infilled hole in the spinopostzygapophyseal fossa (SPOF), and the right epipophysis of CV14, are compressed transversely. The right epipophysis of CV13 is compressed more dorsoventrally, but also slightly transversely, whereas the left epipophysis of CV14 also contains both states, but here, the transverse compression is more prominent. In posterior view, the left TPOL is bent inwards, meeting the right TPOL, which is straighter, above the neural canal. This is more prominent in CV13 compared to CV14, but in both, this is influenced by shear. They both meet in a projection, which protrudes slightly beyond the posterior margin of the neural arch, hanging above the dorsal edge of the cotyle. Lateral to this projection, CV14 shows distinct lateral centropostzygapophyseal laminae (lCPOLs), which are separated by centropostzygapophyseal fossae (CPOFs) from the mCPOLs (or mdCPOL sensu Carballido and Sander, 2014), which run from the projection of the TPOL lateroventrally to the centrum, forming the neural canal margin. In CV13, in contrast to CV14, the lCPOLs

are not distinct from the rest of arch, and probably run alongside the TPOL towards the posterior projection. mCPOLs are present in CV13 and similar in morphology to CV14. The neural canals are not perfectly round due to compression, but more triangular in both anterior and posterior view.

CV15 Description (Figure 5)

As aforementioned, this vertebra is lost, most likely in the fire at Münchehagen. Although the photographs are insufficient to describe CV15 in similar detail, several features can be interpreted from a left anterolateral and posterolateral photograph. Only the anterior half of the vertebra was preserved, and the neural spines were missing. The posterior half was likely destroyed when the field jacket containing the cervical vertebrae and the field jacket containing the anterior dorsal vertebrae were detached from each other. This is supported by the fact that the small jacket containing CV15 fitted perfectly with the jacket containing CV13 and CV14. However, posterior to CV15, the jacket ends, which might be an indication that the posterior half of CV15 was already destroyed during the excavation, due to the crumbly nature of the bones (from which the specimen got its nickname).

The centrum of CV15 is strongly opisthocoelous, with a convex condyle, similar to the previous vertebrae. Posterior to the condyle, an extremely deep pleurocoel is seen. Dorsal to the pleurocoel, the diapophysis has a posterior projection, similar as in CV13 and CV14. A cervical rib loop is also present. A glimpse can be seen in Figure 5C of the anterior process of the cervical rib, which appears small and rounded, similar to the process of the rib of CV13 (see below). Anteroventral to the diapophysis, an ACDL is present. A single CPRL can be seen on this side, with no clear indication of dorsal bifurcation into two rami, although recognizing such a division is hampered by the quality and angle of the photographs. The PRDL is preserved, connecting to a near-horizontal left prezygapophysis. The right prezygapophysis is laterally inclined. No transverse sulcus can be seen posterior to the prezygapophyseal facet. From the left metapophysis, part of an anteriorly compressed SPRL is seen. Ventrally, this lamina protrudes strongly dorsally, to subsequently fade anteroventrally posterolateral to the prezygapophyseal facet. Part of a PODL can also be observed on the left side. From the right prezygapophysis, a similar deformed SPRL is visible as the left SPRL. The TPRL is preserved and

appears similar in morphology as seen in CV13 and CV14. No accessory laminae are observed in the SDF. The PRCDF is filled with matrix, so it cannot be assessed if multiple laminae are present similar to the previous vertebrae. No other morphological details can be gleaned from the photographs.

Cervical Ribs (Figure 5)

Currently, the cervical ribs of both CV13 and CV14 are lost, as well as major parts of the cervical rib loops. However, photographs were taken when the vertebrae were prepared at the SMA, in which CV13 preserved a significant part of the cervical rib loop and the attached rib on the left side. Only the posterior-most end of the rib shaft is missing, and a small part of the anterior process of the rib. A rib was also attached to CV14, but most of the rib is missing in the photographs, preserving only part of the anterior process, a small part of the posterior rib shaft, and the cervical rib loop connecting the diapophysis and parapophysis.

Both ribs are located just slightly ventral to the centrum, unlike those seen apatosaurines (e.g., Gilmore, 1936; Ostrom and McIntosh, 1966; Upchurch et al., 2004b), whereby the ribs are placed significantly below the ventral margin of the centrum. The posterior end of the rib shaft of CV13 is missing in the photo (Figure 5A), but the shaft appears to be tapering towards the posterior end. Both the dorsal and ventral side of the rib shaft is straight, apart from a small indentation caused by deformation/breakage halfway along the visible rib on the posterior side. Anteriorly, the rib is dorsoventrally wider compared to the posterior part of the rib, as the ventral part of the rib shaft curves slowly dorsally towards the anterior process. The anterior process appears rounded in lateral view, although this is difficult to observe in the photograph due to the angle of the photograph, with the dorsal part curving posteriorly against the cervical rib loop. The anterior process appears to be slightly longer anteroposteriorly compared to its height dorsoventrally but is smaller compared to the anterior facets of CV13/14 e.g., *Kaatedocus* (Tschopp and Mateus, 2013, p. 873) or *Galeamopus* (Tschopp and Mateus, 2017, p. 63). In lateral view, it is obscured, but a photograph taken approximately anterolaterally (Figure 5B) reveals that the anterior process is broken in two, and that the process is quite robust, especially compared to the anterior facets of *Kaatedocus* and *Galeamopus*.
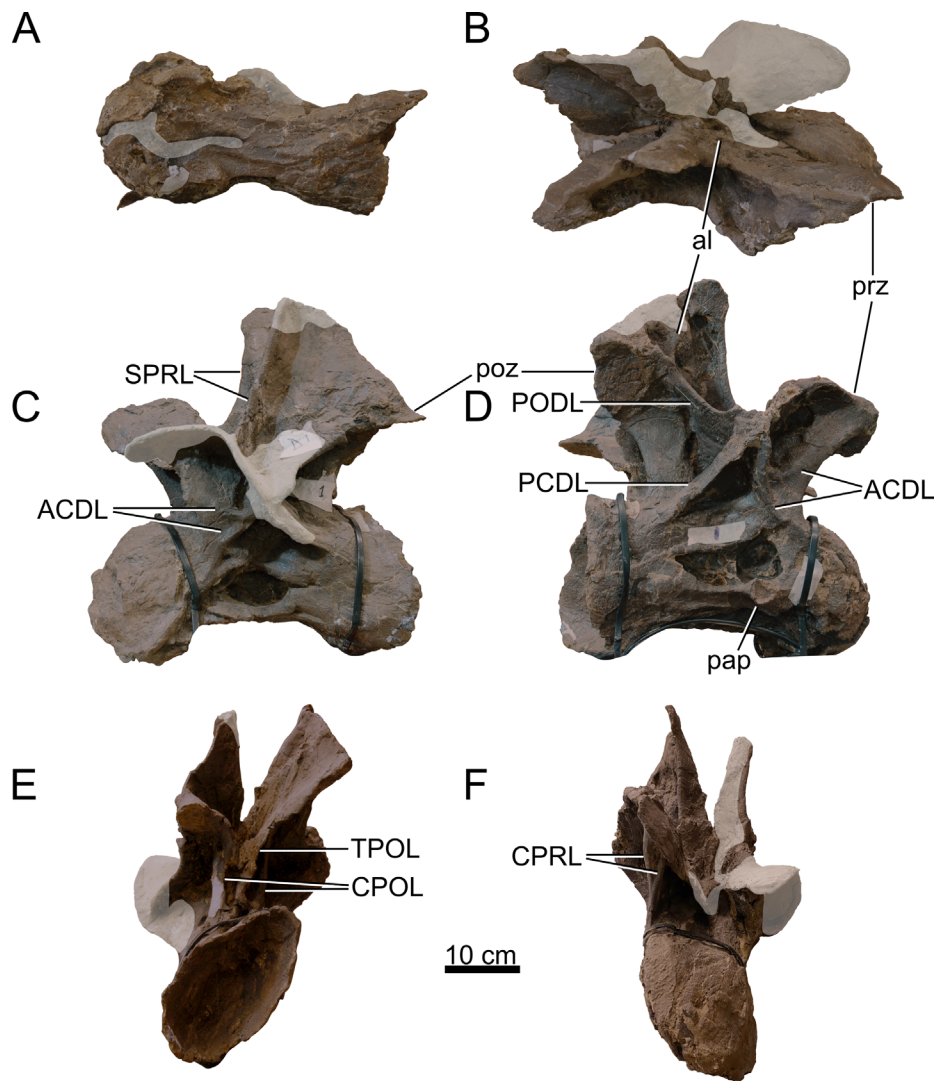
FIGURE 8. Dorsal vertebra 1 of *Ardetosaurus viator* MAB011899. DV1 is shown in A) ventral, B) dorsal, C) left lateral, D) right lateral, E) posterior, and F) anterior view. White shaded areas indicate reconstructed parts. Note the bifurcated ACDLs. Abbreviations: ACDL, anterior centrodiapophyseal lamina; al, accessory lamina; CPOL, centropostzygapophyseal lamina; CPRL, centroprezygapophyseal lamina; pap, parapophysis; PCDL, posterior centrodiapophyseal lamina; PODL, postzygodiapophyseal lamina; poz, postzygapophysis; prz, prezygapophysis; SPRL, spinoprezygapophyseal lamina; TPOL, interpostzygapophyseal lamina.

Dorsal Vertebrae (Figures 8–17, Table 2)

Preservation and orientation. The dorsal vertebrae were preserved in articulation with the cervical and sacral vertebrae, which were all excavated in four separate blocks. Based on the early preparation photographs provided by the SMA, dorsal vertebrae 1-5 and dorsal vertebrae 6-9 were excavated and prepared in separate blocks. The partially preserved tenth dorsal vertebra was recovered and prepared in a block with the sacrum. Distinction between anterior, middle, and posterior dorsal vertebrae is based on Tschopp et al. (2015a): anterior dorsal vertebrae are defined by having the parapophyses still in contact with the centrum, whereas middle and posterior dorsal vertebrae have a numerical subdivision. Generally, the preservation of the dorsal vertebrae becomes worse along the series, and parts that were missing are reconstructed with acrylic resin for mounting purposes. Especially DV10 is modified and reconstructed, as substantial parts of the neural arch were missing, and the preserved parts were crushed. For most of the reconstructed laminae in the dorsal series, however, small parts were present or are reconstructed based on bilateral symme-
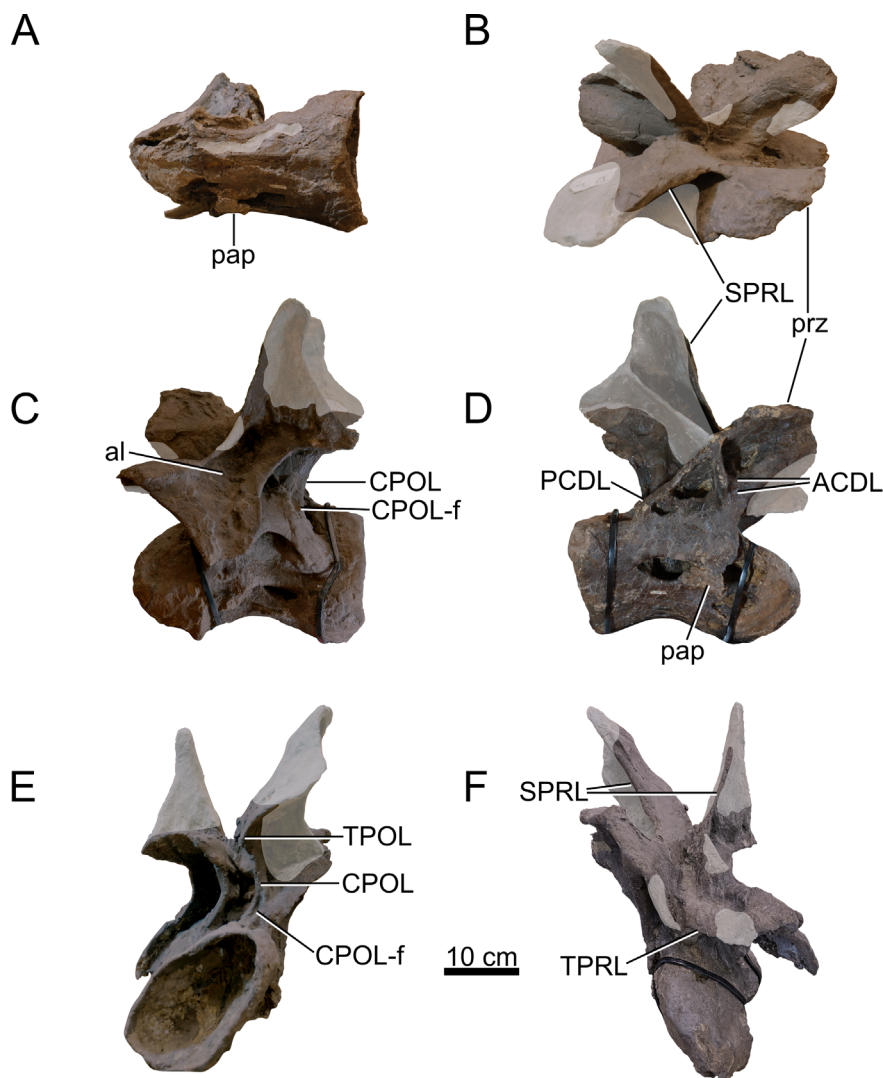
FIGURE 9. Dorsal vertebra 2 of *Ardetosaurus viator* MAB011899. DV2 is shown in A) ventral, B) dorsal, C) left lateral, D) right lateral, E) posterior, and F) anterior view. Note the shallow fossae medial to the ventrally bifurcating CPOLs. White shaded areas indicate reconstructed parts. Note the bifurcated ACDLs. Abbreviations: ACDL, anterior centrodiapophyseal lamina; al, accessory lamina; CPOL, centropostzygapophyseal lamina; CPOL-f, centropostzygapophyseal lamina fossa; pap, parapophysis; PCDL, posterior centrodiapophyseal lamina; SPRL, spinoprezygapophyseal lamina; TPOL, interpostzygapophyseal lamina; TPRL, interprezygapophyseal lamina.

try. All dorsal vertebrae are compressed in an analogous way as the two cervical vertebrae, although compression is more pronounced in the anterior and mid-dorsal vertebrae.

General morphology. All dorsal vertebrae are taller than long, and the centra shorten from DV1 to DV5, after which centrum length remains subequal (Table 2). The condyle is distinct in DV1 and DV2, becomes smaller in DV3, and is reduced in DV4-9 (it is not preserved in DV10). The right lateral side of the condyles of DV2 and DV3 are slightly eroded close to the ventral surface, revealing the internal pneumatic structure as polycamerate (Wedel et al.,

2000). All vertebrae have pleurocoels on the lateral sides of the centra, which vary in shape from oval to more irregularly shaped, but this variation is most likely due to deformation. The true shape of the pleurocoels would have likely been similar to that seen in *Diplodocus carnegii* (Hatcher, 1901), although placed more centrally onto the lateral surface as in *Supersaurus vivianae* (Jensen, 1985), and not invading the neural arch pedicles as in *D. carnegii* or *Galeamopus pabsti* (Tschopp and Mateus, 2017). The size of the pleurocoels increases along the series, with the posterior (DV7-10) centra having pleurocoels with a length roughly
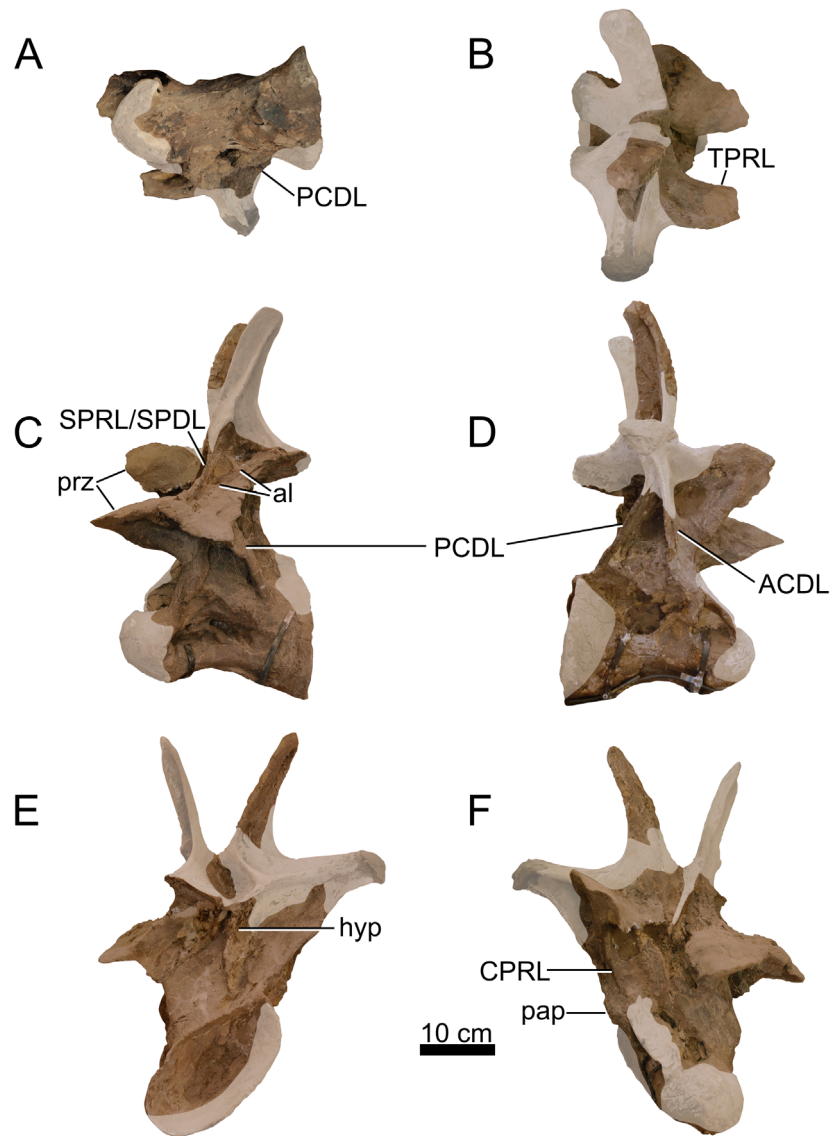
FIGURE 10. Dorsal vertebra 3 of *Ardetosaurus viator* MAB011899. DV3 is shown in A) ventral, B) dorsal, C) left lateral, D) right lateral, E) posterior, and F) anterior view. Note the displacement of the SPRL/SPDL, as well as the first appearance of the hyposphene, albeit crushed. White shaded areas indicate reconstructed parts. Abbreviations: ACDL, anterior centrodiapophyseal lamina; al, accessory lamina; CPRL, centroprezygapophyseal lamina; hyp, hyposphene; pap, parapophysis; PCDL, posterior centrodiapophyseal lamina; prz, prezygapophysis; SPDL, spinodiapophyseal lamina; SPRL, spinoprezygapophyseal lamina.

equal to the anteroposterior length of the neural arch pedicles. Due to compression, the transverse processes on the left lateral side are oriented lateroventrally, whereas the right lateral processes are oriented dorsolaterly. In DV6-8, the transverse processes are nearly horizontal, similar to *Diplodocus* (Hatcher, 1901). The SPDLs, where present, follow the curvature of the neural spine and the diapophyses. They first appear in DV3, as the SPRLs seem to transition laterally along the cervicodorsal junction, and are captured by the dia-

pophysis, sensu Wilson (2012). This capture sequence is best preserved on the left lateral side of DV3, wherein the 'SPDL' ends ventrally in between the prezygapophyses and the diapophysis. The location of the SPDLs (especially their ventral halves) in more posterior dorsal vertebrae gradually moves more posteriorly onto the lateral surface of the neural spine. SPRLs distinct from the captured SPDLs can first be observed in DV4, but preservation in DV3 is incomplete, so the entire serial transition of these two laminae cannot be

clearly identified. Hyposphene-hypantrum articulations are well developed, although most hyposphenes are not preserved, and nearly all hypantra are damaged. The first hyposphene appears in DV3, although poorly preserved. In DV4, the hyposphene is supported by a subvertical lamina ventrally (sTPOL sensu Carballido and Sander, 2014). DV4 is the first dorsal vertebra in which the hyposphene takes a clear rhomboid shape, which is even more prominent in DV6. A supporting lamina is also seen in DV5, but this is a reconstructed lamina. None of the more posterior vertebrae preserve a single, supporting ventral lamina; the hyposphenes in these vertebrae are supported by oblique CPOLs that unite below the hyposphene.

Anterior Dorsal Vertebrae (DV1-3; Figures 8–10, Table 2)

Centrum morphology. The centra are all opisthocoelous and their ventral surface is concave anteroposteriorly. Due to breakage and deformation, it is impossible to say whether the ventral surface was concave, flat or slightly convex transversely. The condyle of DV1 and DV2 preserves a relatively distinct bony rim. This may have been present in DV3, but as parts of the condyle are missing, the condyle of DV3 has been reconstructed without a rim. Due to similar compression patterns as in the cervical vertebrae, the condyles and cotyles of DV1-3 are all compressed ellipses. In DV1, the parapophyses are located anteroventrally to the pleurocoels. They are located more dorsally in DV2, anterior to the pleurocoels, and in DV3, the parapophyses are located anterodorsal to the pleurocoels. The pleurocoels in DV1 are roughly oval and located slightly anterior to the middle of the centrum. The right lateral pleurocoel bears the first signs of a vertical bony ridge dividing the coel in two separate chambers, but this ridge is too shallow to truly divide the pleurocoel. In DV2, the pleurocoels are situated slightly posterior to the middle of the centrum and are suboval in outline. DV3 has a poorly preserved centrum, especially the right lateral side. The pleurocoel on the left lateral side is flattened, suboval, and divided from an anteriorly placed coel by an anterodorsally-posteroventrally oriented bony strut, which resembles an earlier state of the rod-like struts dividing the pleurocoels in the mid- and posterior dorsal vertebrae. The pleurocoel on the right lateral side is almost circular and is positioned slightly posterior to midlength. The posterodorsal edge of the pleurocoel is damaged, as part of the neural arch and the complete cotyle rim of the right side is missing,

which makes it difficult to assess if the pleurocoel was larger posteriorly, and thus more oval shaped rather than subcircular. No bony strut is visible on this side. As the centrum length decreases from DV1 to DV3, the pleurocoel also shortens in anteroposterior length (Table 2). The ventral surface of DV1 is deformed, and the condyle shows signs of breakage. However, an anteroposteriorly oriented keel is present at the anterior side of the ventral surface of the centrum, albeit faint due to the compressed centrum. DV2 does not preserve a keel, is also deformed, and the ventrolateral side of the condyle is missing, revealing the internal pneumatic structures. The internal structure is polycamerate sensu Wedel et al. (2000), consisting of larger camerae which are separated by branching structures, common for diplodocids (Wedel, 2003; Tatehata et al., 2023). The structure seen in DV2 is comparable with the pattern seen in *Apatosaurus* (Wedel et al., 2000, figure 11C). The ventral side of DV3 is better preserved, although compressed similarly to DV1 and DV2. No ventral keel is present.

Neural arch morphology. The prezygapophyses of DV1-3 are largely preserved. DV1 misses the left prezygapophyses, and DV2 misses small parts of the anteromedial sides of both rami. In all three vertebrae, the rami are inclined laterally and slightly convex dorsally. In both DV1 and DV2, the right prezygapophysis is nearly vertical, which is less pronounced in DV3, caused by the shear of the vertebrae. The left prezygapophysis of DV2 is ventrally displaced. Due to deformation, the left prezygapophysis of DV3 is roughly horizontally oriented, with the entire ramus bending slightly ventrally, whereas the right prezygapophysis is steeply inclined laterally, as well as projecting anterodorsally. In DV1, the right CPRL is well preserved, and bifurcates dorsally to form two CPRLs attaching ventrally to the prezygapophyseal facet. The left CPRL misses the dorsal part. Therefore, it cannot be assessed if this lamina also bifurcates dorsally but based on the width of the lamina compared to the right CPRL, it can be assumed that it did bifurcate. In DV2, the CPRLs are relatively vertical (in anterior view) laminae, which are, in lateral view, inclined anteriorly towards the prezygapophyseal facets. No dorsal bifurcation of the CPRLs appears to be present. The right prezygapophysis is oriented similarly as the right prezygapophysis of DV1, being almost vertical in anterior view due to shear. The CPRLs are both preserved in DV3, but due to the different positions of the prezygapophyses, have slightly different trajectories. In lateral

view, the right CPRL is oriented more anterodorsally towards the prezygapophysis. The left CPRL is also oriented anterodorsally, but is bent further anteriorly, therefore appearing closer to the horizontal plane of the centrum. The left half of the TPRL in DV1 is reconstructed. The right half of the TPRL is only posteriorly reconstructed, which in the mount results in a TPRL, which crosses dorsal to the neural canal to the left side. The TPRL of DV2 is largely preserved, missing a small part of the right branch close to the prezygapophysis, and missing half of the left branch, at the same position, but extending further posteriorly. The paired TPRL in DV2 meet dorsal to the neural canal, similar to what is seen in the cervical vertebrae. The TPRL of DV3 is partially preserved, not connecting medially. Most of the left PRCDF of DV1 is preserved, but the fossa does not contain any accessory laminae. The right PRCDF also does not contain any accessory laminae, but it contains a small coel-like depression in the posterodorsal part of the fossa. The neural canal is roughly oval, with the long axis oriented dorsoventrally. The left PRCDF of DV2 is obscured in lateral view by the ventrally displaced PRDL, whereas the right PRCDF is completely visible in lateral view. Neither of the fossae contain any accessory laminae, and only the right fossa contains an additional small depression (similar to DV1). Such a depression, however, might also be present on the other side, but in the left PRCDF, some residual sediment is still present to maintain the stability of the vertebra, which obscures the possible location of this depression. Both PRCDFs of DV3 lack any accessory laminae, but do preserve some additional pneumatic depressions, although the larger depression on the left lateral side is partially reconstructed.

The left transverse process of DV1 is partly reconstructed, but the preserved ACDL and PCDL meet approximately level with the dorsal edge of the cotyle, supporting the diapophysis from below. The right lateral transverse process is located substantially above the dorsal edge of the centrum, halfway between the dorsal edge of the cotyle and the postzygapophysis, but this is probably affected by deformation. In DV2, this shear is more extreme, with the left lateral transverse process projecting even further ventrally, being located in the same plane as the upper third of the centrum, whereas the right lateral process is located just beneath the postzygapophysis at the same side, and is, in posterior view, in the same plane as the left postzygapophysis. In DV3, the shear is less

extreme, but this impression is also caused by the reconstruction of the right lateral transverse process, which follows a more horizontal orientation as would be expected in vivo. On the left lateral surface of DV1, the ACDL bifurcates anteriorly, with the dorsal branch extending almost horizontally, and fading anteriorly close to the CPRL, and the ventral branch connecting to the centrum, anterodorsally to the pleurocoel. Similarly, the right ACDL also bifurcates towards the lateral CPRL, however, because the diapophysis is elevated, the ventral branch of the ACDL is oriented almost vertically and connects to the anterodorsal part of the centrum. The dorsal branch of the ACDL extends anteroventrally from the diapophysis and curves anteriorly at about halfway along its length before it disappears close to the CPRL. In DV2, bifurcating ACDLs are also present, but the bifurcating branches are far less prominent than in DV1. On the left side, the ACDL originates at the ventral surface of the diapophysis, approximately at midlength of the transverse process. From here, it extends medially towards the neural arch, and curves anteroventrally, where the ventral branch meets the CPRL at the anterodorsal edge of the centrum. The bifurcation occurs in a similar position as in DV1, whereby a dorsal branch of the ACDL originates close to the CPRL, is oriented anterodorsally, and nearly connects to the CPRL, but disappears just posterior to the CPRL. The right ACDL is oriented nearly vertically, bifurcates ventrally, with a weakly developed branch extending anteromedially, and a more strongly developed branch continuing in the ventral direction of the dorsal portion of the ACDL. In DV3, no bifurcation of the ACDL is present. The left ACDL is oriented dorsoventrally from the transverse process towards the anterodorsal edge of the centrum. However, due to compression, the lamina projects posterolaterally. The right ACDL is only partially preserved, preserving only the part proximal to the centrum, which is also oriented dorsoventrally, with the dorsal part reconstructed in the mount. The ACDL fuses at the dorsal edge of the centrum, just posterodorsally to the flattened parapophysis. The PCDLs of all three vertebrae differ little on the right lateral side, as they are all oriented diagonally dorsoventrally from the diapophysis towards the posterodorsal edge of the centrum. The dorsal-most part of the right PCDL in DV3, however, is reconstructed. The left PCDLs are different, due to the way this side is compressed. In DV1, the left PCDL is oriented almost horizontally. It lacks the proximal part that connects to the diapophysis, and extends

to the posterodorsal edge of the centrum. In DV2, the left PCDL is slightly more vertical from the centrum towards the diapophysis, but the lamina curves lateroventrally, and ends posterior to the tip of the transverse process. In DV3, the left PCDL is similar to the right, but the proximal end towards the diapophysis is mediolaterally wider. The left PRDL of DV1 is reconstructed. The right PRDL is preserved, and has a roughened lateral side close to the prezygapophysis. In DV2, both PRDLs are preserved and show a roughened lateral aspect. The left PRDL of DV3 is preserved, but the lateral edge is damaged. Only the anterior-most part of the right PRDL is preserved, with the posterior part fully reconstructed. Neither of the PRDLs show similarly distinct rugose areas on the lamina as DV1 and DV2, but some evidence of rugosities is still present. From the diapophyses in DV1, PODLs project posterodorsally towards the postzygapophyses, which connect to the anterior margins of the postzygapophyseal articular facets. In DV2, the left PODL connects from the posterior margin of the diapophysis to the anterior margin of the postzygapophysis and is less posterodorsally inclined compared to the PODLs of DV1. The entire right PODL is reconstructed and connects incorrectly to the middle of the reconstructed right SPOL. In DV3, the left PODL is oriented mostly posteromedially, but as the postzygapophysis is located above the diapophysis, the PODL is also projecting dorsally, which is caused by the dorsally displaced lateral edge of the postzygapophysis. The right PODL is reconstructed. Infradiapophyseal foramina, as also seen in *Giraffatitan brancai* (Janensch, 1950; Taylor, 2009), are present in all anterior dorsal vertebrae, deepening in more posterior elements; these are mainly oval in outline.

The metapophyses in the anterior dorsal vertebrae become less 'wing-like' along the series, and instead become more straight, relatively vertical projections, which are V-shaped in anterior view, especially in DV3, although they do not diverge as widely as seen in *Apatosaurus* (Gilmore, 1936). The metapophyses converge throughout the posterior cervical and anterior dorsal vertebrae, eventually to fully fuse in the middle dorsal vertebrae. However, distance between the spine apices increases in DV2 onwards, becoming more V-like. This distance, however, is influenced by the poor preservation of more posterior elements, whereby all dorsal vertebrae with bifurcating neural spines from DV2 onwards lack one or both metapophyses. Therefore, the increasing distance between the spine apices of DV2-4 is an arti-

fact of the reconstructed metapophyses, which exaggerates this distance. There is evidence in DV4, which preserves the bases of the metapophyses, that a V-shape is the correct shape for DV2 and DV3, but it cannot be ruled out that the neural spine tips become nearly parallel to each other. In lateral view, the metapophyses of DV1-3 are all slightly inclined posteriorly compared to the horizontal long axes of the centra. Medially, the metapophyses of DV1 have a rough surface, with small, obliquely oriented ridge-like structures, whereas the medial surface of the metapophyses of DV3 is smoother. The medial surface of the metapophyses of DV2 is relatively smooth, with some smaller ridges and cracks at the posteromedial side of the metapophysis, but this is also caused by the fact that most of the right metapophysis is overlain with acrylic resin, and is mostly reconstructed. However, the ridges in DV1, and on the left metapophysis in DV2, seem to be the result of compression of the metapophyses, and not true ridges as seen in the cervical vertebrae, or as seen in *A. ajax* (Marsh, 1877; but see Tschopp et al., 2015a, figure 60C). The SPRLs in all three vertebrae mostly project anteriorly/anterolaterally from the spine apex to the prezygapophyses, terminating posterior to the prezygapophyseal rami. The SPRLs in DV1 are both mostly preserved, except for part of the left SPRL close to the prezygapophysis. In DV2, most of the left SPRL is preserved, only missing the dorsal-most part on the metapophysis, and a small part of the SPRL adjacent to the median tubercle. For the right SPRL, only the dorsal-most part is not preserved. Most of the SPRLs of DV3 are reconstructed. As aforementioned, the ventral half of the left SPRL has moved from the prezygapophysis to attach in between the prezygapophysis and the diapophysis. Because most of the left metapophysis is not preserved, the dorsal half of the left SPRL is also missing. From the right SPRL, only the section on the preserved part of the metapophysis is preserved, fading dorsally near the apex of the neural spine. Most of the SPOLs of all three vertebrae are not preserved. Only DV1 preserves parts of both SPOLs. The left SPOL lacks the dorsal third of the lamina, reconstructed for mounting purposes. The right SPOL lacks most of the ventral half of the lamina, except its connection to the dorsal margin of the postzygapophysis. In DV2, only the ventral-most part of the left SPOL is preserved. In DV3, only the dorsal half on the posterior surface of the neural spine is preserved. The left SDF of DV1 bears no accessory lamina. The dorsal part of the left SDF is reinforced and partially recon-

structed, especially the dorsal part towards the neural spine apex. However, based on the preparation pictures provided by the SMA, the left metapophysis including the SDF does have the correct outline, indicating that most of the reconstructive work was aimed at strengthening the metapophysis to prevent further breakage. This becomes more evident based on the right SDF, which bears a more rounded spine apex, or cup of the neural spine sensu Bonaparte and Mateus (1999). Ventral to this dorsally rounded apex, a smaller dorsoventral coel is present on the lateral surface, posteriorly to the right SPRL. Medial to the PODL, an accessory lamina is present on the SDF, likely reaching the SPOL dorsally, and probably the posterior margin of the dorsoventral coel. The main reason for this dubious assignment is the incompleteness of the right SPOL, which is partly covered in acrylic resin, obscuring whether the lamina reaches the SPOL, and whether it is part of the subcircular margin of the coel. In DV2, only the left SDF is preserved, with a short (4 cm) horizontally oriented accessory lamina present on the dorsal surface of the diapophyseal facet. Only the anterior part of the right metapophysis was preserved, which was laterally damaged. Therefore, laterally, the entire metapophysis was reconstructed, whereas medially, some of the bone is still present. Only the ventral part of the postzygapophysis and CPOL are preserved on this side. This is also true for DV3, where the left metapophysis is mostly reconstructed, preserving only the ventral part, anterior to the postzygapophysis. Two accessory laminae are present in the left SDF of DV3. The first is similar to the accessory lamina in DV2, but it connects anteriorly to the displaced SPRL. A second accessory lamina is present more medially, anterior to the postzygapophysis and posterior to the displaced SPRL. This lamina is oriented obliquely. Dorsally, the lamina originates posteromedially to the displaced SPRL. It extends posteroventrally, but also laterally, giving it its oblique orientation, and fuses 4 cm anteriorly to the PODL with the SDF. In contrast to the left side, the right side DV3 only preserves the top half of the metapophysis. Unlike what occurs in *Diplodocus carnegii*, the cup of the neural spine does not bear a sub-horizontal SPOL ventrally. Instead, the SPDL reaches the spine apex, thus no true cup is seen on the lateral surface of the neural spine apex. The presence of distinct SPDLs thus occurs earlier in the dorsal vertebrae compared to *D. carnegii* (Hatcher, 1901, plate VIII). A median tubercle is present in DV1 and DV2 (not preserved in DV3),

with a rugose PRSL in DV1 on the anterodorsal surface of the tubercle. This lamina cannot be assessed in DV2 and DV3 due to the preservation of the tubercle, but some weak rugosity marks the ventral base of the median tubercle of DV2, which may represent the PRSL. Laterally adjacent to the median tubercle, as aforementioned, two accessory laminae occur in DV1, as well as remnants of these laminae in DV2. In DV1, these laminae disappear dorsally halfway in between the medial base of the TPRL and the dorsal edge of the median tubercle. In DV2, the exact limits of the laminae are difficult to elucidate, due to the poor preservation of the median tubercle.

The postzygapophyses of DV1 are laterally inclined. The postzygapophyseal facets of DV2 are more horizontally oriented, although the right postzygapophysis is poorly preserved. In DV3, the posterior side is poorly preserved. Only the left lateral postzygapophysis is preserved, missing the dorsal part. However, based on the position of the postzygapophysis, both postzygapophyses are displaced medially compared to the postzygapophyses of DV1 and DV2. Two singular CPOLs originate on the ventral side of the postzygapophyses in DV1, and project ventrally towards the centrum. In DV2, vertically oriented CPOLs are present on each side, which bifurcate ventrally, creating two small fossae (CPOL-f) between the branches. In DV3, the CPOLs are broad and pillar-like, and less laminar in structure than in DV1 and DV2. Medially to the CPOLs, the paired TPOL originate from the postzygapophyses in DV1. The left half of the TPOL is broken ventrally and therefore does not fuse with the right half of the TPOL dorsal to the neural canal. In DV2, both halves of the TPOL are oriented ventromedially. However, the ventral part of both halves is not preserved. Therefore, both halves do not meet dorsal to the neural canal, which causes the neural arch to have an 'open' appearance in posterior view. Additionally, the ventral part, where the TPOL would meet, is damaged, opening the dorsal side of the neural canal. In DV3, a TPOL is present medially, which connects to a laminar structure, which runs ventrally onto the neural arch, and terminates dorsal to the neural canal. This laminar structure is dorsally wider, but broken, and very likely represents the first hyposphene in the dorsal series, which is supported by a lamina from below (sTPOL sensu Carballido and Sander, 2014). The neural canals in DV1 and DV2 are subcircular in outline. In DV3, the neural canal is dorsoventrally compressed, but is, as is that of DV1 and DV2, subcircular.

Mid-Dorsal Vertebrae (DV4-6; Figures 11–13, Table 2)

Preservation. DV6-9 were all part of a single block, which was partially prepared at the SMA and partially documented photographically. Therefore, DV6, as well as DV7-9 below, are partially described based on these photographs, which were primarily used as a control to elucidate the reconstructed parts from the real bone.

Centrum morphology. The centra of DV4-6 are opisthocoelous, but the anterior condyle and the posterior cotyle become gradually less convex and concave, respectively, along the series. The ventral surfaces are all smooth, apart from cracks caused by the deformation of the vertebrae. The centra are still concave anteroposteriorly and deformed in a similar orientation as the previous vertebrae. Therefore, the posterior articular surfaces are not circular, but more elliptical, with the long axis diagonally oriented, from the right dorsolateral to the left ventrolateral side. This deformation becomes less prominent in DV5 and DV6. Large portions of the anterior surfaces of the condyles are covered in acrylic resin for support, and partly for reconstruction, which is most evident in DV6. As do DV1-3, all mid-dorsal vertebrae bear pleurocoels, however, DV4 is the first dorsal vertebra wherein a true dorsoventral bony strut is present, which separates the pore into chambers. The left and right pleurocoels in DV4 are oval, although the left is close to being circular, and the bony struts are roughly vertical structures in the middle of the pores. In DV5, likely due to compression, the pleurocoels are subtriangular. Bony struts are present, but the right strut is reconstructed. Similar pleurocoels can be found in DV6, where the right pleurocoel is compressed dorsoventrally, flattening the triangular shape of the pore. Bony struts are present, but the left strut is partially reconstructed.

Neural arch morphology. The prezygapophyses of DV4 and DV6 are entirely reconstructed. In DV5, the ventral part of the right prezygapophysis is preserved, but the entire left prezygapophysis is reconstructed. Only the ventral portions of the CPRLs in DV4 and DV6 are preserved. In DV5, both CPRLs no longer directly connect to the prezygapophysis, but connect anteroventrally to the parapophysis (thus becoming an anterior centroparapophyseal lamina - ACPL). This would be similar in DV6.

The parapophyses in DV4 are located in between the centrum and the prezygapophyses at the anterolateral side of the vertebra. The left parapophysis consists of a subcircular bony projection which is heavily deformed. On the right side, the parapophysis is not preserved, but the breakage surface is, which appears to be at the same height as the left parapophysis. DV5 has a relatively well-preserved parapophysis on the right side. The parapophysis is located just ventral to the prezygapophysis on the anterolateral side of the neural arch, and has multiple laminae connected to it. On the left side, the parapophysis is mostly broken off. The lack of a distinct parapophysis results in the appearance of a long 'lamina', which extends from the anterodorsal side of the centrum towards the ventral side of the left transverse process. In the middle of this 'lamina', the breakage surface of the parapophysis is visible. In DV6, the parapophyses would be expected to be located closer to the prezygapophyses. However, the preservation of the anterior part of this vertebra is poor; there are no signs of parapophyses. In the mount, no parapophyses are reconstructed. PCPLs cannot be identified in DV4, due to the poor preservation of the parapophyses and the surrounding surface. A prezygoparapophyseal lamina (PRPL) connects the left parapophysis of DV4 to the prezygapophysis, but the middle part of this lamina is reconstructed. On the right side, a gap is present between the prezygapophysis and parapophysis, wherein the PRPL is not preserved due to weathering, and wherein the PRCDF is quite damaged. Almost entire paradiapophyseal laminae (PPDLs) are preserved, with only their lateral ends reconstructed. On the posterior side of the right parapophysis of DV5, two laminae are present. One of the laminae is a PPDL, which extends posterodorsally from the parapophysis. The second lamina is oriented anteroposteriorly, posterior to the parapophysis, and ends just anterior to the PCDL, and can be identified as the posterior centroparapophyseal lamina (PCPL), which is also seen in this orientation in e.g., *Supersaurus* BYU 725-9044 (Jensen, 1985, p. 698). A PRPL connects to the ventral surface of the prezygapophysis and the anterodorsal surface of the parapophysis. On the left side, ventral to the parapophyseal breakage surface, a short, posteroventrally oriented laminar structure is preserved, which probably represents the PCPL. Two laminae connect the breakage surface of the parapophysis to the ventral side of the prezygapophysis. The dorsal lamina of the two is oriented nearly horizontally, whereas the ventral lamina is oriented ventrolaterally. They are not double PCPLs, as seen in DV9 of *Diplodocus carnegii* (Hatcher, 1901, plates VII and VIII) as the parapophysis is still separate from the prezygapophy-
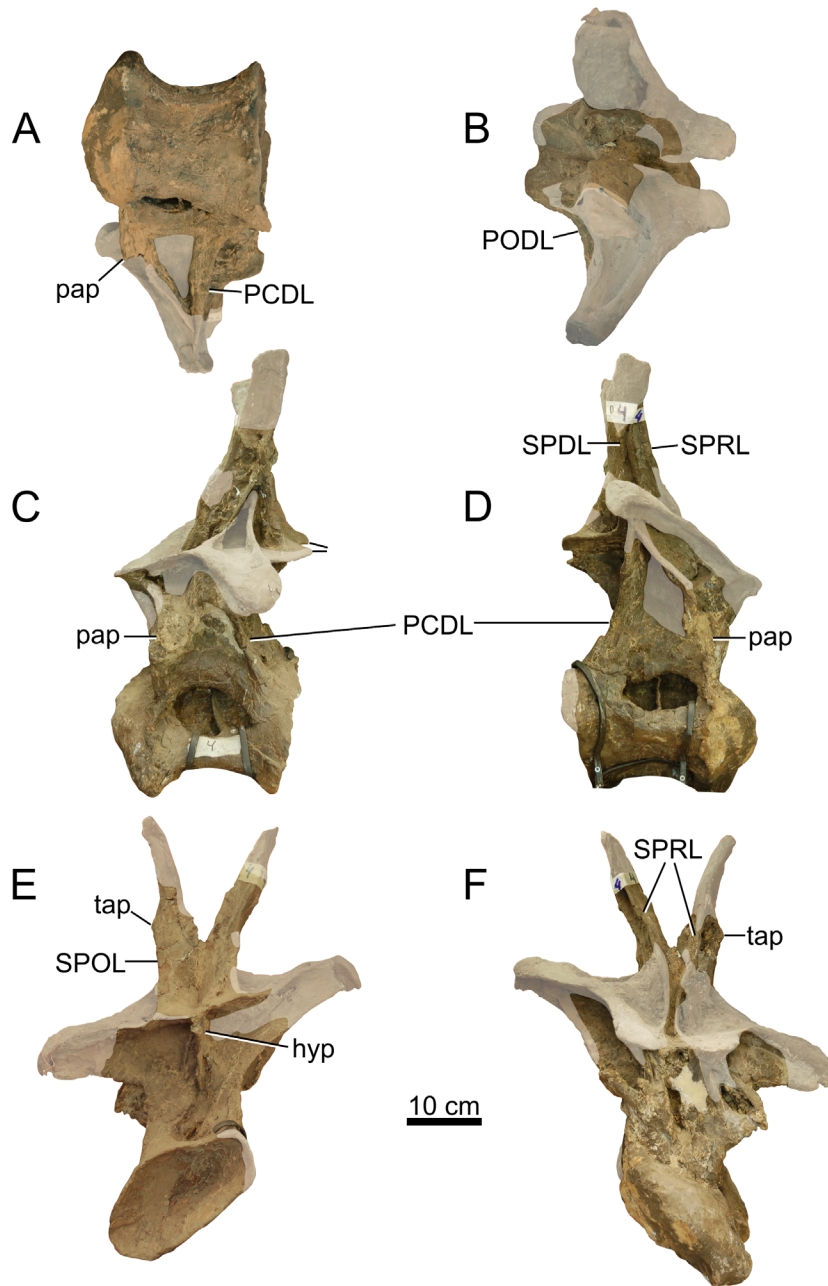
FIGURE 11. Dorsal vertebra 4 of Ardetosaurus viator MAB011899. DV4 is shown in A) ventral, B) dorsal, C) left lateral, D) right lateral, E) posterior, and F) anterior view. White shaded areas indicate reconstructed parts. Abbreviations: hyp, hyposphene; pap, parapophysis; PCDL, posterior centrodiapophyseal lamina; PODL, postzygodiapophyseal lamina; SPDL, spinodiapophyseal lamina; SPOL, spinopostzygapophyseal lamina; SPRL, spinoprezygapophyseal lamina; tap, triangular aliform process.

sis, whereas in DV9 of *D. carnegii*, the parapophysis is laterally adjacent to the prezygapophysis. Instead, the dorsal lamina connecting to the prezygapophysis of DV4 of MAB011899 is short and dorsoventrally thin but does connect to the breakage surface where the parapophysis was located. The ventral lamina is directed more ventrolaterally, and connects to the ACPL, but both laminae connect to the anteromedial part of the parapophysis breakage surface. The dorsal lamina might therefore be an accessory lamina, whereas the ventral lamina can be identified as the PRPL. Interestingly, this PRPL appears to bifurcate ventrolaterally, showing a very small fossa in between the branches. This does not occur on the right side, but this might be due to preservation. Due to the
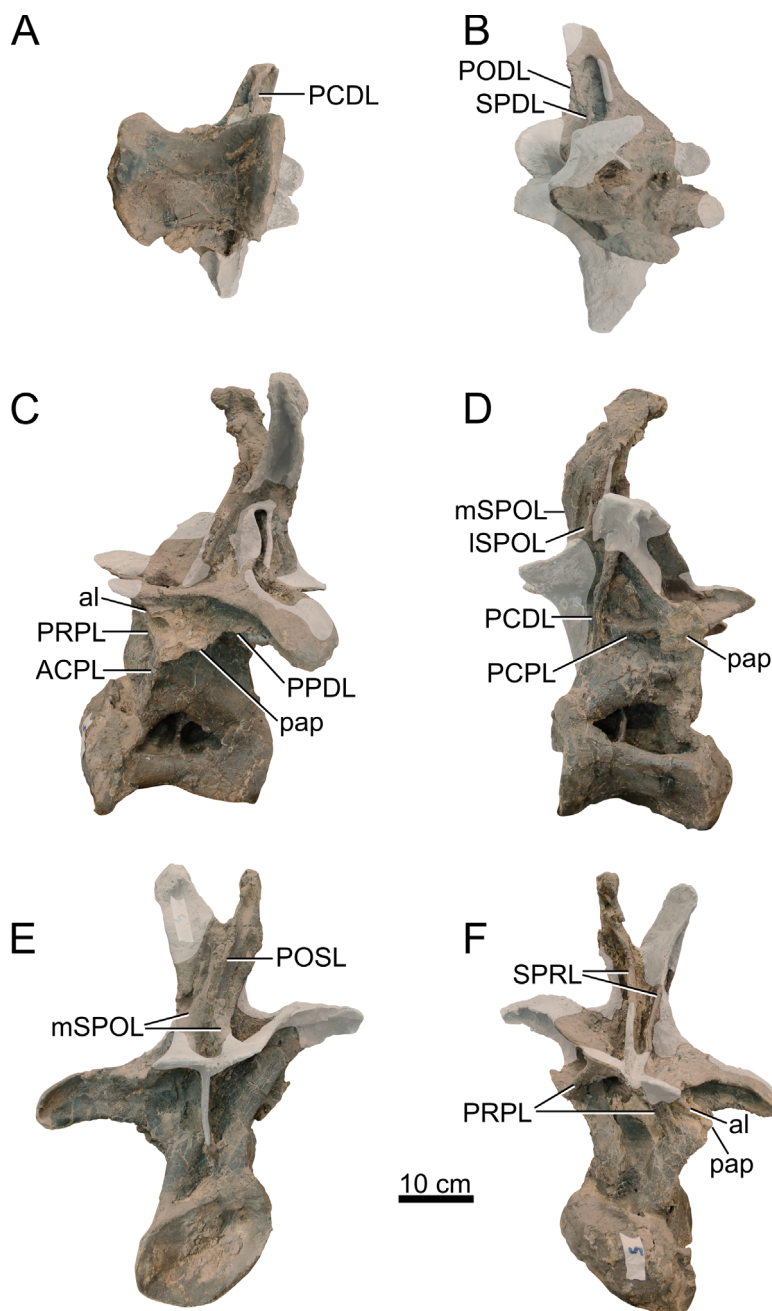
FIGURE 12. Dorsal vertebra 5 of *Ardetosaurus viator* MAB011899. DV5 is shown in A) ventral, B) dorsal, C) left lateral, D) right lateral, E) posterior, and F) anterior view. Note the complex morphology of the left parapophysis and the surrounding laminae. White shaded areas indicate reconstructed parts. Abbreviations: ACPL, anterior centroparapophyseal lamina; al, accessory lamina; mSPOL, medial spinopostzygapophyseal lamina; lSPOL, lateral spinopostzygapophyseal lamina; pap, parapophysis; PCDL, posterior centrodiapophyseal lamina; PCPL. posterior centroparapophyseal lamina; PODL, postzygodiapophyseal lamina; PPDL, paradiapophyseal lamina; PRPL, prezgyoparapophyseal lamina; SPDL, spinodiapophyseal lamina; SPRL, spinoprezygapophyseal lamina.

preservation of the anterior side of DV6, all laminae related to the parapophyses (PCPL, PRPL, PPDL) are not preserved.

The transverse processes of all mid-dorsal vertebrae are poorly preserved. In DV4, only the ventromedial part of the left processes is pre-served. The remaining parts of the processes are entirely reconstructed. In DV5, the left transverse process has a reconstructed dorsolateral tip. The anterior and anterolateral side of the tip is not reconstructed and shows that the lateral-most part of the transverse process was oriented lateroven-
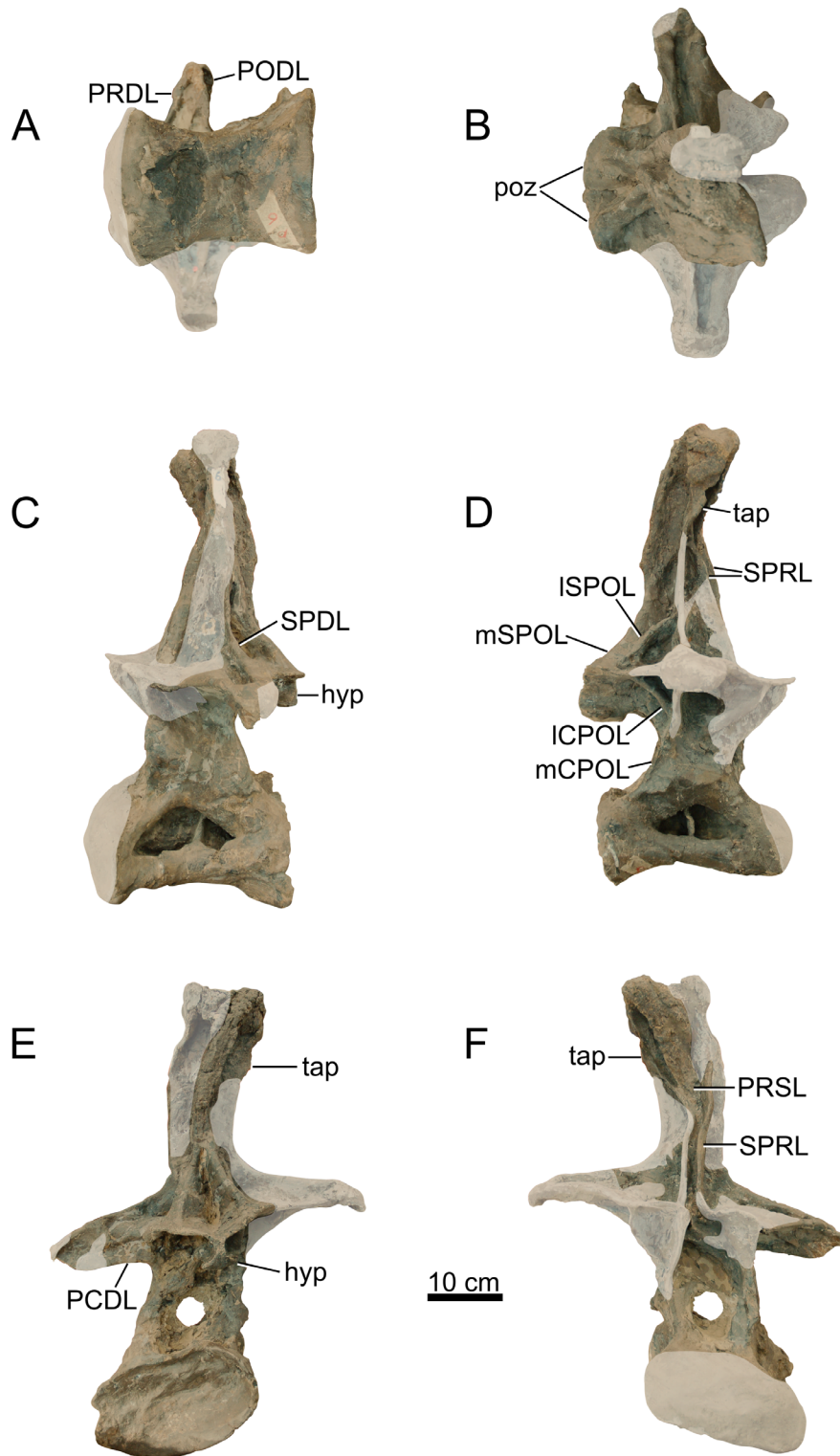
FIGURE 13. Dorsal vertebra 6 of *Ardetosaurus viator* MAB011899. DV6 is shown in A) ventral, B) dorsal, C) left lateral, D) right lateral, E) posterior, and F) anterior view. White shaded areas indicate reconstructed parts. Abbreviations: hyp, hyposphene; mCPOL, medial centropostzygapophyseal lamina; mSPOL, medial spinopostzygapophyseal lamina; lCPOL, lateral centropostzygapophyseal lamina; lSPOL, lateral spinopostzygapophyseal lamina; PCDL, posterior centrodiapophyseal lamina; PODL, postzygodiapophyseal lamina; poz, postzygapophysis; PRDL, prezygodiapophyseal lamina; PRSL, prespinal lamina; SPDL, spinodiapophyseal lamina; SPRL, spinoprezygapophyseal lamina; tap, triangular aliform process.

trally. In DV6, the left transverse process is partially preserved, missing a posterolateral and the medial section towards the anterolateral surface of the neural spine. A feature reconstructed in DV4, but present in DV5 and DV6, are mediolaterally elongated fossae on the dorsal surface of the transverse processes. The anterior rim of this fossa in DV5 is reconstructed on the left process, which transitions into the SPDL. The posterior rim appears to form a lamina medially as well, but because so little is preserved of this lamina, this might have converged towards the SPDL. In DV6, the posterior rim forms the SPDL. In DV4, distinct PCDLs are preserved, which are almost complete, as only the lateral parts which attach to the transverse processes are missing. The left PCDL of DV5 is complete, extending to the tip of the transverse processes. The right PCDL lacks the lateral part on the ventral surface of the transverse process. Only the left PCDL of DV6 is preserved, forming a right angle with the transverse process. The right PCDL is entirely reconstructed. The PRDLs of DV4 are entirely reconstructed. In DV5, the left PRDL is complete, connecting to the posterolateral margin of the prezygapophyses and the anterior surface of the lateral tip of the transverse process. Only the middle part of the right PRDL is preserved. Only the left PRDL is preserved of DV6, lacking only the end towards the prezygapophysis. Both PODLs of DV4 are reconstructed, as well as the right PODLs of DV5 and DV6. The left PODL of DV4, however, was originally present based on preparation pictures of the Oertijdmuseum, but because of the crumbly nature, most of this lamina is supported and reconstructed with acrylic resin. The left PODLs of DV5 and DV6 connect to the lateral margin of the postzygapophyses, extending to the posterior surface of the transverse processes, fusing at midheight of the process. Well-delimited infradiapophyseal foramina are present in DV6. In DV4 and DV5, they are smaller, and in DV4, filled in with acrylic resin to support the vertebra.

The metapophyses of DV4 are distinctly V-shaped. Part of the left metapophysis is preserved, but the apex is fully reconstructed. Similar parts are preserved of the right metapophysis. Interestingly, photographs made by the Oertijdmuseum during preparations show that at least the left apex was preserved originally. However, the apex appears very brittle and was likely lost during preparation. It was subcircular in lateral view, and distinctly rugose. The medial side, where the median tubercle is located, is original bone, and therefore the metapophyses were correctly reconstructed as

separate, as there are no indications yet of a reduced bifurcation of the spine creating a 'shallowly bifid' or 'notched' appearance sensu Wedel and Taylor (2013). The metapophyses of DV5 are shallowly bifid. When separate, the metapophyses are distinctly V-shaped, although the preserved left apex is anteriorly inclined, unlike those of the previous vertebrae. Because this is the only vertebra that shows this feature, and the apex appears brittle, this inclination is likely due to deformation. In DV6, the metapophyses have fused fully, resulting in a vertical neural spine. In DV4, the SPRL and SPDL are distinct from each other, unlike the morphology seen in DV3 where laminar capture sensu Wilson (2012) in still ongoing. However, both the SPRLs and SPDLs are poorly preserved. Only parts on the base of the metapophyses of the SPRLs of DV4 are preserved. At midheight on the metapophyses parts of the SPDLs are preserved. In DV5, the left SPRL has a similar preservation to SPRLs in DV4. The dorsal part of the right SPRL is preserved. Most of the original left SPRL of DV6 is preserved, missing only parts ventrally, and to a limited extent dorsally. Only the dorsal half of the right SPRL is preserved, but both SPRLs do not join dorsally to form a single PRSL. Instead, the PRSL originates medially to the SPRLs in the dorsal half of the neural spine. The right SPRL is oriented dorsolaterally near the neural spine apex, extending into the prezygapophyseal spinodiapophyseal fossa (PRSDF). The left SPDL of DV6 extends dorsally to approximately the midheight of the neural spine. The dorsal half of the lamina is reconstructed. On the right side, most of the SPDL is reconstructed, except the dorsal-most part of the lamina. The SPOLs in DV4 connect ventrally to the dorsal margin of the postzygapophyses, and dorsolaterally to the SPDLs, although the latter connection is only preserved on the left side. They meet on the posterolateral side of the metapophysis, roughly at midheight of the metapophysis, and form a triangular aliform process. DV5 is the first dorsal vertebra to have a clear distinction between the lateral and medial SPOLs. The bifurcation of the SPOL occurs just dorsal to the postzygapophyses, whereby the mSPOLs converge dorsally to form a rugose POSL. The lSPOLs fuse laterally with the reconstructed SPDLs. On the posterior surface of the spine of DV6, the mSPOLs meet at approximately one-third of the neural spine height, fuse, and form the POSL, which is distinctly rugose. In the SPOFs, lSPOLs are present which meet the SPDLs at approximately midheight, which would form lateral spinal laminae. Dorsal to the

ISPOL, in the right SPOF, an accessory lamina is present with the same overall orientation as the ISPOL. Although most of the right SPDL of DV6 is reconstructed, a triangular aliform is preserved, and appears intact. The aliform process, however, is, due to deformation, folded anteriorly. Dorsal to the aliform process, the lateral surface of the neural spine tip bears the neural spine cup, which in DV6, as well as more posterior vertebrae in MAB011899, is a triangular, dorsally widening bony sheet which is slightly rugose. These triangular, rugose sheets are common in diplodocids, as they are present in *Diplodocus* (Hatcher, 1901; Herne and Lucas, 2006; Lucas et al., 2006), *Barosaurus* (Lull, 1919; McIntosh, 2005), *Apatosaurus* (Gilmore, 1936; Upchurch et al., 2004b), *Brontosaurus* (Ostrom and McIntosh, 1966), and *Supersaurus* (Jensen, 1985; Bonaparte and Mateus, 1999). The spine tip is squared dorsally, similar to the posterior-most dorsal vertebra in *Diplodocus carnegii* (Hatcher, 1901, plate VIII), but the left side is reconstructed, and the medial 'notch' shows some breakage, which might indicate that - similar to more posterior vertebrae - the dorsal tip was rounded, and not 'notched' sensu Wedel and Taylor (2013).

Most of the right postzygapophysis of DV4 is preserved, and unlike more posterior vertebrae wherein the articular facets are inclined laterally, the facet is oriented nearly horizontally. The left postzygapophysis is partially reconstructed, including the lateral rim and the section where the PODL attaches to the postzygapophysis. Only the lateral rim of the left postzygapophysis of DV5 is preserved, whereas the remaining bone of the postzygapophyses and the hyposphene are reconstructed using acrylic resin. Only a small part of the ventrally supporting lamina is preserved. In DV6, both postzygapophyses are preserved and are oriented nearly horizontally, inclined laterally similar to DV7 of *Diplodocus* (Hatcher, 1901, plate VIII) or DV8 of *Barosaurus* (McIntosh, 2005, figure 2.5H). The hyposphene of DV4 is partially broken but appears to be too wide to constitute a laminar hyposphene. This is further supported by more posterior vertebrae, which contain a rhomboid hyposphene. The hyposphene in DV4 is ventrally supported by a single dorsoventral lamina (sTPOL sensu Carballido and Sander, 2014), which projects posteriorly in lateral view. DV6, in contrast to DV4 and DV5, preserves a complete hyposphene. The hyposphene is rhomboid, similar in morphology to the hyposphene of DV7 in *Diplodocus carnegii* (Hatcher, 1901, plate VIII). No ventrally

supporting lamina is present, but this part of the neural arch is severely damaged. In DV4 and DV5 the CPOLs are absent. In DV4, lateral to the lamina supporting the hyposphene, two additional laminae extend from the ventral base of the postzygapophyses towards the centrum, which fade ventrally, not extending further ventrally than the supporting lamina of the hyposphene. These supporting laminae could be the presence of mCPOLs in the dorsal series. In DV5, no evidence is present for lateral or mCPOLs, which is also hindered by the poor preservation of this part of the neural arch. The CPOLs are thus more columnar in morphology, indistinguishable from the neural arch. In DV6, the CPOLs are distinct and divided, with lateral branches connecting to the anteroventral side of the postzygapophyses and the medial side of the PCDLs, approximately at the same height as where the PCDLs form a right angle with the transverse processes. The medial branches of the CPOLs connect ventrally to the centrum and dorsolaterally to the neural canal. Dorsally, the mCPOLs connect to the anteroventral margin of the postzygapophyses, medial to the lCPOLs. This is, however, only clear on the left side, as the right side does not preserve the dorsal part of the medial CPOL, which thus appears to connect to the anteroventral part of the hyposphene. The original shape of the neural canal of DV4 is difficult to elucidate, as both anteriorly and posteriorly, the canal is damaged and deformed, and partially infilled with sediment. It was likely subcircular. The neural canal and the surrounding bone of DV5 were damaged, and foam was added internally to stabilize the vertebra, which now obscures the shape and position of the neural canal. The neural canal of DV6 is circular, but the bone surrounding the canal is poorly preserved.

Posterior Dorsal Vertebrae (DV7-10; Figures 14–17, Table 2)

The neural arch and spine morphology of DV7-9 can be described in reasonable detail, aided by the comparisons with the original photographs from the SMA. This is not the case for DV10, because the vertebra was part of the block containing the sacrum, and due to the severe anteroposterior compression of the sacral vertebrae, DV10 is very poorly preserved. It will therefore be discussed separately, mainly based on photographs of the SMA and early photographs from the Oertijdmuseum, because in these photographs the vertebra was yet to undergo reconstructions.
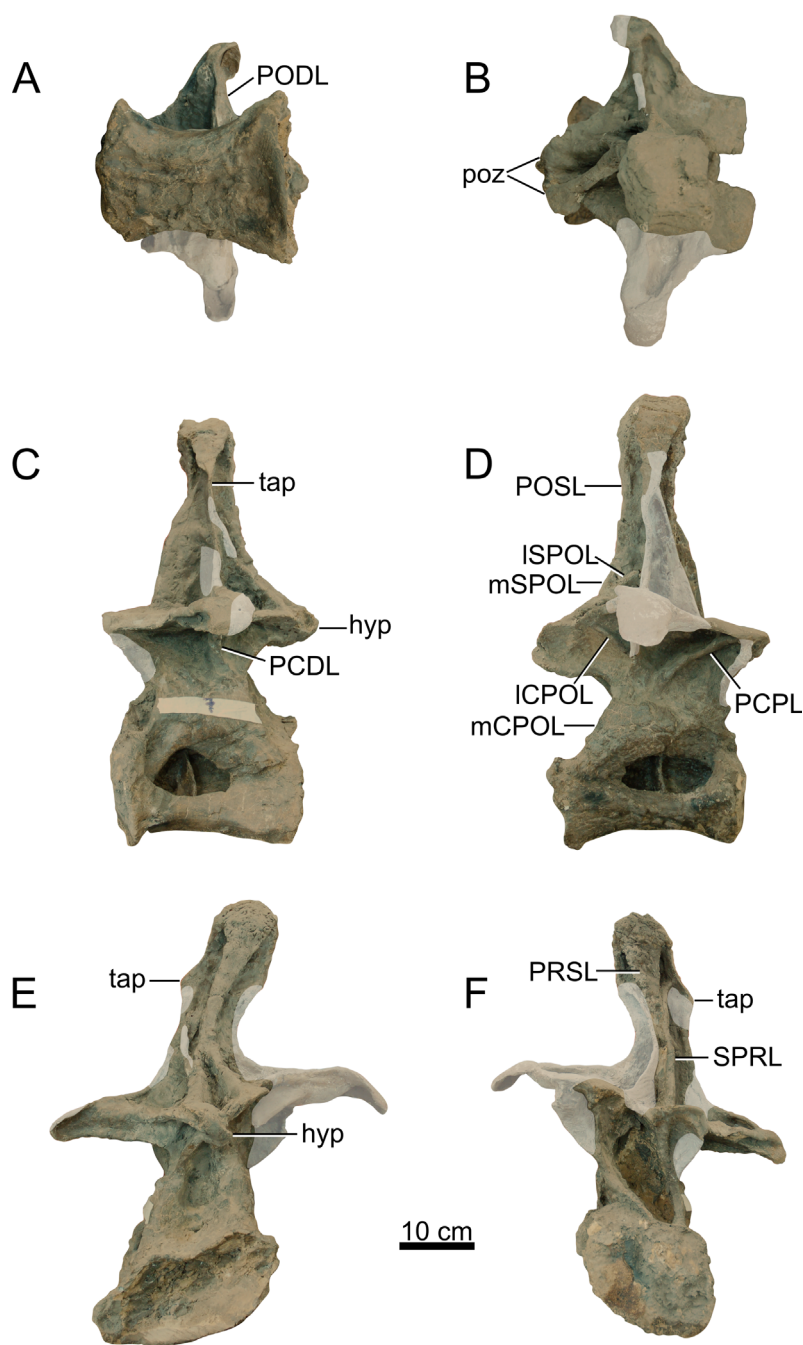
FIGURE 14. Dorsal vertebra 7 of *Ardetosaurus viator* MAB011899. DV7 is shown in A) ventral, B) dorsal, C) left lateral, D) right lateral, E) posterior, and F) anterior view. White shaded areas indicate reconstructed parts. Abbreviations: hyp, hyposphene; mCPOL, medial centropostzygapophyseal lamina; mSPOL, medial spinopostzygapophyseal lamina; lCPOL, lateral centropostzygapophyseal lamina; lSPOL, lateral spinopostzygapophyseal lamina; PCDL, posterior centrodiapophyseal lamina; PCPL, posterior centroparapophyseal lamina; PODL, postzygodiapophyseal lamina; poz, postzygapophysis; PRSL, prespinal lamina; SPRL, spinoprezygapophyseal lamina; tap, triangular aliform process.

Centrum morphology. All posterior vertebral centra are slightly opisthocoelous, with a mildly convex condyle, and a concave posterior articular surface. All centra are ventrally concave in lateral view, but less so than the more anterior dorsal vertebrae.

The pleurocoels of DV7 are roughly triangular (left) and oval (right) in outline and include the dorsoventral bony struts in the middle of the coel. The right bony strut is reconstructed. The centrum of DV8 is deformed in a way that the pleurocoel on the left
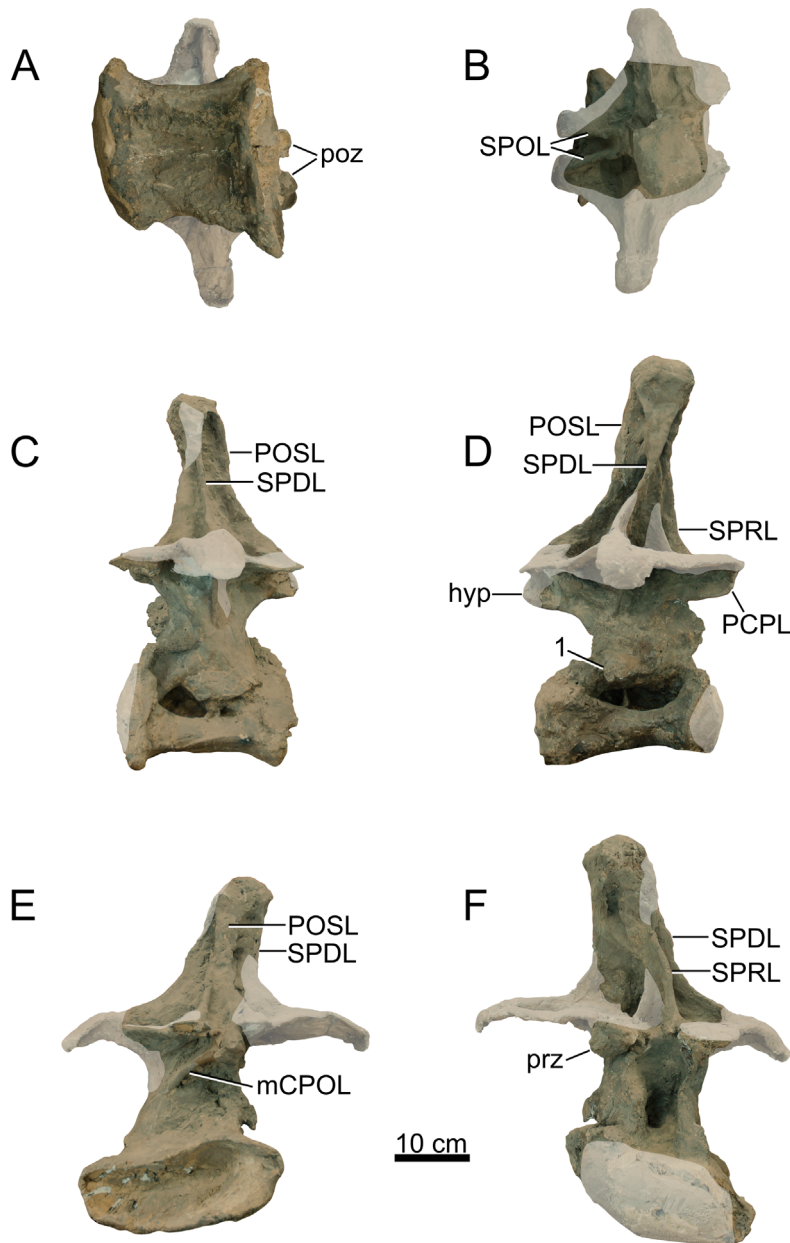
FIGURE 15. Dorsal vertebra 8 of *Ardetosaurus viator* MAB011899. DV8 is shown in A) ventral, B) dorsal, C) left lateral, D) right lateral, E) posterior, and F) anterior view. Note the attached piece of bone (1) to the lateral surface of the neural arch. White shaded areas indicate reconstructed parts. Abbreviations: hyp, hyposphene; mCPOL, medial centropostzygapophyseal lamina; PCDL, posterior centrodiapophyseal lamina; PCPL, posterior centroparapophyseal lamina; PODL, postzygodiapophyseal lamina; POSL, postspinal lamina; poz, postzygapophysis; prz, prezygapophysis; SPDL, spinodiapophyseal lamina; SPOL, spinopostzygapophyseal lamina; SPRL, spinoprezygapophyseal lamina.

side consists of two fossae; a triangular shaped anterior fossa, a thickened bony strut, and a very small posterior coel, which is roughly pentagonal shaped. On the right surface, the pleurocoel is dorsoventrally compressed, resulting in a flattened oval, in which the thin bony strut is located in the posterior half of the coel, similar to its position in the left pleurocoel. On the right side, dorsal to the

pleurocoel, a bulged, irregularly shaped piece of bone projects laterally (Figure 15), which has been attached using acrylic resin. It may potentially represent a deformed, misplaced parapophysis, but this is uncertain. In DV9, the pleurocoels are oval, with the right coel being dorsoventrally compressed. Bony struts are present and are slightly inclined posteriorly. The centrum of DV10 is mostly
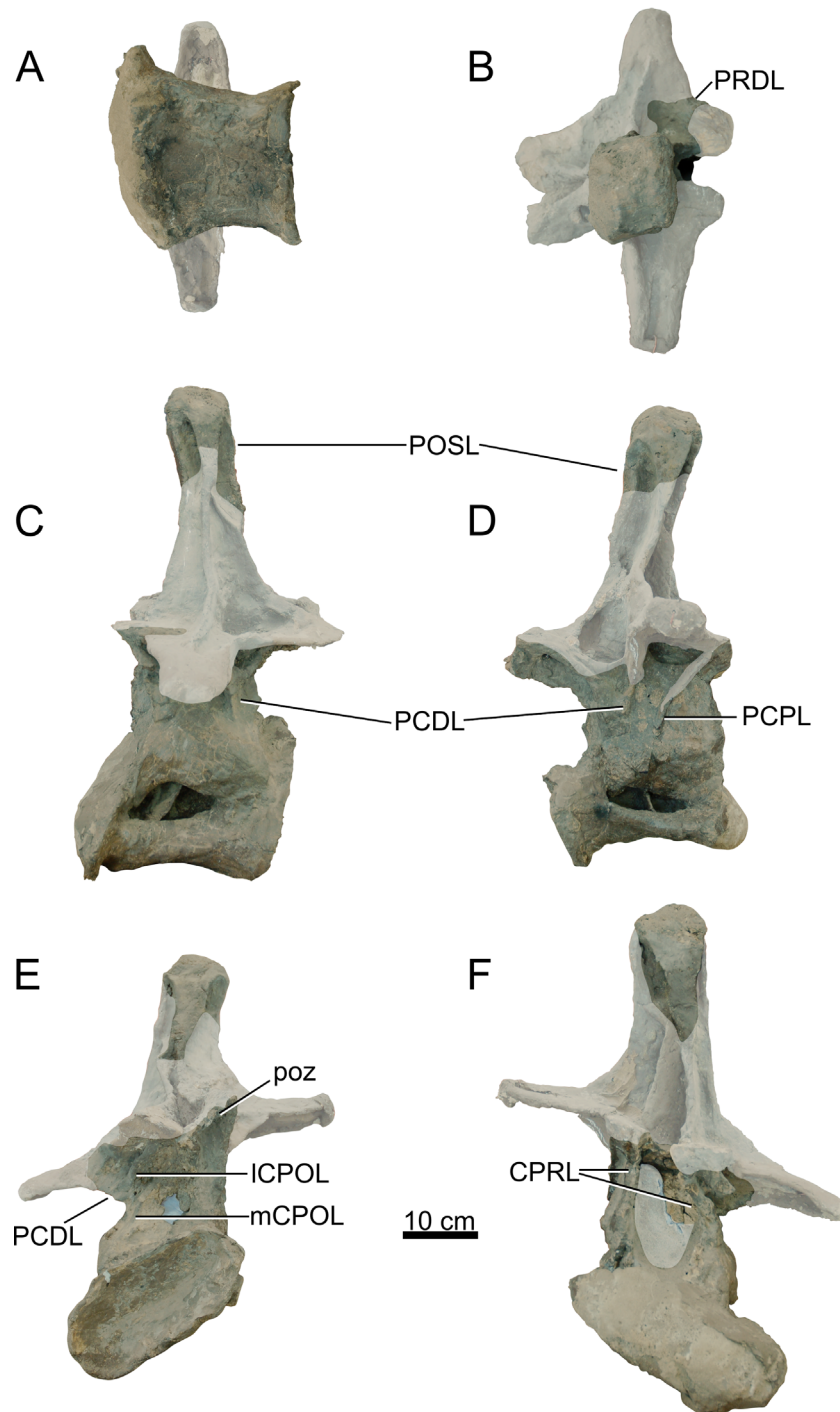
FIGURE 16. Dorsal vertebra 9 of *Ardetosaurus viator* MAB011899. DV9 is shown in A) ventral, B) dorsal, C) left lateral, D) right lateral, E) posterior, and F) anterior view. White shaded areas indicate reconstructed parts. Abbreviations: CPRL, centroprezygapophyseal lamina; mCPOL, medial centropostzygapophyseal lamina; lCPOL, lateral centropostzygapophyseal lamina; PCDL, posterior centrodiapophyseal lamina; PCPL, posterior centroparapophyseal lamina; POSL, postspinal lamina; poz, postzygapophysis.
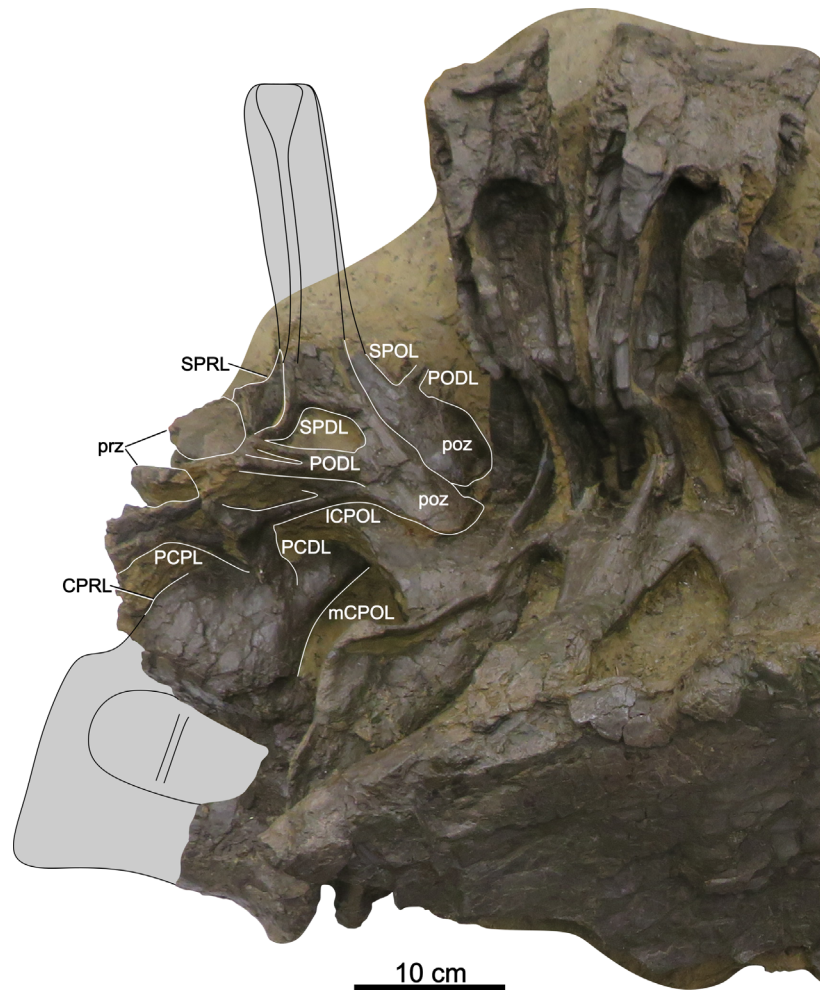
FIGURE 17. Dorsal vertebra 10 of *Ardetosaurus viator* MAB011899. Outline of DV10 is drawn on a left dorsolateral photograph of the sacrum. Photograph is courtesy of René Fraaije. Abbreviations: CPRL, centroprezygapophyseal lamina; lCPOL, lateral centropostzygapophyseal lamina; mCPOL, medial centropostzygapophyseal lamina; PCDL, posterior centrodiapophyseal lamina; PCPL, posterior centroparapophyseal lamina; prz, prezygapophysis; SPDL, spinodiapophyseal lamina; SPOL, spinopostzygapophyseal lamina; SPRL, spinoprezygapophyseal lamina.

reconstructed (see below) and is missing the anterior half and parts of the cotyle. The left pleurocoel is oval, but only the posterior half is preserved. The right pleurocoel is a dorsoventrally compressed oval. At first glance both contain dorsoventral bony struts, but both struts are in fact completely reconstructed.

Neural arch morphology. The neural arches and spines of DV7 and DV8 are relatively well preserved, with DV9 less complete. In DV7, the prezygapophyses are preserved, slightly convex dorsally, and are oriented sub-horizontally. They are ventrally supported by CPRLs, but additional lateral branches have been added using acrylic resin, so the laminae wrongly seem to bifurcate dorsally in the reconstructed vertebra. Therefore,

these additional branches are not considered here. The right prezygapophysis of DV8 is partially preserved. The articular facet is compressed, facing ventrally, and attached to a deformed PCPL. The left prezygapophysis is partially preserved; the dorsal surface is reconstructed. The left CPRL is entirely preserved, but the anterior margin of the ventral half of the lamina is pushed laterally due to shear. The right CPRL misses the dorsal half, which has broken off. The prezygapophyses of DV9 are entirely reconstructed, but the supporting CPRLs are preserved.

In DV7, the parapophyses appear to have broken off, just ventral to the prezygapophyses. In DV8 and DV9 the parapophyses appear not to have been preserved, supported by the SMA pho-

TABLE 2. Measurements of the dorsal vertebrae of *Ardetosaurus viator* MAB011899 (in mm).

Dimension	1	2	3	4	5	6	7	8	9
Greatest height	462		511*		568*	583*	580*	550*	535*
Centrum length	417*	360		266	255*		251*	255	257*
Pleurocoel length (left/right)	102/142	57/84	121/59*	117/101	118/123	135/122	101/113	72/118	97/103
Pleurocoel height (left/right)	53/67	20/46	47/48*	78/53	69/65	56/51	62/53	50/33	44/28
Cotyle width	159	150*	156	184	173	214	199*	214*	194*
Cotyle height	162	174*	151	118	142	150	106	136*	130*
Condyle width	176*	130*	110*	147*	186*	192*	181*	212*	201*
Condyle height	150*	151*		92*	118*	106*	142*	110*	114
Neural spine height	195*	210	234*		251	327*	302	295*	314
Centrum length minus condyle length	322/308	247/268	207*/205*	193/199	197/171	215/224	217/228	200/208	200/202
Neural arch height	153*	170*	157	170		151	151	145	129

Notes: Asterisks indicate estimates, often influenced by shear and transverse compression of the vertebrae. Centrum length includes condyle length. Neural arch height is measured from the dorsal margin of the cotyle rim vertically to an horizontal line joining the posterior-most edge of the postzygapophyses.

tographs. The laminae observed in Figures 14D and 15D are interpreted as PCPLs due to their orientation, placement, and the fact that parapophyses must have been present in vivo in all vertebrae. On the right side, DV9 only preserves the ventral-most part of the lamina. In DV8, the lamina is oriented nearly horizontally, caused by compression, and not posteroventrally as in DV7. PRPLs are not preserved. DV7, however, does preserve a PPDL on the anteroventral corner of the tip of the left transverse process, which quickly fades medially on the ventral side of the process, just posterior to the PRDL. This short PPDL and PRDL thus forms a small horizontal, tear-drop-shaped fossa on the anterior side of the process. This fossa can be identified as a prezygapophyseal paradiapophyseal fossa (PRPADF) sensu Wilson et al. (2011). This fossa occurs in many different sauropods, such as *Camarasaurus supremus* (Osborn and Mook, 1921, plate LXXI), *'Brachiosaurus' brancai* (Wilson et al., 2011, figure 10), *Rapetosaurus krausei* (Rogers, 2009, figure 16), but also in diplodocids such as *Apatosaurus louisae* (Gilmore, 1936; but see Harris, 2006, figure 1). The parapophyseal centrodiapophyseal fossae (PACDFs) in all three vertebrae are ventrally open on all sides, similar to those of *Galeamopus pabsti* (Tschopp and Mateus, 2017).

Most of the right transverse process of DV7 is reconstructed, but the left process is mostly preserved. The lateral tip of the left process is directed lateroventrally, but the lateral-most part has likely broken off sometime between the preparation at the SMA and its arrival at the Oertijdmuseum, as the photographs from the SMA show that the lateral-most tip was directed almost completely ventrally. This lateral tip is partially reconstructed on the posterodorsal side, as shown by a small borehole piercing the transverse process in this area. The medial portion of the left transverse process of DV8 is preserved, but the right process is fully reconstructed. In DV9, both transverse processes are fully reconstructed and misaligned, as the right transverse process is almost fused with the prezygapophysis. Only small, medial parts of the left process are preserved. The left PCDL of DV7 is oriented vertically, with only the ventral-most part extending posteroventrally to reach the posterodorsal side of the centrum. On the right, most of the PCDL is missing, preserving only the ventral part, which shows a similar morphology as the left PCDL. The left PCDL of DV8 is only ventrally well preserved, although the SMA photographs do show that more was present, thus it is likely that acrylic resin was put on top of the lamina, possibly for support. Similarly, only the ventral part of the right PCDL is present. PCDLs are present on both sides in DV9, but most of the right PCDL is reconstructed. A very well-delimited right POSDF is present, resembling a large foramen. However, the entire foramen is reconstructed. DV7 preserves the left PRDL. In DV8 and DV9 they are (except for a very small part halfway of the left PRDL in DV9) reconstructed. The left PODL of DV7 is horizontally

oriented, fusing with the diapophyses at midlength and the anterolateral margin of the postzygapophysis. Only the medial half of the right PODL is preserved. In DV8, only the left PODL is preserved, which was dorsally damaged; this is covered with acrylic resin. In DV9, both PODLs are reconstructed. Infradiapophyseal foramina are present in DV7-9, but due to compression, the ventral rim is not as distinct in DV7 on both sides. This, however, is prominently present on the right lateral side of DV9, and bears resemblance to the foramina in *Giraffatitan* MB.R.3822 (Janensch, 1950). In DV8 of MAB011899, the left foramen is filled in with support material, and the right side only shows a small foramen deep within the PRCDF.

The neural spines of these vertebrae are all inclined anteriorly and are roughly as long anteroposteriorly as they are wide mediolaterally. The dorsal tips of the neural spines are all dorsally rounded and rugose, unlike those of *Apatosaurus* (Gilmore, 1936) or *Diplodocus* (Hatcher, 1901), which are flat, or possess a midline cleft (notched, sensu Wedel and Taylor, 2013). Most of the neural spines of DV7 and DV8 are preserved, whereas DV9 only preserves the dorsal part of the neural spine, missing most of the ventral half. The SPRLs of DV7 and DV8 are partially reconstructed, with reconstruction more extensive in the right SPRLs. Interestingly, at the point of fusion, a lateral branch of the left SPRL extends dorsally in the PRSDF and connects to the anterior side of the SPDL in DV7. These additional laminae can also be seen in the photographs of the SMA of MAB011899, as well as in NSMT-PV 20375 (Upchurch et al., 2004b, plate 3) and NMMNH 3690 (Herne and Lucas, 2006, figure 2). In NMMNH 3690, however, the laminae are more horizontal and appear as accessory laminae instead of continuations of the SPRLs. This lamina also occurs in DV8 of MAB011899, at least in the right PRSDF (the left PRSDF is reconstructed to the point where the PRSL fuses with the SPDL). The SPRLs of DV9 are not preserved, but were likely present, similar in morphology to DV7 and DV8, and thus have been reconstructed as such. These additional laminae are not seen in DV9. The SPRLs in both DV7 and DV8 join dorsally to form a single PRSL. A PRSL is present in DV9 as well, but because most of the spine is missing, it cannot be confirmed if the SPRLs join dorsally to form the PRSL as in preceding vertebrae. The SPDLs of DV7 are largely reconstructed between the ventral- and dorsal-most portions, but the triangular bony sheets on the lateral surface of the neural spine apex are pre-

served, and also seen in the SMA photographs. The left triangular sheet is fully preserved, whereas the right sheet lacks the anteroventral part. The right triangular bony sheet of DV8 is preserved, as well as large parts of the SPDLs. DV9 only shows the dorsal portions of the triangular sheets, as the remainder of the sheet and the SPDLs are fully constructed. Both ISPOLs and mSPOLs are present in DV7. The mSPOLs converge dorsally to form a POSL, which is partially covered with acrylic resin for support reasons. The ventral halves of the ISPOLs is preserved; the left ISPOL is significantly more prominent compared to the right. Both ISPOLs fuse with the SPDLs, presumably at the same height based on their overall orientation. In DV8, the mSPOLs also converge to form a rugose POSL. Only a remnant of the left ISPOL is preserved. In DV9, only the dorsal part of the POSL is preserved. Triangular aliform processes are partially present in DV7; the ventral halves of the aliform processes are reconstructed. DV8 and DV9 do not possess aliform processes; they are also absent in DV9 and DV10 in *D. carnegii* (Hatcher, 1901, plate VIII) indicating that their absence in the posterior two to three dorsal vertebrae of MAB011899 may be real.

The postzygapophyses of DV7 are oriented roughly similarly to their orientation in DV6. The hyposphene of DV7 is rhomboid, but the lateroventral parts are compressed dorsally, resulting in a subcircular appearance. Only the ventral half of the left postzygapophysis is preserved in DV8. The hyposphene of DV8 is similar in morphology as DV7. DV9 is missing part of the posterior side of the neural arch, with major reconstructions of the laminae. Only the ventral half of the right postzygapophysis is preserved, and inclined laterally, but this is likely an artifact of both deformation and the major reconstructions. The hyposphene is damaged such that only its original position can be elucidated. DV7, like DV6, possesses divided CPOLs, with the mCPOLs attached to the anteroventral margin of the hyposphene, directly ventral to the anterior border of the postzygapophyses. The lCPOLs are oriented similarly but attach dorsally to the anterior margin of the postzygapophyses, and ventrally near where the PCDLs originate. DV8 has remnants of these lCPOLs on the left side, but this lamina is less prominent compared to DV7. A short, dorsoventral accessory lamina is present, ventromedial to the lCPOL and lateral to the mCPOL, on the left side of the vertebra. There is no evidence for this lamina on the right side of the vertebra. The same applies for DV9 on the left

side. In DV9, however, the mCPOLs are damaged, as is the bone surrounding the neural canal. lCPOLs are present in DV9, but due to major reconstructions, it is difficult to elucidate the laminae on the lateral and posterior sides of the neural arch. The neural canal shape of DV7 is not exposed, as it is still infilled with matrix. The neural canal of DV8 is rounded anteriorly, but not exposed posteriorly. In DV9, this cannot be assessed, as the arch is filled with supporting material to strengthen the arch.

DV10 neural arch. DV10, although partially preserved, was found in near-perfect articulation with the sacrum. Based on SMA and other early preparation photographs it is missing the anterior half of the vertebra. A left lateral photograph made roughly upon arrival of the sacrum at the Oertijdmuseum elucidates more morphology than any other picture or the current vertebra in the mount, due to extensive reconstruction, see Figure 17. Because the photograph is taken before full preparation, the right side cannot be assessed. Only parts of the neural arch of DV10 are preserved. Based on the current, mounted and reconstructed state of the vertebra, it is nearly impossible to assess which parts of the arch are reconstructed, and which parts still consist of bone. Therefore, the following description is mainly based on the photograph shown in Figure 17.

Both prezygapophyses can be recognized, but they are inclined laterally, and displaced taphonomically posteriorly against the base of the neural spine. Ventral to the left prezygapophysis, the left CPRL can be observed. Posterior to the prezygapophyses, a single left SPRL can be recognized, but it is severely damaged. The right SPRL is not preserved. Dorsal to the CPRL, a PCPL has been pushed anterolaterally due to the breakage of the neural arch. Posterodorsal to the damaged PCPL, the partial left transverse process can be recognized, but most of it is not preserved. A PCDL connects dorsally to the remains of the transverse process and posteroventrally extends to the centrum. The postzygapophyses overhang the prezygapophyses of SV1, and appear slightly inclined laterally. From both postzygapophyses, SPOLs extend dorsally. However, because the neural spine is entirely missing, it is not clear if the SPOLs fuse and form a POSL. From the right postzygapophysis, a single lateral lamina is seen disappearing into the matrix. This is likely the right PODL. From the left postzygapophysis, two anterolaterally projecting laminae can be seen. The lamina that is located more dorsally represents an anteriorly

bifurcating PODL. The more ventral of the two laminae is the lateral branch of the CPOL, which extends from the lateral edge of the postzygapophysis to the posterior side of the left PCDL. A mCPOL is also partially visible, dorsally obscured by the overhanging prezygapophyses of the first sacral vertebrae. A single SPDL originates medially to the medial branch of the PODL. Anterior to the postzygapophysis, and posterior to the SPDL, a very deep POSDF is present. Other structures of the neural arch are too difficult to discern from the pictures.

Thoracic Ribs (Figure 18, Table 3)

Preservation and orientation. A total of nine ribs were found associated with the articulated cervicodorsal series of MAB011899 which still preserve the quarry coordinates, so they can be clearly attributed to their correct position in articulation. More ribs were found (Figure 2), and are likely part of the current composite mount, but it cannot be confidently concluded if these are ribs from MAB011899 or from other individuals in the quarry, as the original SMA coordinates or bone numbers given by the Oertijdmuseum have been lost during the reconstructions. We therefore only describe ribs which can unambiguously assigned to MAB011899.

Three left and four relatively complete right ribs can be identified; one of the right ribs consists of a partial head and is not part of the mount. This partial rib head (RR?4, see below) was found in a storage box, which contained small bone fragments, which are all marked 'G33/90-2', as well as two larger elements: a partial rib shaft and part of a rib head. The rib shaft bears two sets of coordinates, both attached with tape. One is written in German, stating 'G33/90-2 Rippe', and the other appears to be attached later, likely by the Oertijdmuseum, stating 'G33/90-1 Brösmeli'. Unfortunately, the shaft does not bear an original SMA coordinate on the surface, contrary to nearly all other bones of MAB011899. Because the rib head element bears 'G33/90-1 Brösmeli', it seems that the rib shaft element cannot be unambiguously assigned to either the rib head element or RR?4. The quarry sketch of section G33-90 indicates that both ribs numbered 'G33-90-1' and 'G33-90-2' were relatively complete when found. It is likely that during excavations and due to the crumbly nature of the bones, the ribs were only partially recovered. Therefore, neither the quarry map nor sketches elucidate to which of the two ribs the rib shaft ele-
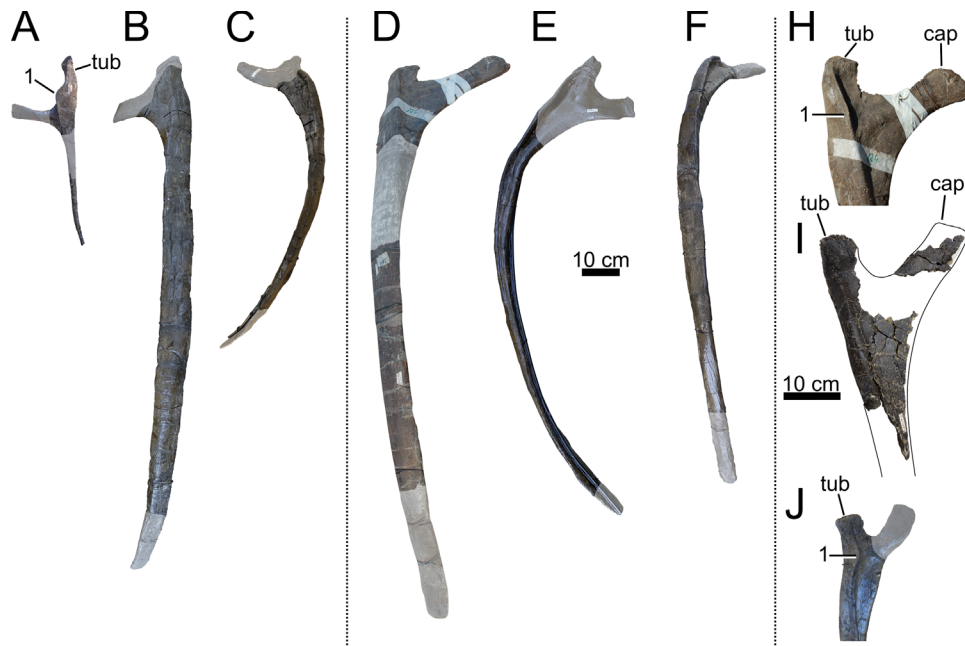
FIGURE 18. Dorsal ribs of *Ardetosaurus viator* MAB011899. Left ribs: A) RL1 in anterolateral view, B) RL?4 in lateral view, and C) RL?8 in anterolateral view. Right ribs: D) RR?3 in lateral view, E) RR?5 in posterior view, and F) RR?6 in lateral view. Rib heads: H) rib head of RR?3 in anterior view, I) rib head of RR?4 in anterior view, and J) rib head of RR?6 in anterior view. Note the pronounced ridges (1) on the rib heads of RL1, RR?3 and RR?6. White shaded areas indicate reconstructed parts. Abbreviations: cap, capitulum; tub, tuberculum.

ment belongs. This element is therefore described separately from the other elements.

It must be noted that large parts of the ribs are reconstructed. The ribs are described as if they are in an anatomical position, whereby the tuberculum is facing medially and the capitulum is facing ventromedially in the anterior ribs, and medially/dorsomedially in more posterior ribs. The ribs are indicated by their in vivo position, which is discussed after the description of the ribs; the ribs are

TABLE 3. Measurements of the thoracic ribs of *Ardetosaurus viator* MAB011899 (in mm).

Dimension	RL1	RL?4	RL?8	RR?3	RR?4	RR?5
Proximodistal length of rib	490*	1050*	605*	980*	900*	875*
Maximum length of capitulum				270		
Anteroposterior length capitular facet				16		
Dorsoventral height capitular facet				83		
Maximum length tuberculum	197			229		90*
Anteroposterior length tubercular facet	18			26		19
Transverse width tubercular facet	30			66		49
Distance between tuberculum and capitulum				161		
Angle between tuberculum and capitulum	~90			55		
Maximum diameter midshaft	16	69	42	75	53	45
Minimum diameter midshaft	6	22	24	38	29	19
Maximum diameter distal shaft	11					
Minimum diameter distal shaft	7					

Notes: Asterisks indicate estimates. Because no rib is complete, the proximodistal length is an estimate of the preserved parts. For RL1, the angle between the tuberculum and capitulum cannot be measured, as only the base is preserved of the capitulum. However, an estimate can be made. For RR?5, the capitulum is absent, resulting in an estimate as the intersecting line cannot confidently be placed on the rib head.

referred to as RL or RR, abbreviations for 'rib left' and 'rib right,' followed by their (possible) serial position. None of the ribs bear any pneumatic foramina or oblique ridges on the posterior surface of the rib head.

Left Thoracic Ribs

RL1 (Figure 18A). RL1 is a small rib, of which only the tuberculum, the head, and part of the distal shaft is preserved. The midshaft and most of the capitulum are reconstructed in the mount, but the base of the capitulum is preserved. It has a short, subcircular shaft, and an approximate right angle between the tuberculum and the preserved base of the capitulum. The tuberculum bears a very distinct ridge on its anterior surface, which originates from the tubercular facet and extends distally onto the shaft. Unlike *Galeamopus pabsti*, however, this ridge is not straight (Tschopp and Mateus, 2017, figure 50), but bulges anteromedially in the middle, thereby slightly folding over the base of the capitulum. The preserved part of the distal shaft tapers distally and is very thin compared to more posterior ribs, see Table 3.

RL?4 (Figure 18B). Only the base of the head is preserved, bearing the ridge which originated from the tuberculum, which connects to the anterior edge of the shaft. The ridge is far less pronounced compared to the ridge in RL1. The midshaft is no longer subcircular, but closer to subtriangular, being wider anteroposteriorly than mediolaterally. The distal part of the shaft is not preserved but reconstructed for mounting purposes.

RL?8 (Figure 18C). It is similar in morphology to RL?4, but more of the head is missing, the shaft is significantly shorter, the ridge is more robust, and the overall curvature of the shaft is stronger, although this is possibly influenced by the reconstructions carried out on the rib. Distally, the preserved shaft becomes more oval than subtriangular and is mediolaterally flattened.

Right Thoracic Ribs

RR?3 (Figure 18D, H). A long, right rib preserves the entire head of the rib, as well as more than half the shaft. A very distinct ridge is present on the anterior surface of the tuberculum, extending from the tuberculum onto the shaft surface, similar to RL1, but not as medially displaced. On the anterior surface of the capitulum, a similarly oriented, broader, less pronounced ridge is present. The surface between the tuberculum and the capitulum is thin and concave medially. The articular ends of the tuberculum and capitulum are rugose. The pos-

terior side of the rib head between the capitulum and tuberculum is flat. The shaft has a subtriangular outline. As mounted, the shaft is incorrectly connected to the rib head in the reconstructed skeleton, as the anterior face of the head is currently confluent with the lateral face of the shaft. Articulation with the corresponding vertebra would be impossible, as the shaft would be directed posteriorly if the tuberculum and capitulum were articulated with the dorsal vertebra.

RR?4 (Figure 18I). This rib is not part of the mount. It consists of a partial head and part of the base of the shaft. The area in between the tuberculum and capitulum is missing, as well as most of the capitulum itself. The tuberculum is well preserved, bearing a ridge on its anterior surface extending onto the shaft. The ridge is straight, similar to the ridge seen in RR?3, but less pronounced.

RR?5 (Figure 18E). This consists of a large section of the, lacking the head and the distal shaft. The curvature of the shaft is more significant in RR?5 compared to RR?3. The shaft, however, has been partially reconstructed, which may have altered the overall outline of the rib. Most of the rib shaft has a subtriangular outline, but the distal part of the preserved shaft is more oval.

RR?6 (Figure 18F, J). The rib head preserves the tuberculum, which bears a distinct ridge, similar to RL1 or RR?3. The ridge is slightly folded medially in its proximal half, which is likely due to deformation. In life, as seen in RR?3 and RR?4, the ridge would have been straighter. The shaft is rather similar in morphology as RR?3, but less curved.

Rib shaft element. The rib shaft is subtriangular in outline and contains a longitudinal ridge on the posteromedial surface. It is probably part of one of the larger ribs (e.g., RR?4, see above), as the shaft is wide, and no edge of the shaft shows tapering.

Rib head element. This element can be identified as part of a rib head based on the ridge that is preserved, which is present on the anterior or dorsal surface of the tuberculum. This rib head fragment is also part of the right side of the rib cage, as the left side of the fragment is the beginning of the tuberculum, whereas a broken surface to the right of the ridge appears to be the beginning of the capitular facet. It shows no different features from the other ribs.

Serial Position of the Thoracic Ribs

Serial positions are difficult to assign for nearly all ribs, because all ribs miss part of the shafts and part of the head, making comparisons

between the ribs and with other taxa nearly impossible. The only rib that is placed unambiguously in the correct position is RL1, due to its short shaft, the approximate right angle between both articular facets, and its similarities with the first rib of *G. pabsti* (Tschopp and Mateus, 2017, fig. 50).

For the other ribs, the serial position is ambiguous. Serially, the fourth, fifth and sixth ribs are usually the largest three ribs in diplodocids (Hatcher, 1901; Gilmore, 1936). Additionally, rib head size can be an indicator of where ribs are placed (Hatcher, 1901), as in *Diplodocus carnegii*, the fourth rib bears the largest rib head. However, the ribs of *Apatosaurus* (Gilmore, 1936) and *Barosaurus*, which according to McIntosh (2005), resemble those of *Apatosaurus*, are different from those of *Diplodocus*. The ribs of YPM VP.000429 appear to be incomplete and damaged (McIntosh, 2005), such that comparisons are near impossible. In *Apatosaurus*, the second rib head is the largest, but based on the shaft length comparisons, the ribs with the largest heads have short shafts. Additionally, the tuberculum becomes less pronounced medially from the fourth rib onwards (Gilmore, 1936). The latter is also present in *Brontosaurus* (Ostrom and McIntosh, 1966), making comparisons with apatosaurines difficult. The ridge on the tubercular facet can aid in positioning the ribs. In both *Apatosaurus louisae* (Gilmore, 1936) and *Galeamopus pabsti* (Tschopp and Mateus, 2017), these ridges become less pronounced in more posterior ribs.

In MAB011899, RR?3 and RL?4 are the largest ribs in terms of shaft length and diameter. RR?4 appears to have an approximately similar head size as RR?3, but the ridge on RR?4 is less pronounced. RR?4 would have been positioned directly after RR?3, or with one rib in between. RL?4 has a slightly smaller midshaft diameter as RR?3, but it falls within the variations seen in *G. pabsti*, whereby the difference in diameter of left and right ribs at the same serial position can be up to 1.5 cm. Therefore, purely based on the slightly less pronounced preserved part of the ridge, RL?4 is placed directly behind RR?3, but it could be the left equivalent of both RR?3 and RR?4. RR?5 and RR?6 are both significantly more convex ribs, but are still quite large, and would be placed behind RL?4. RR?5 is slightly larger compared to RR?6, although it lacks more of the entire rib, and would thus be placed in front of RR?6. RL?8 is the smallest rib apart from RL1, is more convex than any other rib, and should be placed behind RR?6, likely with one or maybe two ribs in between. In vivo, this

could result in the following sequence: RL1 is the first left rib, RR?3 is the third or fourth right rib, RR?4 is the fourth or fifth right rib, RL?4 is the fourth or fifth left rib, RR?5 is the fifth or sixth right rib, RR?6 is the sixth or seventh right rib, and RL?8 is the eighth or ninth left rib. The rib head element preserves a distinct ridge, which could place it in front or behind RR?3. However, because most of this rib head is missing, this is difficult to assess.

Sacrum (Figure 19, Table 4)

Preservation. The sacral vertebrae are only partially preserved and have been heavily reconstructed since the first preparations by the SMA. Several photographs from mostly approximately lateral and dorsal views were made at the time and also subsequently when the sacrum arrived at the Oertijdmuseum, and are used here extensively for further reference, as the reconstructions made during the mounting process are difficult to distinguish from the real bone. The entire sacrum was excavated and prepared as a single block consisting of the remaining parts of DV10, four fused vertebrae that are firmly attached to the left ilium, and SV5, the centrum of which had not fused to SV4 anteriorly. However, the sacral rib of SV5 is fused laterally to the medial surface of the ilium, just as the other sacral ribs. The entire right side of the sacrum, including the right ilium and some of the righthand parts of the neural spines, is missing.

On excavation SV5 was preserved in a near-horizontal orientation, with the neural spine directed anterodorsally and the centrum was directed posteroventrally. This caused the sacrum to have an anteroposteriorly folded appearance in older photographs. Because SV5 was reoriented in this manner, the anterodorsal surface of the neural spine of SV5 was displaced anteriorly into the posterior surface of the neural spine of SV4, which caused the neural spine of SV4 to break at mid-height. Subsequently, the forward displacement of SV5 caused the neural spines of SV2 and SV3 to bulge, and become convex anteriorly, as the neural spine of SV4 was pushed into the preceding vertebrae. During preparation, it became clear that both the dorsal halves of the neural spines of SV4 and SV5 were lost. In the mount, the neural spines have been straightened as to approach in vivo position; both the dorsal halves of the neural spines of SV4 and SV5 are reconstructed. During the mounting and preparation processes, an additional sixth sacral neural spine was wrongly added as a reconstruction. To avoid future confusion when studying the specimen, it is important to note
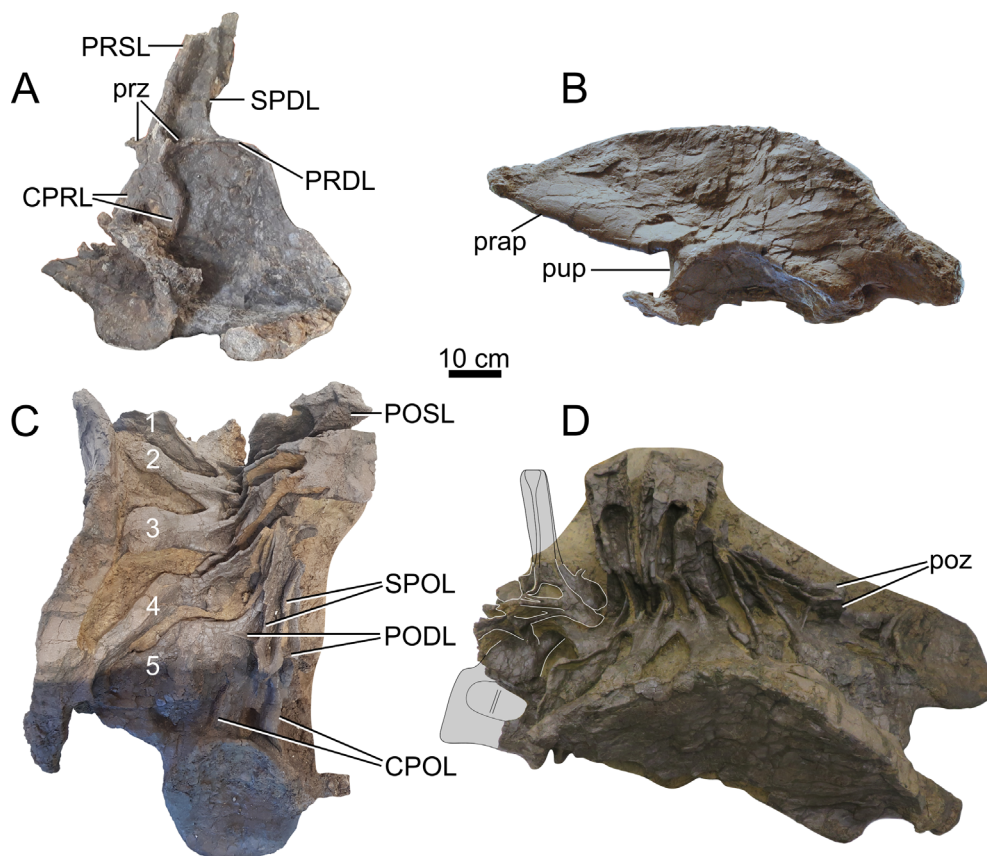
FIGURE 19. Sacrum, dorsal vertebra 10 and ilium of *Ardetosaurus viator* MAB011899. Composite figure of the sacral elements. A) Fifth sacral vertebrae in left anterolateral view. B) Left ilium in lateral view. C) Sacrum in posterodorsal view. D) Sacrum and outline of DV10 in left dorsolateral view. Markings 1, 2, 3, 4, and 5 indicate the sacral ribs in anteroposterior order. Note that in Figure D, the anterior part of the preacetabular process is missing, which had broken off during transport. Figures A, C, and D are courtesy of René Fraaije, made during the preparation and mounting process. Abbreviations: CPRL, centroprezygapophyseal lamina; CPOL, centropostzygapophyseal lamina; PODL, postzygodiapophyseal lamina; POSL, postspinal lamina; poz, postzygapophysis; prap, preacetabular process; PRDL, prezygodiapophyseal lamina; prz, prezygapophysis; pup, pubic peduncle; SPDL, spinodiapophyseal lamina; SPOL, spinopostzygapophyseal lamina.

which neural spine is reconstructed. Based on the trajectory of the SPDL of the fourth neural spine (as mounted) and the enlarged, both anteroposteriorly and transversely, fifth spine, it appears that this fifth mounted spine is reconstructed and was wrongly added to the sacrum, which is composed of five vertebrae as is ubiquitous in diplodocids and many other eusauropods except derived macronarians (Filippini et al., 2017).

Description. The sacral neural spines project significantly above the dorsal rim of the ilium, similar to the situation in other diplodocid taxa (Hatcher, 1901; Gilmore, 1936; McIntosh, 2005). The first sacral neural spine is oriented nearly vertically. The left SPDL of SV1 is located on the anterolateral side of the spine. The lamina is prominent, protruding laterally, and bifurcates ventrally, approximately at midheight. The anterior branch connects to the

TABLE 4. Measurements of the sacrum of *Ardetosaurus viator* MAB011899 (in mm).

Dimension	
Centrum length SV1	220
Centrum length SV2	140
Centrum length SV3	180
Centrum length SV4	190
Centrum length SV5	115
Cotyle width SV5	280
Cotyle height SV5	258
Rib width SV5	202
Neural arch height SV5	145

Notes: Due to the way the sacrum was mounted, measuring most parts of the sacrum was impossible. Rib width is measured mediolaterally on the ventral surface of the rib, from the lateral-most point to where the centrum is reached.

dorsal surface of the first sacral diapophysis, which is indistinguishable from the tuberculum of the sacral rib, but which are still separate elements sensu Wilson (2011). The posterior branch is attached to the ventral-most part of the spine, close to the posterior edge of the spine and the antero-medial side of the diapophysis of SV2. Dorsally, the SPDL of SV1 becomes a single stout lamina, and expands anteroposteriorly when reaching the spine tip, forming a triangular, rugose sheet of bone. A small part, ventral to the triangular bony sheet, of the SPDL is reconstructed. The POSDF is dorsally bordered by a prominent ventral rim of this bony sheet, and anteriorly by the SPDL. Both SPRLs can be recognized, albeit only partially preserved, which join dorsally to form a single rugose PRSL. The rugose POSL extends dorsally above the dorsal edge of the spine.

The second and third sacral neural spines are fused, similar to e.g., SMF R462 (formerly AMNH FARB 516; Osborn, 1904, figure 3) and UW 15556 (formerly CM 563; Hatcher, 1903, plate IV). A PRSL and POSL can be observed, as well as two SPDLs. The two SPDLs expand dorsally in antero-posterior direction to form a single, expanded bony sheet on the lateral side of the neural spine tip. Ventrally, the SPDL of SV2 is not bifurcated, but single. The SPDL of SV2 is ventrally attached to the dorsal surface of the second diapophysis.

The SPDL of SV3 is ventrally bifurcated, but unlike the SPDL of SV1, the bifurcation occurs near the neural spine tip. The anterior lamina can be confidently identified as the SPDL, as the ventral part of the lamina attaches to the dorsal surface of the third diapophysis. The posterior branch, however, is either a second SPDL as in SV1, or it is a ISPOL which dorsally fuses to the SPDL. The edge of the lamina faces posteriorly, but this appears to be influenced by compression. Ventrally, the lamina either attaches to where the post-zygapophysis and prezygapophysis of SV3 and SV4 fuse, thus identifying the lamina as a ISPOL, or, which can't be elucidated with confidence, the lamina attaches to the anterodorsal surface of the fourth diapophysis, thereby identifying the lamina as a second SPDL. The continuation of this lamina towards the fourth diapophysis is difficult to judge, as the lamina shows some breakage near the post-zygapophysis, whereby the lamina could terminate, but also could continue towards the diapophysis of SV4.

The anatomy of the fourth neural spine is difficult to discern due to reconstruction and poor preservation. Only the left ventrolateral half was preserved. Additionally, the neural spine was not fully separated from the third spine, but also not fully fused, due to the prominent POSL of SV3. This appears similar to the sacrum of SMF R462 (Osborn, 1904, figure 3A), which also, although obscured, seems to have a partially fused fourth neural spine. Only a single SPDL is present. The SPDL attaches ventrally to the dorsal surface of the fourth diapophysis. This SPDL, however, does extend further laterally compared to the SPDLs of more anterior neural spines. Part of the ventral portion of the POSL is exposed, as the dorsal half of the spine is lost.

Because it is separated from the rest, SV5 can be described in more detail. The vertebra resembles an anterior-most caudal vertebra sensu Tschopp et al. (2015a). However, the lateral rim of the left rib folds anteriorly and attaches laterally to the posteromedial margin of the ilium, contacting the fourth rib where both ribs contact the ilium. The centrum is anteroposteriorly short, mildly opisthoc-oelous, and ventrally concave. The posterior articular surface is subcircular. The neural canal is oval and is taller than wide. The neural canal is bordered by two transversely wide CPOLs. The post-zygapophyses are distinctly V-shaped in posterior view and supported by a TPOL from below. A rhomboid-shaped hyposphene is added in the mount, however, this is not found in earlier pictures. This could, however, be an artifact of the age and detail of the pictures from the SMA, which renders it difficult to discern whether a hyposphene was present, as hyposphenes are known to be present in post-dorsal vertebrae (Apesteguía, 2005). However, it is more likely, based on the SMA photographs, that if the hyposphene was present, it would be more of a laminar structure, instead of the reconstructed rhomboid hypo-sphene. From the postzygapophyses, two vertical, parallel SPOLs are present, which project posteri-orly, and are separate from the POSL. The POSL originates approximately at midheight, medial to the SPOLs, is distinctly rugose, and runs towards the dorsal edge of the remainder of the spine. It is likely, as seen in SV3 and the posterior dorsal ver-tebrae, that the POSL would have reached the neural spine tip. Just above the dorsal-most point of the postzygapophyses, horizontal PODLs are present which meet where the SPDLs fade into the 'wing-like' transverse processes. On the right side, only a small part of the ventral border of the rib is preserved.

The anterior part of the vertebra is poorly pre-served, also due to breakage caused by detach-

ment of the vertebra from the fused sacral vertebrae and ilium. A convex, dorsoventrally flattened, small condyle is present. Posterolaterally, the ventral borders of the transverse processes originate. On the left dorsolateral side of the condyle, a half circle of bone is present which likely would have been attached to the fourth sacral rib, bending dorsolaterally towards the neural canal. The neural canal is surrounded by two CPRLs, which like the CPOLs, are stout laminae, with a 'horseshoe'-like appearance, thus fusing dorsomedially. Dorsal to the CPRLs, two laminar structures are present, oriented dorsolaterally, which likely represented the prezygapophyses. These structures are no longer visible in the mount, as they are overlain by reconstructed prezygapophyses. Medial to the prezygapophyses, a single stout PRSL is present, which is dorsally interrupted as the dorsal half of the neural spine is missing. Posteromedially to the prezygapophyses, the PRDLs originate. On the left side, the edge of the PRDL is dorsally oriented anteriorly, facing laterally towards the lateral side of the rib, and facing anteriorly again ventrally. In posterior view, the margin of the rib curves ventrally approximately halfway along the mediolateral lengths of the rib. This is true for a third of the dorsoventral length of the rib, after which the margin curves lateroventrally. Finally, when the margin meets its lateral-most point, anterior curvature of the rim begins, extending beyond the anterior edge of the neural arch. On the posterior surface of the rib, an enclosed fossa is present lateral to the left CPOL. It is bordered by the neural arch and can be identified as the final transverse foramen sensu Wilson (2011). No intracostal foramen or fossa is observed in this final rib.

The sacral centra are all smooth ventrally, and mildly concave. The first and fourth centra bear pleurocoels, although the first is only partially preserved and infilled with residual sediment, and the fourth is infilled with acrylic resin. The second and third centra cannot be assessed for pleurocoels, due to extensive reconstruction. Intercostal foramina which are anteroposteriorly open are not visible and have likely been infilled with acrylic resin. Intercostal and transverse foramina are present. As the first sacral rib is broken laterally, only a small oval shaped transverse foramen can be observed. This rib would have fused with the anterodorsal-most part of the ilium. Transverse foramina may have been present in the second, third and fourth sacral ribs, but everything has been filled in and covered with acrylic resin for support, resulting in fully enclosed reconstructed ribs. Similarly, describing the intracostal foramina in detail is not possible due to reconstruction, but it appears that at least the third and fourth ribs have them. For the first rib, due to breakage, it is unknown if an intracostal foramen was present. Ventrally, two distinct intercostal foramina are present, laterally in between the second and third, and third and fourth centra. Because only the anterodorsal part of the anterior extension of the fifth rib is attached to the ilium, ventrally, this space is entirely open. For the first rib, because of the breakage, similar to the fifth rib, the ventral space is entirely open. A sacricostal yoke is present, fusing the ventrolateral parts of the ribs in a single anteroposterior elongated block, which is laterally fused to the ventromedial side of the ilium. A small foramen is present in the yoke, lateral to the second intercostal foramen, posterior to the pubic peduncle, but this is probably an artifact of a borehole for supporting the sacrum in earlier stages of the mounting process. The dorsal surface of all ribs is smooth, bearing no ridges or rugose surfaces, with the second and third rib being anteroposteriorly wider compared to the other three ribs.

Caudal Vertebrae (Figures 20–24, Table 5)

Preservation and mounting. Initially, an in-situ plan was made for MAB011899 in 1994, wherein more than 20 caudal vertebrae were assigned to

FIGURE 20. Caudal vertebra Cd1 of *Ardetosaurus viator* MAB011899. Cd1 is shown in A) left lateral, B) right lateral, C) posterior, and D) anterior view. White shaded areas indicate reconstructed parts.
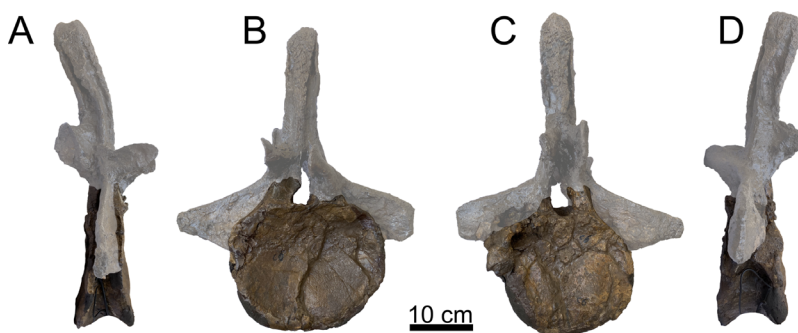
FIGURE 21. Caudal vertebra Cd2 of *Ardetosaurus viator* MAB011899. Cd2 is shown in A) left lateral, B) right lateral, C) posterior, and D) anterior view. White shaded areas indicate reconstructed parts.

FIGURE 22. Caudal vertebra Cd3 of *Ardetosaurus viator* MAB011899. Cd3 is shown in A) left lateral, B) right lateral, C) posterior, and D) anterior view. White shaded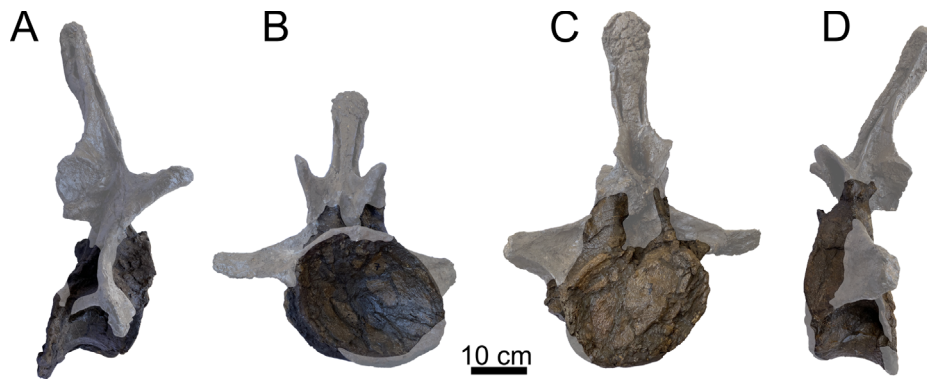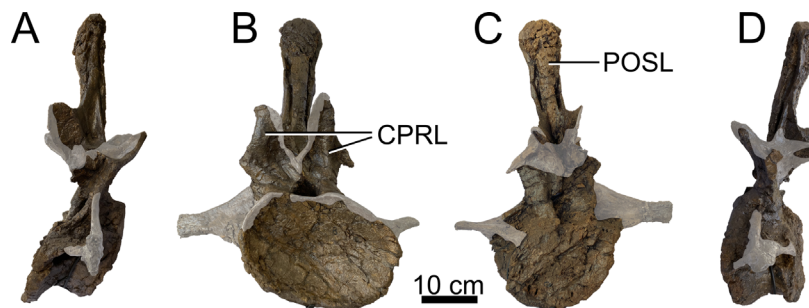 areas indicate reconstructed parts. Note the presence of distinct CPRLs ventral to the prezygapophyseal rami. Abbreviations: CPRL, centroprezygapophyseal lamina; POSL, postspinal lamina.

MAB011899. However, in subsequent years, most of these caudal vertebrae were determined to belong to the individuals 'Twin' and 'Triplo' (Figure 2), as more material was found of these individuals. Figure 2 shows seven caudal vertebrae assigned to MAB011899, three of them articulated with the sacrum. However, the jacket containing most of the material of quarry section G34/93 did only include four caudal vertebrae. The side of the jacket was therefore marked with the numbers "17" (G33/93-1), "18" (G33/93-2), "19" (G34/93-4) and "20" (G34/94-3), indicative of the four vertebrae which were present in this jacket. These numbers were subsequently used by the Oertijdmuseum to indicate each vertebra, as a temporary bone number. Early preparations, however, revealed that the jacket contained five vertebrae. Vertebra '17' turned out to be a very poorly preserved cervical vertebra. This vertebra was not drawn on the quarry map, probably because not enough was exposed to identify this bone as such. It is probable that this vertebra does not belong to MAB011899,

as the cervical column was found far from the caudal region, but to either 'Twin' or 'Triplo' based on flow direction (Figure 2). No anatomical characteristics could be gleaned from the vertebra to further support this.

During the early preparation of this jacket, another caudal vertebra was recognized in front of caudal vertebra (Cd)20. This vertebra was given the number "20.1" (G34/93-2), and was recovered displaced relative to the other vertebrae in the jacket. Further exposure revealed that Cd20 and Cd19 were articulated with each other, and that Cd18 was lying with its anterior articular surface facing towards the neural spine of Cd19, partially on top of the neural arch of Cd19. It thus seems that Cd20.1 very likely articulated posteriorly with Cd20 and Cd19, and that Cd18, and possibly the now lost other vertebrae in quarry sections G33/93 and G34/92, are part of the anterior portion of the tail, but do not necessarily articulate with Cd19. Another caudal vertebra can also be assigned to MAB011899 with confidence. It was numbered
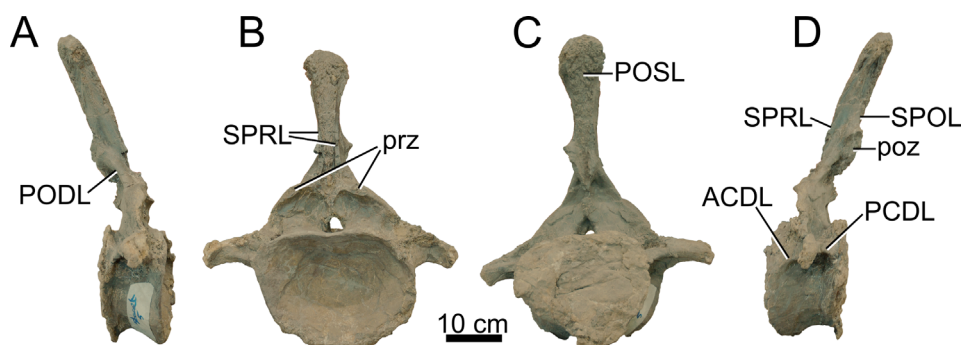
FIGURE 23. Caudal vertebra Cd?4-6 of *Ardetosaurus viator* MAB011899. Cd?4-6 is shown in A) left lateral, B) right lateral, C) posterior, and D) anterior view. Note the absence of distinct CPRLs ventral to the prezygapophyseal rami. Abbreviations: ACDL, anterior centrodiapophyseal lamina; PCDL, posterior centrodiapophyseal lamina; PODL, postzygodiapophyseal lamina; POSL, postspinal lamina; poz, postzygapophysis; prz, prezygapophysis; SPOL, spinopostzygapophyseal lamina; SPRL, spinoprezygapophyseal lamina.
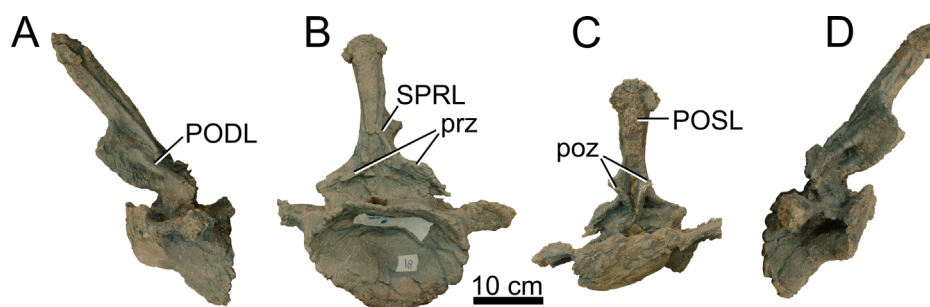

FIGURE 24. Caudal vertebra Cd?5-8 of *Ardetosaurus viator* MAB011899. Cd?5-8 is shown in A) left lateral, B) right lateral, C) posterior, and D) anterior view. Note the absence of distinct CPRLs ventral to the prezygapophyseal rami. Abbreviations: PODL, postzygodiapophyseal lamina; POSL, postspinal lamina; poz, postzygapophysis; prz, prezygapophysis; SPRL, spinoprezygapophyseal lamina.

"322" and was found next to the lower jaw of SMA 0002/NMZ 100002 in quarry section G33/92-1. In the final maps, Cd322 was assigned to Triplo. However, this assignment is likely incorrect for the following reasons: 1) Cd322 is still quite close to the caudal region of MAB011899, especially compared to most bones assigned to Triplo; 2) the caudal vertebrae that are not drawn as articulated are all displaced in a west-southwest direction, such as Cd18; 3) earlier versions of the map indicate that Cd322 was found much earlier than the bones of Triplo, and when more material of Triplo was found, not directly assigned to Triplo; 4) Cd322 is nearly identical to Cd18 in morphology, apart from size and spine inclination; and 5) the bone preservation of Cd322 is much closer to the bone preservation of Cd18 compared to the bones of Triplo.

Serial position and orientation. Cd20.1, Cd20, and Cd19 were roughly articulated with no space left in between the vertebrae to fit another caudal vertebra. Cd20.1, although anteroposteriorly com-

pressed, is larger in articular surface diameter, and could articulate with SV5. Therefore, from anterior to posterior, Cd20.1, Cd20, and Cd19 is the correct order for their in vivo placement. Because the jackets were separated, and no pictures are known to capture the direct articulation between SV5 and Cd20.1, the quarry map (Figure 2) and sketches are the only evidence of near direct articulation between these vertebrae. Based on the quarry map and sketches, as well as the minor difference between the articular surface diameters (Tables 4-5), we can confidently conclude that Cd20.1 did articulate with SV5, so we interpret Cd20.1 as being the first caudal vertebra.

Cd18 and Cd322 are more difficult to place because anterior caudal vertebrae are generally similar in their morphology apart from their size and the development of the transverse processes. Although Cd18 was found on top of Cd19, direct articulation between both vertebrae is unlikely, because of the overall smaller size of Cd18.

TABLE 5. Measurements of the caudal vertebrae of *Ardetosaurus viator* MAB011899 (in mm).

Dimension	Cd1	Cd2	Cd3	Cd?4-6	Cd?5-8
Greatest height				513	461
Centrum length	110	144	125	142	165
Pleurocoel length (left/right)	50/30	57/80	88/70	80/59	73/80
Pleurocoel height (left/right)	65/50	50/55	24/43	35/42	38/35
Cotyle width	268	249	207	240	
Cotyle height	230	187	165	195	
Condyle width	296	252	277	271	285
Condyle height	246	246	213	211	202
Neural arch height				164	157
Mount position	5	6	7	8	10
Former vertebral numbers	20.1	20	19	322	18

Notes: The cotyle measurements of all vertebrae are influenced by the poor preservation of the vertebrae, with the exception of Cd?4-6. The cotyle of Cd?5-8 is too deformed to provide a useful measurement.

Because of the morphological variation among anterior diplodocid caudal vertebrae when the serial position is known, assigning a range of serial positions for each vertebra is a more appropriate approach than definite positions. Measurements of the first five caudal vertebrae of *Diplodocus* CM 84 (Hatcher, 1901), *Barosaurus* YPM VP.000429 (Lull, 1919), AMNH FARB 6341 (McIntosh, 2005), and *Apatosaurus* CM 3018 (Gilmore, 1936) indicate a slow decline in articular surface diameter along the sequence. Especially when following the measurements of CM 84, the presence of one or two additional vertebrae between Cd19 and Cd18 cannot be excluded. Cd322 has a slightly taller anterior articular surface, and the neural spine inclination is not as strong as in Cd18, although this might be affected by distortion in the latter. Cd322 likely preceded Cd18. Because the articular surface diameter shows such a slow decline in other diplodocids, there is a possibility that Cd322 and Cd18 did not articulate but were separated from each other along the sequence by a single vertebra. It is possible that Cd322 articulated with Cd19, or that one or two vertebrae were present in between both vertebrae.

Therefore, to account for all variability in serial positions, Cd322 is assigned to a serial position between caudal vertebra four and six, and Cd18 positioned between five and eight. From here, all caudal vertebrae will be referred to by their serial position. Therefore, Cd20.1, Cd20, and Cd19 are referred to as Cd1, Cd2, and Cd3, respectively. Cd18 and Cd322 are referred to as Cd?5-8 and Cd?4-6, to account for the variability in their serial position. The caudal vertebrae are described with the ventral surface of the neural canal parallel to the horizontal.

Descriptions (Figures 20–24)

Cd1 (20.1). Only the centrum of Cd1 is preserved (Figure 20), which is the largest in terms of articular diameter of all preserved caudal vertebrae. The centrum is strongly anteroposteriorly compressed, resulting in a flattened centrum in lateral view. The anterior articular surface is slightly concave, whereas the posterior surface is flat. Pleurocoels are present, but weakly developed. Foramina are present on the ventral surface. The remainder of the vertebra is reconstructed.

Cd2 (20). This vertebra is, similarly to Cd1, poorly preserved (Figure 21). It is anteroposteriorly longer than Cd1 (Table 5), but this is most likely influenced by the compression of Cd1. Most of the neural arch is missing, including the neural spine, pre- and postzygapophyses and transverse processes. The pleurocoels are far less pronounced, lacking a clear ventral rim on the left side. The ventral rim of the posterior articular surface is sheared ventrally. The ventral part of the arch is preserved, but it bears no clear remnants of CPRLs.

Cd3 (19). Parts of the neural arch are missing from Cd3 (Figure 22), as well as part of the posterior articular surface. The vertebra is anteroposteriorly obliquely deformed. Additionally, the left dorsolateral surface of the centrum is displaced medially. The posterior articular surface was flat based on the preserved parts of the articular surface and comparisons with the more complete Cd?4-6 and Cd?5-8. The surface contains numerous cracks. The ventral side of the vertebra is concave antero-

posteriorly and does not possess any foramina. This is the only vertebra with well-delimited pleurocoels, albeit deformed. The anterior articular surface is concave, similar to Cd?4-6 and Cd?5-8. The rim is damaged ventrally and dorsally. The neural canal is shaped roughly like an equilateral triangle in anterior view, with the apex placed directly dorsally. Posteriorly, the margins of the canal are broken off, so the original outline of the canal is not preserved. Attached to the centrum are two reconstructed transverse processes. These processes are ventrally reconstructed just dorsal to the pleurocoel, as seen in *Diplodocus carnegii* (Hatcher, 1901, plate IX). However, the left process is dorsally connected to the dorsal margin of the centrum, and the right process is dorsally connected to the dorsolateral edge of the PCDL. The left process should connect to the small remnant of the preserved transverse process that is still seen posterolateral to the left prezygapophysis, whereas the right process should connect slightly further dorsally. In vivo, the transverse processes would be distinctly 'wing'-like, as seen in *Diplodocus* (Hatcher, 1901) and *Barosaurus* (Lull, 1919). The neural arch bears a hyposphenal ridge posteriorly; the ridge is partially broken, and because of the overall deformation of the vertebra, it is not straight dorsoventrally. Only the lateroventral parts of the prezygapophyses are preserved, oriented anterodorsally. They are both pointed processes, although the distal ends are not fully preserved, and the end of the right prezygapophysis looks similar to those seen in Cd4-6 of *Diplodocus* (Hatcher, 1901, plate IX). This vertebra does preserve CPRLs, but these laminae do not connect to the dorsal surface of the centrum. Instead, they extend approximately level to the dorsal margin of the neural canal and are not nearly as robust as in *Diplodocus* (Hatcher, 1901) or *Leinkupal* (Gallina et al., 2014). The neural spine is mostly preserved. However, anatomical detail of the spine is obscured by reconstructions, as the neural spine was separated from the rest of the vertebra during preparations and was ventrally damaged. Therefore, the neural spine is described mostly based on the photographs taken during the preparations. The neural spine was posteriorly inclined. It bears the dorsal parts of the postzygapophyses, which are dorsally rounded. On the lateral sides, the SPRLs and SPOLs can be discerned, which dorsally join to form lateral spinal laminae. Anterior and posterior to these laminae, dorsoventral depressions are present. A PRSL and POSL are present. They are distinct laminae, and both are rugose dorsoventrally.

Cd?4-6 (322). Cd?4-6 (Figure 23) consists of a relatively undeformed centrum and a relatively complete neural arch. Partially preserved pre- and postzygapophyses were reconstructed in the mount. Anteriorly, the articular surface of the centrum is sub-oval, of which the dorsal edge of the rim is compressed ventrally, and the right lateral side of the rim is compressed medially. The posterior articular surface has a distinct, distally projecting rim, but this could be an artifact of deformation. The centrum is concave anteriorly, and flat to mildly convex posteriorly [procoelous-distoplatyan sensu Tidwell et al. (2001), or procoelous-opisthoplatyan sensu González Riga et al. (2009)]. Ventrally, the centrum is concave anteroposteriorly, and bears several elliptical foramina, which are significantly smaller compared to *Suuwassea* (Harris, 2006). Pleurocoels on both sides are significantly reduced compared to the cervical and dorsal vertebrae and consist of rounded depressions ventral to the transverse processes with no distinct borders. Both the left and right ACDL project anteroventrally from the transverse processes. The PCDLs differ, however, as the left PCDL projects posteriorly, with the edge facing laterally. Only the posterior end of the lamina bends ventrally. The right PCDL, however, projects almost fully ventrally from the transverse processes and attaches to the centrum ventral to the ventral margin of the pleurocoel. The dorsal portions of the transverse processes are damaged, and parts of the processes are missing, which would have formed a distinct connection between the processes and the neural arch, creating a 'wing'-like shape. The processes project laterally to lateroventrally, and terminate laterally as damaged, bulged surfaces. The dorsal edge of the left transverse process contacts the posterolateral side of the prezygapophysis. This cannot be assessed due to breakage for the right side, but a similar structure lateral to the prezygapophysis appears to be present. The neural canal is sub-oval in anterior view, with the rounded edge projecting dorsally, whereas in posterior view, the canal is almost a perfect triangle. Dorsal to the neural canal, the two branches of the TPRL diverge laterally, connecting to the medial edge of the oval prezygapophyses. Interestingly, there is no evidence for the presence of CPRLs in either Cd?4-6 or Cd?5-8, which are notably present in, e.g., *Diplodocus* (Hatcher, 1901, plate IX) or *Leinkupal* (Gallina et al., 2014, p. 4). The prezygapophyses appear to have projected anterodorsally. The lateral parts of the prezyga-

pophyses project towards the transverse processes lateroventrally. SPRLs are present, but the ventral part is broken off, so the anterior portion of the SPRLs connecting the prezygapophyses to the neural spine is missing. The postzygapophyses are V-shaped based on the remaining parts. The left postzygapophysis is best preserved, although broken posteriorly, and based on the left SPOL, projects dorsolaterally at the top. The postzygapophyses occupy the ventral third of the neural spine, similar to e.g., *Diplodocus carnegii* (Hatcher, 1901). A single, posteriorly projecting hyposphenal ridge connects the dorsal margin of the neural canal to the ventral margin of the postzygapophyses. The ridge is broken in some parts, but is still recognizable. Lateral to the ridge, the PODLs are present, each of which is connected to the anterolateral edge of the postzygapophyses and to the dorsomedial surface of the transverse processes, just posterior to the prezygapophyses. Medial to both PODLs, dorsolateral to the hyposphenal ridge and lateral to the ventral margin of the postzygapophyses, two distinct triangular fossae are present which are ventrally open. The neural spine bears a broad PRSL and POSL, which both are entirely rugose. The PRSL terminates at the dorsal margin of the spine, whereas the POSL projects beyond the dorsal margin, forming a small projection at the posterodorsal side of the spine tip. The neural spine widens dorsally, strongly in the dorsal third. At midheight, the SPRL and SPOL fuse laterally to form a single, rugose lateral spinal lamina, which projects laterally towards the dorsal tip of the spine, creating a rounded outline in anterior view for the top of the neural spine. Lateral to the POSL, posterior to the lateral spinal laminae, dorsoventral depressions are present, similar to *D. carnegii* (Hatcher, 1901). A similar depression is present anterior to the left lateral spinal lamina. The entire neural spine is inclined posteriorly, including the postzygapophyses.

Cd?5-8 (18). Cd?5-8 (Figure 24) is significantly more deformed compared to Cd?4-6. This deformation is most notable in centrum morphology. Anteriorly, the articular facet is heart-shaped, caused by the mediodorsal compression of the ventrolateral sides of the rim. Like Cd?4-6, the anterior articular surface of the centrum is concave, and the posterior surface is flat to mildly convex. The posterior articular surface, however, is severely obliquely compressed, resulting in a facet that is at least two times smaller compared to the anterior facet. This facet is reconstructed in the mount to similar proportions as the anterior facet.

Ventrally, the centrum is anteroposteriorly concave, but lacks the small foramina found in Cd?4-6. A pleurocoel is present on the left side, but on the right side, the pleurocoel is absent, which may be caused by the severe oblique compression. It is likely that both pleurocoels resemble those seen in Cd?4-6. The pleurocoels are oval and located beneath the transverse processes towards the posterior end of the centrum. Transverse processes are partially broken, lacking most of the dorsal parts that connect the processes with the neural arch, as well as the distal extremities. The missing dorsal parts preclude any assessment of the presence of foramina in the transverse processes, but their absence on the left side of Cd?4-6 leaves their presence in Cd?5-8 unlikely. The transverse processes project laterally, with a sub-circular distal end in lateral view. The PCDLs are oriented anteroposteriorly and attach to the rim of the posterior articular facet. The ACDLs are oriented similarly towards the anterior articular facet. The neural canal is ovate, both anteriorly and posteriorly, but this is influenced by the compression of the vertebra. The apex of the neural canal is dorsally with the long axis oriented dorsoventrally. The TPRL is similar in morphology as in Cd?4-6. The prezygapophyses are poorly preserved. However, based on photographs taken during the preparation, the right prezygapophysis was partially present. It projected anterodorsally, had a rounded end, and was quite long compared to the prezygapophyses seen in *Diplodocus carnegii* (Hatcher, 1901, plate IX). This prezygapophysis, however, was severely damaged, both dorsally and anteriorly, and it was lost during the mounting process. As currently mounted, the right prezygapophysis is almost entirely broken off, now consisting only of a small bony protrusion. The left prezygapophysis consists of a partially broken facet, which projected anterodorsally, and is roughly elliptical in shape. Like Cd?4-6, the transverse processes fuse medially to the posterolateral side of the prezygapophysis. From the prezygapophyses, two SPRLs extend dorsally onto the lateral side of the neural spine. Posteriorly, partially broken V-shaped, laterally concave postzygapophyses are preserved. They are very large, nearly half the neural spine length, although they do not extend as far dorsally as in *Brontosaurus* (Ostrom and McIntosh, 1966). Only the posterodorsal margin of both postzygapophyses is damaged. Ventral to the postzygapophyses, no clear hyposphenal ridge is present, which is a result of damage. Dorsally, two SPOLs extend onto the posterior, and more dorsally, lateral side of the
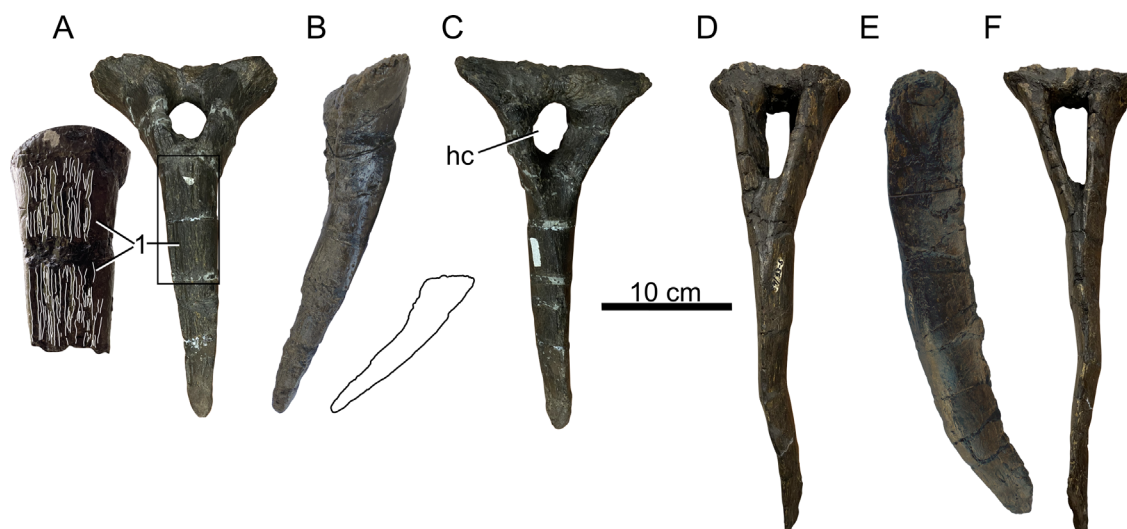
FIGURE 25. Chevrons of *Ardetosaurus viator* MAB011899. First chevron in A) anterior, B) right lateral and C) posterior view. Third chevron in D) anterior, E) left lateral, and F) posterior view. Note the (1) vertical striations on the anterior surface of the blade in Figure A. The rectangle in Figure A shows the chevron portion shown left of the chevron, wherein the striations are highlighted in white. Figure B includes the outline of the first chevron angled as it would be in vivo. Figure E already shows the third chevron angled as in vivo. Abbreviation: hc, haemal canal.

neural spine. Like Cd?4-6, the distinct, triangular, and ventrally open fossae are present lateral to the postzygapophyses and medial to the PODLs. The neural spine is inclined posteriorly, significantly more so than in Cd?4-6. However, the stronger inclination in Cd?5-8 might be affected by the oblique compression. The remaining neural spine morphology is identical to Cd?4-6, with fusing SPRLs and SPOLs, a rugose PRSL and POSL, of which the latter projects beyond the dorsal margin of the neural spine tip, and the lateral spinal laminae extend to the top of the neural spine.

Chevrons (Figure 25, Table 6)

Two anterior chevrons were found close to the anterior-most caudal centra. Although they were not found in direct articulation with the caudal centra, the first chevron (G34/93-8) was found beneath Cd1. The second chevron (G34/93-5) was found beneath Cd3. They are described as if they are in anatomical connection with the caudal vertebrae.

Both chevrons are 'Y-shaped', with a bony crus closing the dorsal side, similar to most flagellicaudatans (Otero et al., 2012). The haemal canal enclosed by both chevrons is oval, with the dorsoventral axis being longer than the transverse axis. However, there are clear differences between both chevrons. The first chevron (Figure 25A-C) has a flattened anterior surface along the blade of the chevron. On this surface, many dorsoventral ridges are present extending parallel to each other; these ridges form a rugose surface for ligament attach-

TABLE 6. Measurements of the chevrons of *Ardetosaurus viator* MAB011899 (in mm).

Dimension	1	3
Proximodistal length	251	330
Proximal transverse width	134	107
Haemal canal greatest height	42	66
Haemal canal greatest width	29	35
Proximal anteroposterior length	45	54

ment, and fade at the ventral-most part of the anterior surface of the chevron. Based on *Alligator*, a fascial layer was attached to the anterior surfaces of the chevrons, including the first, which connected the chevron to the cloaca, also serving as an attachment point for the *M. caudofemoralis longus* (Wilhite, 2023, unpublished data). The ridges are dorsoventrally interrupted by several breaks (Figure 25A), as the chevron was broken into multiple parts; these breaks are restored using acrylic resin. The ventral part of the blade tapers anteroposteriorly. In lateral view, the blade is flat. Based on the morphology and the fact that it was found beneath Cd1, as well as comparisons with FMNH P25112, confirms that this chevron is most probably the first chevron in the series. The second chevron (Figure 25D-F) is slightly larger, and the haemal canal enclosed is shaped more like a trapezium, with rounded corners. The bony crus is flat and almost horizontal. The blade is morphologically similar to most diplodocid chevrons: thin
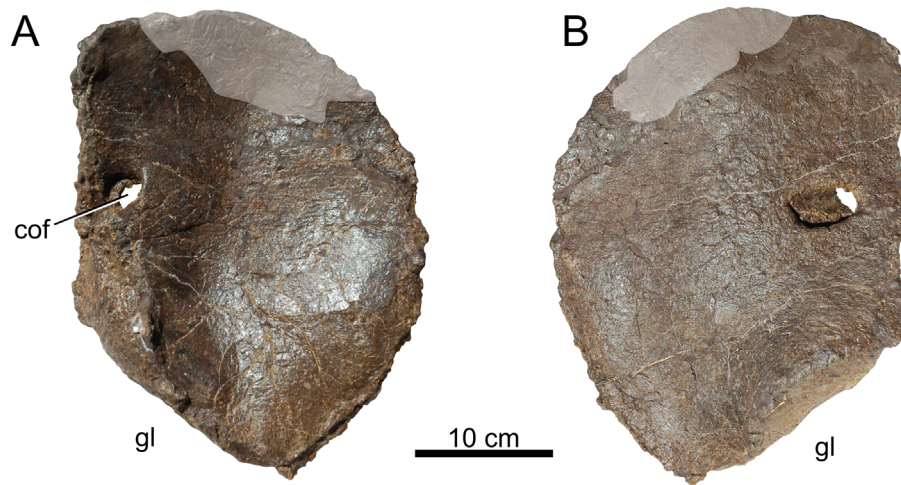
FIGURE 26. Left coracoid of *Ardetosaurus viator* MAB011899. Coracoid in shown in A) medial and B) lateral view. White shaded areas indicate reconstructed parts. Abbreviations: cof, coracoid foramen; gl, glenoid.

mediolaterally, and anteroposteriorly wide, tapering ventrally. Unlike e.g., *Brontosaurus* (Ostrom and McIntosh, 1966), the posterior side of the blade does not bear a stepped expansion of the blade. This chevron is, as it was found beneath Cd3, the third chevron in the series.

APPENDICULAR SKELETON

Forelimb Element

Left coracoid (Figure 26, Table 7). The coracoid is described with the articular surface with the scapula parallel to the vertical. The coracoid was found (coordinate: G35/87-1, not drawn in any of the quarry maps made by the SMA) between MAB011899 and the specimen nicknamed 'XL', close to a bone, likely a pubis, which was assigned to XL by the SMA. Several lines of evidence connect this coracoid to MAB011899, rather than XL. First, a single scapula appears to have been assigned to XL, located in the quarry sections G41/88 and G41/89, which may or may not have had an associated coracoid. However, based on the quarry map (Figure 2), a coracoid foramen is drawn on the west end of the drawn scapula, indicating that a coracoid was likely fused to the scapula of XL. If this coracoid foramen is not a true foramen, but a possible large crack which was drawn by the SMA, a coracoid is drawn in quarry sections G85/45 and G86/45, which would be more likely to be the coracoid of XL. Second, the coracoid of MAB011899 is smaller than that of *G. pabsti* (Tschopp and Mateus, 2017). XL, however, is considered to be the largest sauropod from the Howe-Stephens Quarry, much larger than both

TABLE 7. Measurements of the coracoid of *Ardetosaurus viator* MAB011899 (in mm).

Dimension	
Proximodistal length	338
Dorsoventral height	387
Scapula-coracoid articular length	276
Longest diameter glenoid	174
Transverse width glenoid	87

MAB011899 and *Galeamopus pabsti*. It would therefore be highly unlikely that the coracoid was part of XL. Third, XL was found in a layer above MAB011899, causing a different preservation (Ayer, 2000), which is supported by the crumbly nature of the bones of MAB011899, including the coracoid. Because the coracoid is closer to MAB011899, is quite small, and has a different preservation, this coracoid can be relatively safely assigned to MAB011899.

The coracoid was not fused with the scapula, as there are no signs of breakage on the coracoid where it articulated with the scapula. Parts of the dorsal surface have broken off but have been restored for mounting purposes (Figure 26). The outline of the coracoid is semi-circular. The outer margin of the coracoid is rough. The anterior margin curves slightly medially. In anterior view, the coracoid is slightly concave medially. In lateral view, the enclosed coracoid foramen is oval, oriented anterodorsally posteroventrally. Medially, the foramen is more circular. The glenoid surface is teardrop-shaped and transversely expanded in the middle. On both ends, the glenoid surface tapers

into two sharp points, whereby the posterodorsal end transitions into the articular surface with the scapula. The anteroventral end transitions into the anterior margin of the coracoid.

Hindlimb Elements

Left ilium (Figure 19, Table 8). The ilium is described as it is oriented in its in vivo position. It is preserved in its entirety. The preacetabular process is pointed and directed anterolaterally in dorsal view with an approximate angle of 30° relative to the body axis. The ventral surface of the anterior lobe of the ilium extends relatively straight towards the pubic peduncle and forms an obtuse angle with the anterior surface of the peduncle. The dorsal margin of the ilium is round anteroposteriorly in lateral view and is highest above the posterolateral margin of the pubic peduncle. The dorsal margin ends, in lateral view, in a pointed, postacetabular process, which has a rough posterior surface. The ischial peduncle, which is present anteroventrally to the postacetabular posterior margin, is distinct and faces posteroventrally. The pubic peduncle is heavily compressed dorsoventrally. The peduncle as preserved is a small extension ventral to the iliac blade. The compression resulted in the ventral-most point of the peduncle forming a flat disc, of which most projects anteriorly and laterally. The base of the peduncle is angled more than 90° from the ventral surface of the preacetabular process. Due to the number of cracks on the surface of the iliac blade, it is difficult to assess if there are any

TABLE 8. Measurements of the left ilium of *Ardetosaurus viator* MAB011899 (in mm).

Dimension	
Proximodistal length	930
Anteroposterior length pubic peduncle	70
Mediolateral width pubic peduncle	80
Preacetabular process length	412

distinct fossae on the surface, however, the triangular fossa, formerly considered to be an autapomorphy of *Cetiosaurus oxoniensis* (Upchurch and Martin, 2003), present in most diplodocines (Hatcher, 1901; McIntosh, 2005; Lucas et al., 2006; Lovelace et al., 2007; Tschopp and Mateus, 2017), is absent dorsal to the pubic peduncle.

Pubes (Figure 27, Table 9). Both pubes are nearly complete, with only the right pubis lacking part of the anterodorsal part of the iliac peduncle including the ambiens process. They are described with the long axis of the shaft parallel to the vertical. The obturator foramen is completely enclosed in both pubes, oval in the left pubis, and slightly triangular in the right pubis, and in both elements, it is located above the midline of the ischial articular surface. The ischial articular surface is concave medially. Ventral to the ischial articular surface, the pubic surface sensu Osborn and Mook (1921), which form the pubic apron (Wilhite, 2003), ends ventrally in a hook-like projection, whereby the pubic surface is not confluent with the rest of the shaft. A projection is also present in e.g., *Camarasaurus*
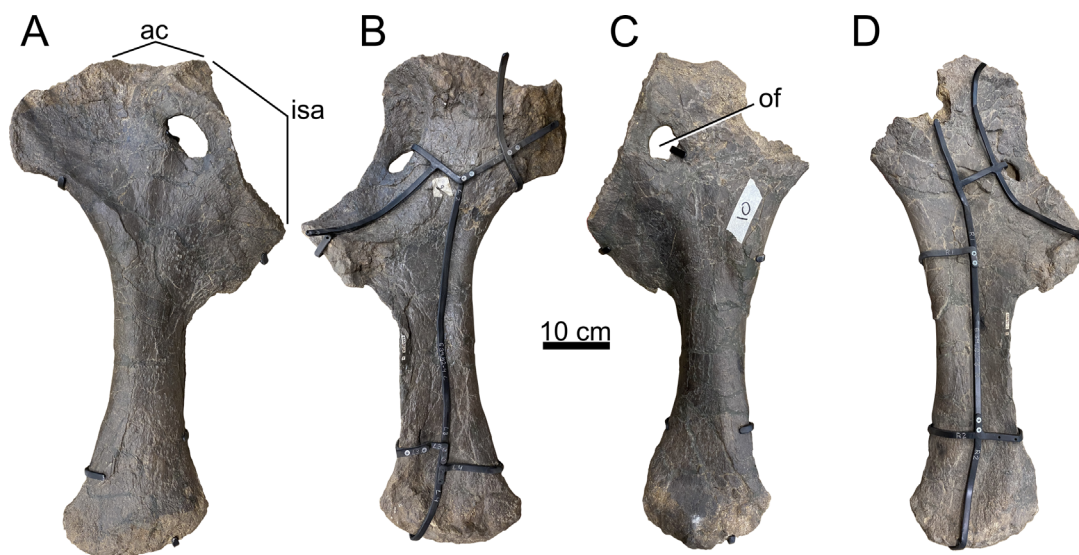

FIGURE 27. Pubes of *Ardetosaurus viator* MAB011899. Left pubis is shown in A) lateral and B) medial view. Right pubis is shown in C) lateral and D) medial view. Abbreviations: ac, acetabular surface; isa, ischial articular surface; of, obturator foramen.

TABLE 9. Measurements of the pubes of *Ardetosaurus viator* MAB011899 (in mm).

Dimension	L	R
Proximodistal length	730	740
Mediolateral minimum shaft width	55	53
Minimum anteroposterior shaft length	123	106
Proximal anteroposterior length	328	
Distal anteroposterior length	224	196
Maximum proximal mediolateral width	120	
Ischial articulation surface length	278	265
Acetabular articulation surface length	159	

supremus AMNH FARB 5761/Pb.1 (Osborn and Mook, 1921) and *Supersaurus* BYU 725-12424 (Lovelace et al., 2007), however, in these specimens the projection is not hook-like, but more rounded. This part of the shaft tapers distally. The ambiens process present on the left pubis is evident but shows no sign of a protruding hook-like structure as that seen in, e.g., *Diplodocus carnegii* (Hatcher, 1901). The pubes are elongated, with the posteroventral surface nearly straight towards the distal end of the pubes. The distal end is rounded,

rugose, and projects slightly anteriorly. The anterior edge of the shaft is smooth, slightly concave, ending almost horizontally as the ventral surface of the ambiens process.

Ischia (Figure 28, Table 10). The ischia are nearly complete and distally fused, and therefore figured together (Figure 28). They are described with the long axis of the shaft parallel to the horizontal. Parts of the articular surfaces have suffered damage. The proximal sections of the ischia are concave medially and convex laterally. The articular surfaces, both the iliac peduncle and the pubic articular surface, are rugose. The pubic articular surface of the right ischium is pushed laterally. The acetabular surface is distinctly concave, and not flat as seen in *Galeamopus pabsti* (Tschopp and Mateus, 2017). The acetabular surface and the pubic articular surface are compressed laterally.

Both the ventral and dorsal margins of the shaft are parallel to each other proximodistally. At the base of the shaft, a fossa occurs on the dorsolateral surface. This fossa is elliptical, and rugose; these rugosities extend proximally outside the fossa. Therefore, both fossae and muscle scars are present in the ischia of MAB011899. The ventral margins of the shafts are relatively straight from
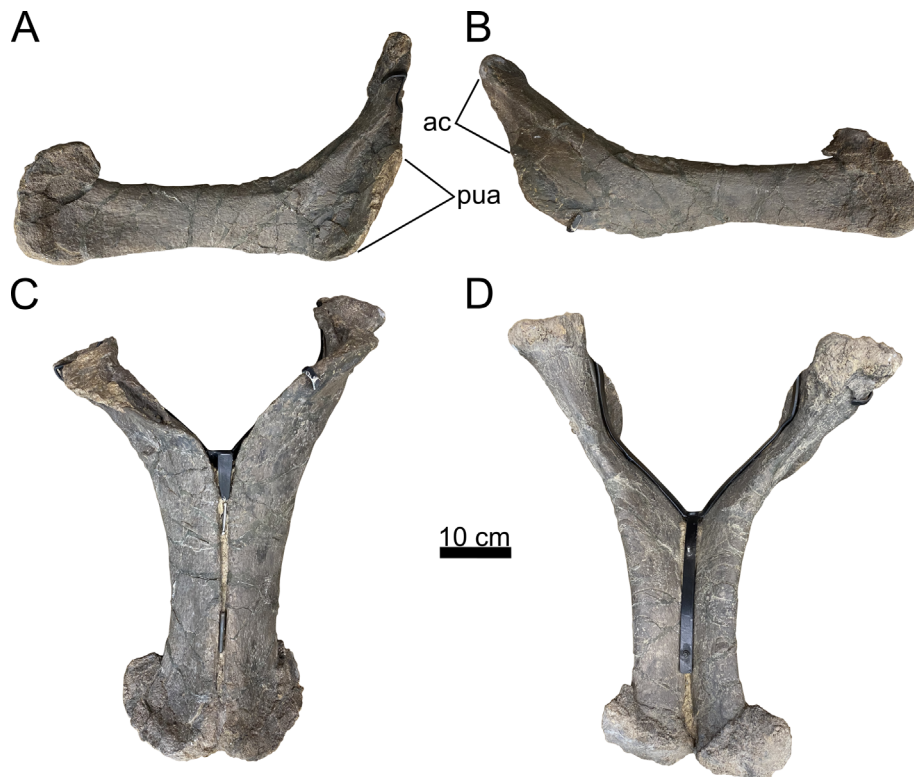

FIGURE 28. Ischia of *Ardetosaurus viator* MAB011899. Ischia are shown in A) right lateral (left ischium cut out), B) left lateral (right ischium cut out), C) ventral, and D) dorsal view. Abbreviations: ac, acetabular surface; pua, pubic articular surface.

TABLE 10. Measurements of the ischia of *Ardetosaurus viator* MAB011899 (in mm).

Dimension	L	R
Proximodistal length	553	490
Mediolateral minimum shaft width	44	40
Minimum anteroposterior shaft length	129	107
Proximal anteroposterior length	295	375
Distal anteroposterior length	194	193
Maximum mediolateral width	88	105
Pubic articulation surface length	130	203
Acetabular articulation surface length	196	190

the pubic articular surface towards the distal end of the shaft. The distal end expands both transversely and dorsoventrally/posterodorsally. In posterior view, the distal shafts are oval shaped, rugose, and fused in an obtuse, V-shaped angle. This morphology is similar to *Brontosaurus excelsus* (Ostrom and McIntosh, 1966, plate 67), except for the triangular shape being expanded in all directions and more rounded. The dorsal margin of the distal end of the shaft projects dorsally, and is not confluent with dorsal edge of the shaft, unlike *Diplodocus*

(Hatcher, 1901; Lucas et al., 2006) or *Apatosaurus* (Gilmore, 1936), in which this distinct dorsal expansion is absent.

Femur (Figure 29, Table 11). Originally, a complete femur was excavated from the quarry (Figure 2). However, this femur was part of the bones sent to Münchehagen. Subsequent exposure to fire and water damage caused the femur to fall apart, whereby some parts of the femur completely disintegrated. The femoral head, distal condyles and part of the distal shaft are still preserved, with element in the mounted skeleton reconstructed based on other diplodocid femora for mounting purposes. A length for the complete femur is provided in Waskow (2019) as 1344 mm, and the femur is supposedly figured as SMA 0013 (the original specimen number of MAB011899) in Woodruff et al. (2017), but both the measurement and the figure are not of MAB011899, but of SMA 0086 'David', which was found in the northern part of the quarry (Figure 2). A femur length of approximately 1300 mm can be calculated from the quarry map, which would imply, combined with the measurements of Table 11, a rather gracile femur (robustness index is 0.19, sensu Wilson and Upchurch (2003)). Although cal-
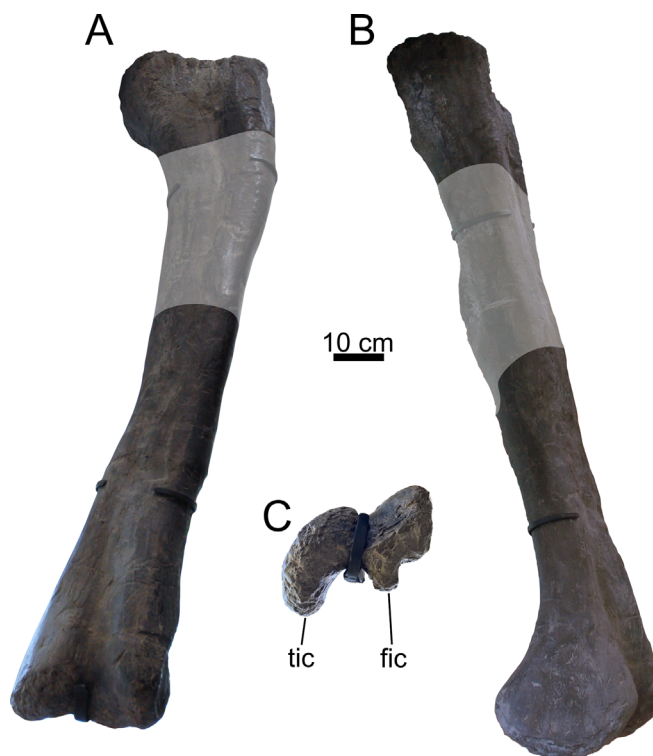

FIGURE 29. Left femur of *Ardetosaurus viator* MAB011899. Femur is shown in A) anterolateral, B) anteromedial, and C) distal views. Femur could be photographed only from the mount during the mounting process, hence the awkward position and angles. White shaded areas indicate reconstructed parts. Abbreviations: fic, fibular condyle; tic, tibial condyle.

TABLE 11. Measurements of the hindlimbs of *Ardetosaurus viator* MAB011899 (in mm).

Dimension	Femur	Tibia	Fibula
Proximodistal length		915	
Mediolateral width midshaft	167	133	79
Anteroposterior depth midshaft	82	67	
Proximal mediolateral width	310	290*	
Distal mediolateral width	260	188	77
Proximal anteroposterior depth	200	140	
Distal anteroposterior depth	179	112	148
Minimum circumference	438	332	220

Notes: Asterisk indicates estimate.

culating femoral length from the quarry map has considerable drawbacks in accuracy, the obtained femoral length is certainly a reasonable estimate given that the femora of SMA 0086 and MAB011899 are approximately the same size. The femur is described with the long axis vertical.

Both the femoral head and the distal condyles have rugose surfaces. The femoral head is separated medially from the shaft. The ventral surface of the head is confluent ventrally with the shaft, and not stepped as seen in e.g., *Dicraeosaurus* (Janensch, 1961, p. 208). The femoral head is transversely wider than anteroposteriorly. From the three pieces, it is clear that the shaft tapers distally from the femoral head and widens again closer to the distal end. The shaft is elliptical, and twice as mediolaterally wide as anteroposteriorly thick. There are no clear indications of severe anteroposterior compression, thus this elliptical outline is more extreme than seen in *Diplodocus* (Hatcher, 1901) or *Galeamopus* (Tschopp and Mateus, 2017). The distal condyles are pronounced posteriorly from the posterior side of the shaft, especially the tibial condyle, which is shifted posteriorly, like NSMT-PV 20375 (Upchurch et al., 2004b). This projection is more pronounced due to shear but is certainly partly biological.

Tibia (Figure 30, Table 11). The tibia of MAB011899 was found next to the femur and will be described with the shaft parallel to the vertical, whereby the cnemial crest is placed to the right in anterior view. The tibia is nearly complete and has only suffered minor damage to its posterior surface, both proximally and distally, and is anteroposteriorly compressed as a result of deformation. Additionally, some burn marks are visible from the fire in Münchehagen, mainly at the proximal end. The proximal end is wider compared to the distal end, and has a subtriangular outline, with the cnemial crest strongly expanding. Presence of a second crest sensu (Bonaparte et al., 2000) cannot be assessed due to the posterolateral damage of the tibia. The distal end is concave, with the posterior part projecting further distally compared to the anterior part of the articular facet, creating the step-like morphology for the insertion of the astragalus. A fibular trochanter is present, posteromedial to the ventral half of the cnemial crest.

Fibula (Figure 31, Table 11). Only the left fibula is preserved, missing the proximal part. It is described with the long axis vertical. The fibula is slender in anteroposterior view. In lateral view, the fibula tapers towards midlength, and expands again thereafter towards the distal articular surface. In posterior view, the lateral side of the fibula is slightly concave. The insertion of the *M. iliofibularis* is present just above the narrowest part of the fibula, but its relative position along the bone cannot be accurately determined due to the missing proximal part. The distal articular surface is oval, rugose, and anteroposteriorly wider than mediolaterally.

DISCUSSION

Comparison with Other Diplodocines

MAB011899 can be excluded from being interpreted as a non-neosauropod eusauropod or macronarian sauropod by having a different dorsal and sacral vertebral count, and/or the bifurcation of the neural spine of both the cervical and anterior/middle dorsal vertebrae (Upchurch, 1998; Wilson and Sereno 1998; Wedel and Taylor, 2013; Tschopp et al., 2015a). Inclusion in Diplodocoidea is supported by having short cervical ribs, an exclusive synapomorphy sensu Tschopp et al. (2015a) for this clade (Wilson, 2002; Tschopp et al. 2015a). MAB011899 can be identified as part of Diplodocidae based on the presence of 10 dorsal vertebrae (Huene, 1929; Upchurch et al., 2004a). The presence of 14/15 cervical vertebrae similarly is a diplodocid feature (Huene, 1929; Tschopp et al., 2015a), assuming a presacral vertebral count of 25 for diplodocids (McIntosh, 2005), which, although ambiguous, is likely in the case of MAB011899 based on a dorsal vertebral count of 10. However, MAB011899 also lacks several synapomorphies for Diplodocidae provided by previous phylogenetic analyses. Only synapomorphies that can be tested in MAB011899 are discussed here. Wilson (2002) and Whitlock (2011) recovered dorsally divided CPRLs in middle and posterior cervical vertebrae as a distinct cervical character for Diplodocidae,
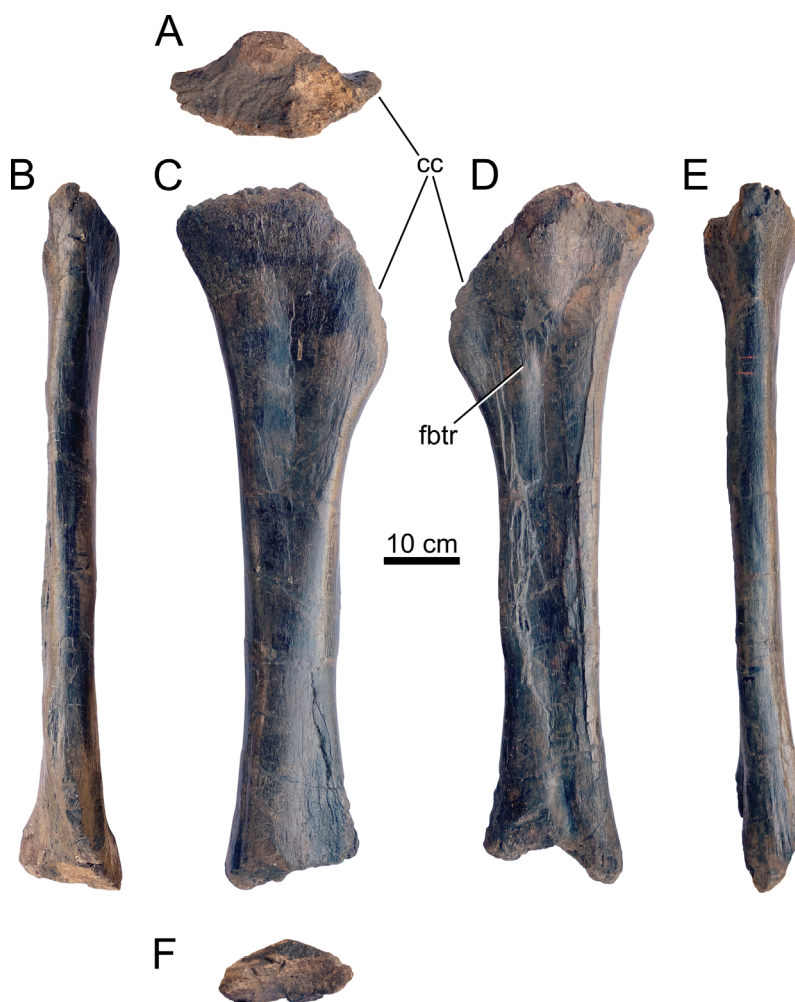
FIGURE 30. Left tibia of *Ardetosaurus viator* MAB011899. Tibia is shown in A) proximal, B) lateral, C) anterior, D) posterior, E) medial, and F) distal views. Abbreviations: cc, cnemial crest; fbtr, fibular trochanter.

which in MAB011899 remain single except for the first dorsal vertebra. This character was not recovered as a synapomorphy by Tschopp et al. (2015a), because *Supersaurus* also lacks dorsally divided CPRLs. We exclude the possibility here of ontogenetic influence for the single CPRLs, because MAB011899 is identified as an adult individual, and the first dorsal vertebra does show this feature. Wilson (2002) listed the presence of PCPLs in mid- and posterior dorsal vertebrae as a diplodocid synapomorphy, but this lamina is also present in rebbachisaurids (Tschopp et al., 2015a). Whitlock (2011) listed the presence of ventral sulci in the cervical vertebrae as another diplodocid synapomorphy; this sulcus rarely occurs in apatosaurines (Tschopp et al., 2015a), whereas it is present in most diplodocines including MAB011899. A median tubercle in the posterior cervical and anterior dorsal vertebrae is present in MAB011899, but

not recovered as a synapomorphy in Tschopp et al. (2015a), because this feature may be (ambiguously) synapomorphic for flagellicaudatans, although not recovered as such.

MAB011899 can be excluded from Apatosaurinae based on its slender cervical vertebrae, and its cervical ribs that do not project far ventrally (Gilmore, 1936; Upchurch et al., 2004b). The assignment of MAB011899 to Diplodocinae is supported by the dorsoventrally elongate coel on the lateral surface of posterior cervical neural spines, as well as several characters shared by most diplodocines, which are, however, not exclusive to the clade. These traits are transversely convex prezygapophyseal articular facets in the middle and posterior cervical vertebrae (incorrectly stated as 'flat' by Tschopp et al. (2015a, p. 249), the presence of triangular aliform processes in the middle and posterior dorsal vertebrae, the presence of a

FIGURE 31. Left fibula of *Ardetosaurus viator* MAB011899. Fibula is shown in A) lateral, B) anterior, C) medial, D), posterior view. The proximal end is lacking. The number '13' attached with tape to the lateral surface of the fibular is an old catalogue number of the Oertijdmuseum. Abbreviation: tilf, *M. iliofibularis* trochanter.

muscle scar on the proximal surface of the ischia, and a subtriangular proximal surface of the tibia (Tschopp et al., 2015a). Although MAB011899 lacks some features diagnostic for diplodocids, such as the dorsally divided CPRLs in mid- and posterior cervical vertebrae and the presence of distinct pleurocoels in anterior caudal vertebrae, which herein are treated as reduced, it is clear based on most features that MAB011899 (Figure 32) should be placed within Diplodocinae.

Below, MAB011899 will be compared to all currently valid diplodocines, *Barosaurus lentus* Marsh, 1890, *Diplodocus carnegii* Hatcher, 1901, *Diplodocus hallorum* (Gillette, 1991), *Galeamopus hayi* (Holland, 1924), *G. pabsti* Tschopp and Mateus, 2017, *Kaatedocus siberi* Tschopp and Mateus, 2013, *Leinkupal laticauda* Gallina et al., 2014*, Supersaurus lourinhanensis* (Bonaparte and Mateus, 1999)*, Supersaurus vivianae* Jensen, 1985, and *Tornieria africana* (Fraas, 1908). MAB011899 will also be compared with *Amphicoelias altus* Cope, 1877, because this species has

been recovered in various positions within Diplodocidae (Tschopp et al., 2015a; Tschopp and Mateus, 2017; Mannion et al., 2021).

Amphicoelias altus. Several characteristics can be used to distinguish MAB011899 from *A. altus.* The latter can be recognized by the distinct shape of the lateral projections on the apex of posterior dorsal neural spines, as well as the subcircular cross section of the femoral shaft (Mannion et al., 2021). The dorsal projections, originating from the SPDLs, independent from the more common aliform processes, are absent in MAB011899. The cross section of the femoral shaft in MAB011899 is highly elliptical, uniquely so among diplodocines, and rare among apatosaurines. Additionally, *A. altus* does not show the dorsoventral bony struts in the pleurocoels of dorsal vertebrae, has more dorsoventrally oval posterior articular surfaces, compared to the more transversely oval articular surfaces in MAB011899, and has a distinctive thin base of the neural spine compared to MAB011899. *A. altus* also lacks all potential autapomorphies of

FIGURE 32. Life reconstruction of *Ardetosaurus viator* MAB011899. Illustration by Ole Zant.

Ardetosaurus viator in the elements preserved in both type specimens.

Barosaurus. Although several characteristics between MAB011899 and *Barosaurus* are shared, such as the cervical EI, the position of the postzygapophyses relative to the cotyle edge and the presence of multiple laminae in the PRCDF (Tschopp et al., 2015a, figure 38), notable differences are present between YPM VP.000429 and MAB011899. All differences discussed here differ also between MAB011899 and AMNH FARB 6341, another specimen referred to *Barosaurus* (McIntosh, 2005). Both YPM VP.000429 and MAB011899 are considered sexually and skeletally mature specimens (Waskow 2019), but MAB011899 is significantly smaller compared to *Barosaurus*. *Barosaurus*, according to McIntosh (2005), has a dorsal vertebral count of nine, whereas other diplodocines including MAB011899 have ten dorsal vertebrae. Additionally, *Barosaurus* has a distinctly low neural spine in posterior cervical vertebrae, notches on the prezygapophyseal rami creating additional anterior projections on the lateral edge of the rami, which is an extension of the PRDL, and a posteriorly bifurcated ventral keel (Lull, 1919; Tschopp et al., 2015a). Lull (1919) notes on page 11 that the pleurocoels of YPM VP.000429 are similar in depth as those of *Diplodocus*, but not nearly as extensive anteroposteriorly as in *Diplodocus*. Lateral pneumatization in

MAB011899 is similarly extensive as in *Diplodocus* (Hatcher, 1901), thus differing from *Barosaurus*. The prezygapophyseal rami are quite wide mediolaterally in YPM VP.000429, something not seen in MAB011899, wherein it is more similar to *Kaatedocus*. Another significant difference is the broad diapophyseal 'wing' of *Barosaurus*, which results in a nearly anteroposteriorly straight PRDL in dorsal view. In MAB011899, as well as in *Kaatedocus* and (possibly) *Diplodocus* (Hatcher, 1901; Tschopp and Mateus, 2013), the PRDL curves further posterolaterally to reach the diapophyses and the cervical rib loops. Other obvious differences between the cervical vertebrae of YPM VP.000429 and MAB011899 include the dorsal bifurcation of the CPRLs, which are absent in MAB011899, and the presence of foramina piercing the POCDF and SPOF in MAB011899. There are several differences between the dorsal vertebrae of YPM VP.000429 and MAB011899: in MAB011899, the hyposphene is supported by two oblique laminae in posterior middle and posterior dorsals, only single PCPLs are present, the PACDFs are ventrally open, and the neural spines are anteriorly inclined.

Diplodocus. There is no overlap between the elements of MAB011899 and YPM VP.001920 *(Diplodocus longus),* and thus no comparison can be made. This is also true for *Diplodocus lacustris* (YPM VP.001922), which consists only of a set of teeth (see Tschopp et al. (2015a) for revision of the

material), and is currently considered to be a nomen dubium. Therefore, comparisons can only be made with the other two, more complete species of *Diplodocus*: *D. carnegii* (Hatcher, 1901) and *D. hallorum* (Gillette, 1991; Lucas et al., 2006; Tschopp et al., 2015a). The differences between both species of *Diplodocus* and MAB011899 are numerous. The posterior cervical vertebrae of *Diplodocus* (for *D. carnegii* based on CM 84, see Hatcher, 1901; for *D. hallorum*, based on scores and personal observations of DMNS 1494) can be distinguished from those of MAB011899 because the former have SPRLs that remain vertical throughout their anterior extend, rather than laterally inclined. *Diplodocus* lacks the foramina connecting the POCDF and SPOF, shows only a single lamina present in the PRCDF, has CPRLs which are dorsally divided, forming two rami, lacks anteriorly bifurcating PCDLs, shows accessory spinal laminae posterior to the SPRL, present within the SDF, and the lacks a PRSL. Additionally, MAB011899 shows an EI for CV13 and CV14 of 3.1 and 2.4, respectively. Given that cervical vertebrae become dorsoventrally taller than anteroposteriorly long in more posterior elements throughout the sequence in diplodocines (Hatcher, 1901; Lull, 1919; McIntosh, 2005; Tschopp and Mateus, 2013), we can assume that CV11 and CV12 would have been more elongate than CV13, so that the majority of posterior cervical vertebrae of MAB011899 would have had an EI of >3, which is higher than the ratios seen in *Diplodocus.* Furthermore, the last two cervical vertebrae in *Diplodocus*, which also applies to *Barosaurus* and *Kaatedocus* (McIntosh, 2005; Tschopp and Mateus, 2013), usually show the steepest decline in EI, thus further supporting the fact that MAB011899 likely had more elongate posterior cervical vertebrae compared to *Diplodocus*, similar to *Barosaurus* and possibly *Tornieria* (Remes, 2006). Finally, the postzygapophyses in MAB011899 terminate in front of the cotyle rim, a characteristic especially prominent in *Giraffatitan* (Janensch, 1950), but also present in *Barosaurus* (McIntosh, 2005, figure 2.1). In MAB011899, the difference is small (not more than 4 cm) and difficult to see due to deformation, but it compares well with CV13 and CV14 in McIntosh (2005), in which the difference equals roughly 4-5 cm (distance was measured from McIntosh, 2005, figure 2.1). Similarly, vertebra 'A' of BYU 601-20815, possibly *Barosaurus* (Taylor and Wedel, 2016), also shows this 4-5 cm difference, albeit that this vertebra may be a mid-cervical vertebra. This difference can thus be assumed to be valid,

and thus a notable difference between MAB011899 and *Diplodocus.*

Additionally, there are numerous differences between the dorsal vertebrae of MAB011899 and *Diplodocus*: both CM 84 (the holotype of *D. carnegii*) and NMMNH 3690 (the holotype of *D. hallorum*) show a gradual anteroposterior pattern of metapophyseal fusion, whereas MAB011899 shows a relatively abrupt pattern, which cannot solely be explained by ontogenetic differences, as all three specimens are assumed to be adult (Waskow, 2019). Neither CM 84 and NMMNH 3690 show infradiapophyseal foramina. Both *Diplodocus* species show the continuous presence of a midline cleft in the posterior dorsal and sacral neural spines, which is absent in MAB011899, and the ratio between centrum length and cotyle height is different between *Diplodocus* and MAB011899 (this will be further discussed below in relation to the height of the vertebrae). Figure 2 of Herne and Lucas (2006) shows that the posterior dorsal vertebrae are of NMMNH 3690 are distinctly different from those of MAB011899. There are substantially more laminae present on the lateral side of the vertebra from each of the neural arch landmarks sensu Wilson (1999), as well as a more squared neural spine, which is relatively low compared to the remainder of the vertebra. Caudal vertebral characteristics are primarily important for *D. hallorum*, but differences can be found between both species of *Diplodocus* (Hatcher, 1901; Gillette, 1991; Lucas et al., 2006) and MAB011899. Differences between both species of *Diplodocus* and MAB011899 include the absence of the lateral processes on the lateral side of the apex of the neural spines, which are very prominent in MAB011899; the more procoelous centra in *Diplodocus*; and the distinct dorsally projecting POSL in MAB011899, compared to the notched neural spines of *Diplodocus*. The latter is also evident in the sacral spines of MAB011899, whereas NMMNH 3690 clearly shows notched, laterally expanded neural spine apices. In the neural spines of the dorsal vertebrae, the dorsal ends of the POSLs of NMMNH 3690 are concave transversely (Herne and Lucas, 2006; Lucas et al., 2006), which is a unique feature amongst diplodocines.

Diplodocus hallorum, formerly *Seismosaurus halli* Gillette, 1991, could originally be diagnosed based on characteristics in the pubis, ischium, caudal vertebrae and chevrons (Gillette, 1991). As discussed in Lucas et al. (2006) and Tschopp et al. (2015a), the robustness of the pubis is difficult to quantify, and may represent variation within *Diplod-*

ocus, such that the more anteroposteriorly expanded shaft of *D. hallorum* compared to *Ardetosaurus viator* is simply due size differences of NMMNH 3690 and MAB011899. Moreover, both species of *Diplodocus* have a strongly developed, hooked ambiens process, which projects parallel to the shaft, whereas in MAB011899, the process is not nearly as developed. Additionally, MAB011899 has a more distinct anteriorly concave ischial articular surface compared to *D. hallorum*, which in NMMNH 3690 is less concave anteriorly. Comparisons of the caudal vertebrae of NMMNH 3690 and MAB011899 beyond the neural spines are not possible, as the remainder of the arches and centra remain unprepared. The chevrons are very similar, apart from the distal ends of the blades. In lateral view, the distal end of the anterior chevron of NMMNH 3690 is petal-shaped, expanding both anteriorly and posteriorly. In MAB011899, however, the distal end of the blade of either the first or third chevron continues to taper, and shows no expansion of the distal end.

Like *Diplodocus hallorum*, *Diplodocus carnegii* possesses specific traits which differ from MAB011899. The most recent diagnosis of this species is provided in Tschopp et al. (2015a), however, only a single autapomorphy of the recovered set can be compared to *Ardetosaurus viator*. In posterior dorsal vertebrae of CM 84, the SPOLs bifurcate ventrally near the postzygapophyses; this does not occur in MAB011899. Additional differences between *D. carnegii* and *A. viator* include: the anteriorly inclined posterior cervical neural spines in *D. carnegii* (Hatcher, 1901, plate III, CV12-15), which remain vertical in MAB011899, the presence of posterior projections on the cervical diapophyses in MAB011899, the capping of the SDF by a rugose horizontal ridge in the cervical vertebrae in *D. carnegii*, the dorsoventrally tall, invading pleurocoels in the dorsal vertebrae in *D. carnegii*, which are more restricted dorsoventrally in MAB011899, the ventrally divided SPOLs in the dorsal vertebrae in *D. carnegii* (recovered as autapomorphic in Tschopp et al. (2015a)), the double PCPLs in the dorsal vertebrae in *D. carnegii*, the large number of accessory laminae in the caudal 'wings' in *D. carnegii*, the lateroventral orientation of the 'wings', compared to the more lateral orientation in MAB011899, and the difference in the distal expansion of the caudal neural spines.

Galeamopus. Comparisons between MAB011899 and *Galeamopus* are possible, albeit mainly between *Galeamopus pabsti*, SMA 0011/NMZ 1000011 (see Demuth et al. (2022) for explanation

of the specimen numbers) and MAB011899, and not with HMNS 175. The latter specimen, the holotype of *G. hayi*, consists of a relatively complete skeleton (Holland, 1906; McIntosh, 1981; Tschopp et al., 2015a), and was named '*Diplodocus*' *hayi* by Holland (1924). However, no postcranial material has been described of *Galeamopus hayi*, so the comparison between MAB011899 and HMNS 175 is done based on photographs of the mount at the HMNS, as well as the scoring of the updated matrix of Tschopp et al. (2015a) and the mentions of the specimen in Tschopp and Mateus (2017). *Galeamopus* can be identified based on nine autapomorphies according to the analysis of Tschopp and Mateus (2017), some of which were also recovered in Tschopp et al. (2015a).

The TPOL in mid- and posterior cervical neural arches of *Galeamopus* does not project posteriorly, a unique feature within Diplodocinae, which is notably different from MAB011899. The second autapomorphy concerns the pubic peduncle, and its angle with the preacetabular lobe. Although the peduncle in MAB011899 is dorsoventrally compressed, the proximal-most part shows no indication of crushing compared to the rest of the ilium, and therefore it appears it can be measured with confidence. In MAB011899, the angle between the anterior side of the peduncle and the ventral margin of the preacetabular lobe exceeds 90° significantly, which is even more extreme compared to *G. pabsti* (Tschopp and Mateus, 2017, p. 84) and *G. hayi,* where the angle is roughly 90°, although the angle is difficult to measure in HMNS 175, which might thus also exceed 90°. The third autapomorphy concerns the 'second' cnemial crest on the tibiae of *Galeamopus*, which is probably absent in MAB011899. One additional autapomorphy is of interest, as the anterior dorsal centra in *Galeamopus* lose their strong opisthocoelous nature very rapidly anteroposteriorly. This does not occur in MAB011899, similar to *Diplodocus* (Hatcher, 1901, plate VII).

Tschopp and Mateus (2017) also list the autapomorphies for *Galeamopus hayi* and *Galeamopus pabsti* for the specific separation. The autapomorphies for *G. hayi* cannot be compared, because none of the elements with specific autapomorphies are preserved in MAB011899. However, some additional differences in morphology can be discussed, supporting the distinction of MAB011899 from *G. hayi*. Comparing the cervical vertebrae, no foramina can be observed in the POCDF of *G. hayi*. Additionally, a second PCDL can be observed ventral to the diapophysis in *G. hayi*. Fossae are

present in *G. hayi* posterolateral to the prezyga-pophyseal rami, similar to *Kaatedocus*. Contrary to *Barosaurus* and MAB011899, the postzygapophy-ses terminate on, or just posterior to the cotyle rim in *G. hayi*. The posterior-most cervical and anterior-most dorsal vertebrae of *G. hayi* show anteriorly inclined metapophyses, either based on the entire metapophyses, or in the case of the twelfth pre-sacral vertebra, based on the orientation of the SPRLs, as the apices appear to be reconstructed. Tschopp and Mateus (2017, p. 100) mention rounded neural spines in *G. hayi*, whereas in *G. pabsti* and MAB011899, they are laterally com-pressed. Finally, some additional differences can be observed in the pelvic region. There is a distinct fossa on the left ilium of *G. hayi*, which is absent in MAB011899. The SPDLs of the sacral neural spines converge towards the spine apex in *G. hayi*, whereas these laminae remain vertical in MAB011899, which is rare in diplodocines. Finally, there are differences between the distal ends of the ischia. It is impossible to assess the extent of medi-olateral compression in the ischia of *G. hayi,* but the right ischium appears relatively undeformed. The distal ends of the ischia of *G. hayi* have medio-laterally compressed, oval outlines in posterior view. In addition, they lack the extreme transverse 'stepped' expansion of the distal end, which is seen in MAB011899.

For *Galeamopus pabsti*, fourteen autapomor-phies were recovered, some of which can be com-pared between MAB011899 and SMA 0011/NMZ 1000011. The first comparable autapomorphy is the junction of the PCDL and PODL in the posterior cervical vertebrae. In *G. pabsti*, these laminae meet on the posterior face of the transverse processes, and not at the base of the process. Additionally, the PCDLs in *G. pabsti* bifurcate anteriorly, and although this does occur in MAB011899, it is not nearly as extreme as seen in *G. pabsti*. Although SMA 0011/NMZ 1000011 was sexually mature before death, no EFS was detected, and thus was probably not a skeletally mature specimen (Was-kow, 2019). However, re-fusion of the PCDLs in older specimens is unlikely, as exemplified by the skeletally mature YPM VP.000429 specimen (Lull, 1919; Waskow, 2019). The second autapomorphy for *G. pabsti* is the presence of foramina connect-ing the POCDF and SPOF, which is not shared with the other species in the matrix of Tschopp and Mateus (2017).

In *Galeamopus pabsti*, these foramina are present in CV4-10, but only in CV6-9 they are freed from matrix. It is therefore not certain that all of

these would open up to form foramina. In MAB011899, foramina are present in CV14, and most probably in CV13 as well, but the latter are obscured by reconstructions. These foramina thus appear more widespread amongst diplodocines, and may not be a specific autapomorphy for *G. pabsti*. A third autapomorphy of *G. pabsti*, unique within Diplodocinae, is the low EI for the posterior cervical vertebrae. This is opposite to MAB011899 and *Barosaurus*, which have strongly elongated vertebrae. The cervical vertebrae of *G. pabsti* are indeed relatively short, especially when CV13 and 14 of both specimens are directly compared. Fur-thermore, the proximal surface of the tibia of *G. pabsti* is autapomorphically rectangular, and even correcting for the obvious anteroposterior com-pression, it does not result in a similarly subtriangu-lar shape as that seen in MAB011899. There are several additional differences between *G. pabsti* and MAB011899. Notably absent are the posterior projections on the diapophyses in *G. pabsti*, the presence of dorsally bifurcated CPRLs in *G. pabsti*, the absence of the posteriorly projecting TPOLs in *G. pabsti*, the different offset of the postzygapophy-ses to the cotyle rim in *G. pabsti*, and the more anteriorly inclined metapophyses in the cervical vertebrae in *G. pabsti*. Additionally, differences occur in the dorsal vertebrae. The pleurocoels are dorsoventrally taller in *G. pabsti*, thereby invading the neural arch, and more triangular-shaped than in MAB011899. Aliform processes are absent in *G. pabsti*. The neural spine bases of the mid- and posterior dorsal vertebrae are much longer antero-posteriorly than wide mediolaterally in *G. pabsti*. Similar to *Galeamopus hayi*, the ilium of *G. pabsti* contains a triangular fossa dorsal to the pubic peduncle, which is absent in MAB011899. The femur cross section is, as already discussed previ-ously, more elliptical in MAB011899 compared to other diplodocines, including *G. pabsti*.

Kaatedocus. Comparing MAB011899 with *Kaate-docus* is hampered by the fact that all specimens currently referred to *Kaatedocus* lack post-cervical vertebrae as well as all appendicular bones. Hence, only the posterior cervical vertebrae can be compared. In these elements, *Kaatedocus* is diag-nosable based on rugose tuberosities on the anterodorsal corner of posterior cervical vertebrae, and transverse sulci posterior to the prezygapoph-yseal facets (Tschopp and Mateus, 2013). Neither are present in MAB011899. In addition, *Kaatedo-cus* shows, unlike most diplodocines including MAB011899, no evidence for a dorsoventrally elon-gate coel on the lateral side of the neural spines.

Kaatedocus also lacks a foramen connecting the POCDF and SPOF, present in both MAB011899 and *G. pabsti* (Tschopp and Mateus, 2013, 2017). The CPRLs are dorsally divided in *Kaatedocus*, as in most diplodocines. Although the SPRLs are laterally inclined in both individuals, in *Kaatedocus* they create distinct lateral fossae on the prezygapophyseal facet, which do not occur in MAB011899. The PRCDFs in *Kaatedocus* do not contain any accessory laminae, so the PRCDFs are undivided. The PCDLs in *Kaatedocus*, unlike those of MAB011899, do not bifurcate anteriorly.

The postzygapophyses of MAB011899 terminate in front of the posterior edge of the cotyle, a characteristic only shared with sauropods such as *Barosaurus* and *Giraffatitan*. The epipophyses of *Kaatedocus* are not pneumatized, but in MAB011899, they are distinctly pneumatized. This could, however, be influenced by ontogeny, because no fully skeletally mature specimen is known from *Kaatedocus* to date (Woodruff et al., 2017; Mannion et al., 2021). Finally, the neural spine morphology differs, with the distance between the metapophyses being very narrow in *Kaatedocus*, although this may be influenced by transverse compression. However, the vertebrae of MAB011899 are also influenced by transverse compression, in the case of CV13 possibly even more so than *Kaatedocus*, given the appearance of the cotyle and the diapophyses. Additionally, the cotyle of CV14 is relatively similar in outline as those of CV12-14 of *Kaatedocus*, but still shows a relatively wider gap between the metapophyses than those vertebrae. Assuming affinities with *Kaatedocus* (see Tschopp et al., 2015a), AMNH FARB 7530 is also a subadult specimen according to Woodruff et al. (2017). This specimen is represented by relatively similar material as SMA 0004/ NMZ 1000004. The vertebrae of AMNH FARB 7530 appear to lack the posterior projections on the diapophyses, as well as the complex lateral pneumaticity, although lateral pneumaticity may be ontogenetically influenced (Woodruff et al., 2017). The postzygapophyses are firmly positioned beyond the edge of the cotyle. The posterior cervical vertebrae of AMNH FARB 7530 lack the posteriorly projecting TPOLs, which are clearly present in MAB011899. The neural spines apices are substantially higher in the final two cervical vertebrae preserved of AMNH FARB 7530 relative to the postzygapophyses. SMA 0004/NMZ 1000004 also shows this feature. In MAB011899, the difference is minor in CV14, and in CV13, the neural spine tips are nearly aligned with the postzygapophyses.

No bifurcation of the PCDL appears present in AMNH FARB 7530, but the rugose tuberosities appear present, as well as the dorsally bifurcated CPRLs. It appears unlikely, based on these differences, that MAB011899 is synonymous with *Kaatedocus*, especially when these differences are summed with the below mentioned autapomorphies of MAB011899, as well as the high probability that the number of differences would increase when more overlapping material would be found for *Kaatedocus*.

Leinkupal. The holotype of *Leinkupal* consists of a single anterior caudal vertebra, and the paratype comprises more axial elements (Gallina et al., 2014). Additional axial elements were referred to the same taxon by (Gallina et al. (2018), and a braincase by Garderes et al. (2022). Comparison of the cervical vertebrae between both taxa is hampered by the fact that there is no anatomical overlap. MMCh-Pv 63-4 is the only posterior cervical vertebra preserved that has been described, and based on Gallina et al. (2014), it most likely represents the eleventh cervical vertebra. Although the preservation of the lateral surface is poor, the cervical vertebra of *Leinkupal* appears to lack the highly complex lateral pneumaticity seen in MAB011899. Although not described, it appears that no additional accessory laminae are present in the SDF and the POCDF of *Leinkupal*. Additionally, it lacks the pneumatic foramen connecting the POCDF with the SPOF. The PCDL appears not to bifurcate anteriorly, and as stated in Gallina et al. (2014), the ACDLs are reduced in all elements. Comparing the anterior dorsal vertebrae, this becomes more evident, as the ACDL seems to have disappeared or is reduced beneath the diapophysis in *Leinkupal*, whereas MAB011899 shows bifurcating ACDLs in both DV1 and DV2. Information on other morphological characters cannot be gleaned from the description and the illustrations of the anterior dorsal vertebra. Comparing the anterior caudal vertebrae is probably most useful, as *Leinkupal* is only diagnosable based on these elements, although the braincase tentatively assigned to *Leinkupal* (Garderes et al., 2022) may reveal additional autapomorphies for this taxon (but this cannot be compared to MAB011899). *Leinkupal* can be recognized by the extreme development of the transverse processes, which are equal or wider than the centrum width. This is clearly not the case for MAB011899, of which the transverse processes are relatively small. Additionally, the dorsal and ventral bars of the processes of MAB011899 are not nearly as robust as those in

61

Leinkupal. Paired pneumatic fossae occur at the base of the postzygapophyses in *Leinkupal*, which are absent in MAB011899. Finally, *Leinkupal* preserves very robust CPRLs in the anterior caudal vertebrae. These are notably absent in MAB011899. A future, full anatomical description of the material mentioned by Gallina et al. (2018) would probably reveal additional morphological differences between MAB011899 and *Leinkupal*. Furthermore, geographic and temporal separation should be considered here, as *Leinkupal* is an Early Cretaceous Patagonian diplodocine.

Supersaurus. MAB011899 can easily be distinguished from both species of *Supersaurus*, primarily based on differences in the cervical and dorsal vertebrae. Moreover, *Supersaurus vivianae,* assuming that both individuals are known from adult material, is much larger compared to MAB011899 (Lovelace et al., 2007). *Supersaurus lourinhanensis* lacks bifurcated vertebrae, and both species of *Supersaurus* show distinct grooves posterolateral to the parapophyses in the cervical vertebrae, as well as paired pneumatic fossae lateral to the midline keel in the cervical vertebrae (Lovelace et al., 2007; Mannion et al., 2012). Other differences can be found in the dorsal vertebrae, including accessory laminae connecting the SPOL and POSL in the middle dorsal vertebrae, enclosed PACDFs in *Supersaurus*, the presence of medial SPOLs in the posterior dorsal vertebrae in *Supersaurus*, and vertical neural spines in *Supersaurus*, which are anteriorly inclined in MAB011899. The thoracic ribs of *Supersaurus* contain pneumatic foramina and oblique ridges, which are both absent in MAB011899.

Tornieria. As *Leinkupal*, *Tornieria* is also geographically separated from the Morrison diplodocines, being a taxon from the Tendaguru Formation from Tanzania. MAB011899 can be compared to both the holotype individual (MB.R.2672, 2713, 2728; SMNS 12140, 2141a, 12142, 12143, 12145a, c; Remes, 2006), and skeleton 'k' (MB.R.2386, 2572, 2586, 2669, 2673, 2726, 2730, 2733, 2913, 3816; Remes, 2006). The caudal centrum (SMNS 12141a) is distinctly more procoelous compared to the caudal vertebrae of MAB011899, and possesses more distinct pleurocoels, which are reduced in most centra of MAB011899. The pleurocoels are located in the dorsal third of the centrum in *Tornieria* (Remes, 2006), who determined this as autapomorphic for *Tornieria*. Tschopp et al. (2015a), however, considered this unclear. In MAB011899, the reduced pleurocoels are restricted below the dorsal half of the centrum. The left side of the centrum (SMNS 12141a) is compressed dorsally, as seen in the anterior view of the vertebra, possibly causing this shift in pleurocoel position. Similarly, the transverse processes are situated further dorsally in *Tornieria*, whereas in MAB011899, they are located more at midheight, but this might also be caused by the compression of the *Tornieria* vertebra. The ventral hollow in the caudal centra of MAB011899 are not nearly as prominent as in *Tornieria*. Only very small, irregularly placed foramina are present in Cd?4-6 of MAB011899. Similar to *Leinkupal, Tornieria* preserves very robust CPRLs, which are absent in MAB011899. The ischia (SMNS 12143) are distinctly different, as the acetabular margin is strongly concave in both specimens of *Tornieria* (SMNS 12143, MB.R.2733), but flat to convex in MAB011899. Additionally, elongated lateral fossae mark the ischial shaft in MAB011899; these are absent in *Tornieria*. The distal ends differ substantially, too, with the transverse expansion being more extreme, and the dorsal expansion resulting in a more triangular shape in MAB011899 compared to *Tornieria*, where the distal outline is more oval. *Tornieria* (SMNS 12140) and MAB011899 differ in the elliptical outline of the femoral shaft, which in *Tornieria* is less elliptical. The fibulae of *Tornieria* (SMNS 12142) and MAB011899 show no notable distinctions from each other. Skeleton 'k' of *Tornieria* preserved a mid-cervical vertebra, lost during World War II, which is figured in right lateral view in (Janensch, 1929c). This vertebra lacks the distinct fossae on the dorsal surface of the parapophyses seen in both mid- and posterior cervical vertebrae of, e.g., *Diplodocus carnegii* (Hatcher, 1901), *G. pabsti* (Tschopp and Mateus, 2017) and MAB011899. Similarly, the posteroventral fossae on the centrum are missing, and the PCDL appears not the bifurcate anteriorly in *Tornieria*; these features both occur in MAB011899. No other important anatomical differences can be gleaned from the figure in Janensch (1929c).

Autapomorphies of MAB011899

Five main features distinguish MAB011899 apart from all currently known diplodocids, and possibly other flagellicaudatans. The first of these are the accessory laminae in the SPRF of the posterior cervical vertebrae. They are not connected to any landmarks. These accessory laminae migrate posteriorly and slightly dorsally from CV13 to DV2 and disappear in DV3. A similar posterior migration occurs in the SPRL of CV13 to DV2, and these SPRLs are 'captured' by the diapophysis of DV3 so

they now form SPDLs, with novel SPRLs occurring simultaneously. Although very likely, poor preservation of the metapophyses and the SPDLs/SPRLs in DV3 renders it unclear whether these novel SPRLs truly represent the posteriorly migrated accessory laminae that were captured by the prezygapophyses. Wilson (2012) discussed lamina capture, wherein he exemplified laminar capture of the SPRL and SPDL in *Jobaria*. This process occurs in MAB011899 and is also clearly visible in *Diplodocus carnegii* (Hatcher, 1901, plate VIII), wherein true SPDLs are formed in DV4. In contrast, laminar capture is absent in *Haplocanthosaurus* (Hatcher, 1903), whereas *Apatosaurus* (Gilmore, 1936) shows laminar capture occurring in DV1. In *Apatosaurus louisae,* SPDLs are immediately present in DV1, without an intermediate state such as seen in DV3 in MAB011899 and CM 84. In addition, unlike what is seen in *D. carnegii*, SPRLs are present in DV1 of *A. louisae*, whereas *D. carnegii* shows only partial SPRLs in DV4 and DV5, which do not reach the prezygapophyseal rami.

Although it is uncertain if these accessory laminae are captured in DV3, it is clear that this set of laminae are present in the preceding vertebrae, where they are independent of the SPRLs, the PRSL and the median tubercle. Their participation in laminar capture can be questioned due to their size, as the laminae are very thin - ± 2 mm - and would not function well as the supporting laminae between the functional landmarks, as well as their rugose nature in the cervical vertebrae, probably related to muscle tendon attachments. Assessing laminar capture is difficult, however, due to the lack of complete cervico-dorsal transitions preserved in diplodocid specimens. Despite the process of laminar capture, neither NSMT-PV 20375 (Upchurch et al., 2004b), *Apatosaurus louisae* CM 3018 (Gilmore, 1936), *Brontosaurus yahnahpin* Tate-001 (Filla and Redman, 1994), *Diplodocus carnegii* CM 84 (Hatcher, 1901)*, Kaatedocus* SMA 0004/NMZ 1000004 (Tschopp and Mateus, 2013), *Barosaurus* (Lull, 1919; McIntosh, 2005), nor *Leinkupal* (Gallina et al., 2014) possess these structures in their posterior cervical and/or anterior dorsal vertebrae. They are also absent in *Australodocus*, but the type material consists only of mid-cervical material, which might not be eligible to test for these structures (Remes, 2007). There is no mention of these structures in Bonaparte and Mateus (1999) or Mannion et al. (2012) for *Supersaurus lourinhanensis*, and it cannot be assessed from the figures of the specimen. *Supersaurus vivianae* BYU 725-9024 does not show these structures either (Taylor

and Wedel 2016). Lovelace et al. (2007) also did not describe this feature for *S. vivianae* WDC DMJ-021, because the description of all elements is brief. This feature cannot be assessed in *Galeamopus*, because the posterior cervical vertebrae of SMA 0011/NMZ 1000011 are still embedded in matrix (Tschopp and Mateus, 2017), obscuring the SPRF, and axial material of HMNS 175 is not described. It appears, however, that although for several type specimens the feature cannot be tested, this set of additional laminae in the SPRF is a unique feature of MAB011899 and can thus be tentatively considered to be autapomorphic.

A second feature is the anteriorly bifurcating ACDL in anterior dorsal vertebrae. Similar to the previous feature, these laminae are best observed in anterolateral view, because the PRDL can obscure this feature in photographs in lateral view. Bifurcating ACDLs are not mentioned by Wilson (1999, 2012), apart from the usual distinction between the PPDL and ACPL, which causes the ACDL to split due to the dorsal migration of the parapophysis in the dorsal vertebral sequence. However, in anterior dorsal vertebrae, the parapophysis is located partially on the centrum, wherein the distinction between the PPDL and ACPL has yet to occur. Bifurcating ACDLs are absent in *Apatosaurus louisae* CM 3018 (Gilmore, 1936), *Diplodocus carnegii* CM 84 (Hatcher, 1901), *Diplodocus hallorum* DMNS 1494, *Haplocanthosaurus priscus* CM 879 (Hatcher, 1903), *Leinkupal* (Gallina et al., 2014), *Supersaurus lourinhanensis* ML 414 (Mannion et al., 2012), *Supersaurus vivianae* BYU 725-4503 (the serial position of this vertebra is unknown), *Galeamopus hayi* HMNS 175 and possibly in a dorsal vertebra of *Tornieria* (Janensch, 1929b), but this dorsal vertebra is lost, the serial position is unknown and it is only figured in anterior view. In the case of NSMT-PV 20375, DV1 cannot be assessed in lateral view, because the PRDLs obscure the ACDLs. Anterior view of the vertebrae suggests there is no bifurcation (Upchurch et al., 2004b, plate 3, M). Bifurcation is absent in DV3 of *Diplodocus hallorum* NMMNH 3690 (Herne and Lucas, 2006). In the case of *Barosaurus*, ACDLs are difficult to spot in both YPM VP.000429 (Lull, 1919) and AMNH FARB 6341 (McIntosh, 2005) for the anterior dorsal vertebrae. Descriptions of DV1 in Lull (1919) and DV1-3 in McIntosh (2005) are concise, and do not elaborate on the presence and orientation of all laminae. Plate III of Lull (1919) shows DV1 in lateral view, and no ACDL can be observed. If the bifurcation of the possibly obscured ACDL occurs, resembling

MAB011899, it would be expected that the ventral ramus would be seen in lateral view. AMNH FARB 6341 lacks bifurcation of the ACDLs. For *Galeamopus pabsti*, it is debatable if the bifurcation is present. The penultimate cervical vertebra (Tschopp and Mateus, 2017, figure 31) appears to lack anterior bifurcation of the ACDL, but this is also obscured by the preceding vertebra, so this cannot be confirmed with confidence. This uncertainty also applies to the posterior-most cervical vertebra (Tschopp and Mateus, 2017, figure 32), which is not obscured, but the ACDL is not preserved. A breakage pattern is present which bifurcates and could have held the lamina, but this might be coincidental. In the possible first dorsal vertebra of *Galeamopus pabsti,* the lateral surface is too damaged to assess the presence of an ACDL. It thus seems unlikely that a similar structure is present in *G. pabsti*. This seems to suggest that most type- and other important diplodocid specimens appear to lack this feature for which it can be assessed. Its presence as an autapomorphy is thus well-supported within Diplodocidae.

A third feature which is here determined to be autapomorphic for *Ardetosaurus viator*, are the CPOL-f in DV2. These fossae are absent in diplodocoids which preserve anterior dorsal vertebrae (Hatcher 1901, 1903; Lull, 1919; Janensch, 1929a; Gilmore, 1936; Salgado and Bonaparte, 1991; Calvo and Salgado, 1995; Upchurch et al., 2004b; McIntosh, 2005; Rauhut et al., 2005; Carballido et al., 2012b; Mannion et al., 2012; Xu et al., 2018) but have been identified in a number of other sauropods. Wilson et al. (2011) provides examples for *Camarasaurus supremus* (AMNH FARB 5761-a/D-X-106) and *Giraffatitan* (MB.R.2180), and Wilson (2012) states that divided CPOLs (enclosing CPOL-f) are also present in *Argentinosaurus*. However, *Camarasaurus supremus* (AMNH FARB 5761-a/D-X-106) does not have the CPOL-f which Wilson et al. (2011, figure 9) illustrate. There is no bifurcation of the CPOL, either dorsally as suggested, or ventrally as seen in MAB011899, in AMNH FARB 5761-a/D-X-106. Instead, in the upper third of the left CPOL of AMNH FARB 5761-a/D-X-106, the lateral edge of the lamina bends slightly laterally, suggesting a bifurcation. However, there is no clear separation from the 'main' CPOL, thus the lamina remains single throughout its length, and simply widens when observed in posterior view. In *Giraffatitan*, similar to MAB011899, the bifurcation of the CPOL occurs ventrally, but is present in CV7, and not in the dorsal vertebrae. Additionally, the fossae are much

deeper than in MAB011899. In the titanosaur *Ninjatitan*, a similar, but deeper fossa is created between the lateral and medial CPOL (Gallina et al., 2021). As *Giraffatitan, Ninjatitan* and *Argentinosaurus* are very distantly related to *Ardetosaurus viator,* the presence of CPOL-f in DV2 can be used as an autapomorphy for *Ardetosaurus viator* among diplodocoid sauropods.

A fourth unique feature is the vertebral height/centrum length ratio of the posterior dorsal vertebrae of MAB011899, and primarily its change along the series. Although the condyles of the mid- and posterior dorsal vertebrae are poorly preserved, estimates can be made for most, as the SMA photographs show that only the outer-most surface is reconstructed. Centrum length minus condyle length differs only minorly as the condyles become less pronounced along the vertebral series antero-posteriorly. The centrum lengths of DV7-9 (Hatcher, 1901, p. 38, column 2) of *Diplodocus carnegii* are 13, 20 and 33 mm larger, respectively, than those of MAB011899. Comparing this to the vertebral height, dorsal vertebrae 7-9 are all significantly taller in *D. carnegii.* However, all greatest height measurements of MAB011899 are influenced by compression (Table 2). Based on the compressed morphology, it is expected that DV6 and DV7 are slightly larger, as the neural spines deflect laterally. DV8 and DV9 are also assumed to be slightly larger compared to the current length, as the centra are severely compressed. We estimate that DV6-9 are all approximately 600 mm tall, and did not differ much in total height, which is also supported by the SMA photographs prior to the reconstructions. This is unusual, as *Diplodocus* shows a distinct increase in overall vertebral height (Hatcher, 1901; Herne and Lucas, 2006). Herne and Lucas (2006, table 1) provide ratios for total vertebral height to total centrum length of *Diplodocus hallorum* NMMNH 3690, *D. carnegii* CM 84, *Apatosaurus louisae* CM 3018 and FMNH P25112 (formerly FMNH 7163). Table 12 provides updated ratios for these specimens, including MAB011899, as well as other diplodocoid specimens. MAB011899 stands out from all other specimens; the ratios of *Diplodocus, Barosaurus, Supersaurus lourinhanensis, Galeamopus pabsti, Amphicoelias altus,* as well as the specimens ascribed to Apatosaurinae are >3, whereas in MAB011899, they are all below 2.4. Only the two *Supersaurus vivianae* specimens have a ratio below 3. Comparing the vertebral heights with table 2 in Herne and Lucas (2006), is it obvious that in *D. hallorum, D. carnegii, A. louisae* and FMNH P25112 the vertebral height

TABLE 12. Ratios of vertebral height to centrum length of posterior dorsal vertebrae of several diplodocoid specimen.

Vertebra	*Ardetosaurus viator* MAB011899	*Diplodocus carnegii* CM 84	*Diplodocus hallorum* NMMNH 3690	*Galeamopus pabsti* SMA 0011/NMZ 1000011	*Barosaurus lentus* YPM VP.000429	*Barosaurus lentus* AMNH FARB 6341	*Amphicoelias altus* AMNH FARB 5764
DV7	2.31	3.07	3.32	4.76		3.26	4.07
DV8	2.15	3.08	4.20	5.52	4.01	3.29	
DV9	2.08	4.20	4.38	5.63		3.24	
DV10		3.69	4.64				

Vertebra	*Supersaurus vivianae* BYU 725-9044	*Supersaurus vivianae* WDC DMJ-021	*Supersaurus lourinhanensis* ML 414	*Apatosaurus louisae* CM 3018	Diplodocidae indet. FMNH P25112	Apatosaurinae indet. NSMT-PV 20375	*Haplocanthosaurus pricus* CM 572
DV7	2.65	2.82	3.91	4.90	4.62	4.69	3.51*
DV8				4.87	4.30	4.74	4.05*
DV9				5.29	5.24		4.18*
DV10					5.36	5.48	4.92*

Notes: Herne and Lucas (2006) compared total vertebral height of NMMNH 3690 to other diplodocids. However, Hatcher (1901), Riggs (1903) and Gilmore (1936) used greatest height measurements for CM 84, FMNH P25112 and CM 3018. In addition, for CM 3018, Herne and Lucas (2006) used incorrect values. Ratios for MAB011899, CM 84, SMA 0011/NMZ 1000011, AMNH FARB 5764, BYU 725-9044, WDC DMJ-021, CM 3018, FMNH P25112 and CM 572 are based on greatest height measurements. Ratios for NMMNH 3690, YPM VP.000429, AMNH FARB 6341, ML 414 and NSMT-PV 20375 are based on total height measurements. Measurements of CM 84 are taken from Hatcher (1901) and Lull (1919), of NMMNH 3690 from Herne and Lucas (2006), of SMA 0011/NMZ 1000011 from Tschopp and Mateus (2017), of YPM VP.000429 from Lull (1919), of AMNH FARB 6341 from McIntosh (2005), of AMNH FARB 5764 measured from figure 5 and table 2 in Mannion et al. (2021), of BYU 725-9044 measured from figure 1 in Jensen (1985), of WDC DMJ-021 measured from figure 5 in Mannion et al. (2012), of ML 414 from Mannion et al. (2012), of CM 3018 from Gilmore (1936), of FMNH P25112 from Gilmore (1936), of NSMT-PV 20375 from Upchurch et al. (2004b), of CM 572 from Hatcher (1903). Note that for SMA 0011/NMZ 1000011, ML 414 and NSMT-PV 20375, centrum length is provided as centrum length minus condyle. However, in all three specimens, a true convex condyle is absent, such that centrum length is nearly equal to centrum length minus condyle. For AMNH FARB 5764, BYU 725-9044 and WDC DMJ-021, the serial position of the vertebrae is unknown, so their ratios are placed in the top row. *These are dorsal vertebrae 11, 12, 13 and 14 *sensu* Hatcher (1903), as *Haplocanthosaurus* possesses more dorsal vertebrae than diplodocids.

keeps increasing from DV6 onwards. This is not the case in MAB011899, wherein the ratio is low, and the vertebral height remains roughly stable throughout the posterior dorsal vertebrae. We do recognize the compression of the vertebrae, which could have led to the equalization of vertebral height in these elements, but also recognize that the ratio is substantially lower than should be expected for these vertebrae. For *Brontosaurus yahnapin*, only a single centrum length is provided in Filla and Redman (1994), but no figure is provided for this vertebra. Dicraeosaurids are not a useful comparison, due to their highly elongated neural spines (Janensch 1929a; Salgado and Bonaparte, 1991; Rauhut et al., 2005), resulting in ratios >5. *Haplocanthosaurus priscus* CM 572 is the only other diplodocoid which shows a relatively stable posterior dorsal series in terms of vertebral height, wherein vertebral height of DV8-13 are all

within 3 cm of each other (Hatcher, 1903, but vertebral count follows Mannion et al., 2012 and Tschopp et al., 2015a). However, all of these vertebrae have a ratio >3.0. Neither *Brontosaurus parvus, Kaatedocus, Leinkupal,* or *Tornieria* preserve dorsal vertebrae, and the dorsal vertebrae of *G. hayi* are not described or measured, so these taxa cannot be compared to MAB011899 (Peterson and Gilmore, 1902; Remes, 2006; Tschopp and Mateus, 2013; Gallina et al., 2014, 2018). It thus appears probable, especially because MAB011899 is an adult specimen, that the low ratio of vertebral height/centrum length is unique amongst diplodocids.

A fifth feature that may be considered autapomorphic, is the lack of distinct CPRLs in the anterior caudal vertebrae. The absence of distinct CPRLs is, however, influenced by serial variation. This is exemplified by *Brontosaurus excelsus* YPM

VP.001980 (Ostrom and McIntosh, 1966, plates 32 and 35), wherein the second caudal vertebra shows very distinct CPRLs, which have faded in the fifth caudal vertebra. There is no anterior view of the fourth vertebra, so these laminae could have faded earlier than Cd5. In *Apatosaurus louisae* CM 3018, the CPRLs are distinct up to seventh caudal vertebra, posterior to which the CPRLs also fade into the arch pedicles and become indistinguishable from the transverse processes and the remainder of the arch (Gilmore, 1936). NSMT-PV 20375 is described as having CPRLs in Cd1 and Cd2, and losing distinct medial and lateral CPRLs in Cd5 (Upchurch et al., 2004b). Instead, the prezygapophyses are ventrally connected to the dorsal expansion of the neural canal, and medially connected by a TPRL. However, sensu Wilson (1999) and Wilson (2012), the medial branches of the CPRLs in Cd1-4 should in fact be termed TPRLs, because they are connected to the dorsal roof of the neural canal and the prezygapophyses, as is clearly visible on plate 5 in Upchurch et al. (2004b). Clear CPRLs are already difficult to make out in Cd4, but following Upchurch et al. (2004b), true CPRLs disappear in Cd5 in NSMT-PV 20375. In apatosaurines CPRLs disappear early in the caudal sequence. There appears to be a relationship between the presence of these laminae, and the presence of clear 'wing'-like transverse processes in caudal vertebrae, which are ubiquitous in diplodocids (Hatcher, 1901; Lull, 1919; Gilmore, 1936; Ostrom and McIntosh, 1966; Upchurch et al., 2004b; Lucas et al., 2006). As the transverse processes migrate ventrally, and lose their connection to the neural arch, the CPRLs become no longer distinct from the arch, and simply become the dorsal expansion of the neural canal. This is supported, to an extent, by comparison with *Giraffatitan brancai*, wherein CPRLs appear absent in the second caudal vertebra (Taylor, 2009, figure 3). This vertebra also lacks true 'wing'-like transverse processes, and has more simple, horizontal transverse processes, similar to more posterior caudal elements in *A. louisae* (Gilmore, 1936). Only a handful of diplodocine specimens preserve anterior caudal vertebrae in sequence, so comparisons of serial variation are difficult. *Diplodocus carnegii* clearly possesses 'wing'-like transverse processes up to the twelfth element, all containing distinct CPRLs (Hatcher, 1901). For *Diplodocus hallorum* NMMNH 3690, CPRLs are difficult to compare, because the anterior caudal vertebrae are part of articulated blocks, which are only partially prepared. 'Wing'-like transverse processes

disappear quickly after Cd8 according to Herne and Lucas (2006), with Cd8 still showing distinct CPRLs (Lucas et al., 2006). However, *D. hallorum* is unique, as the prezygapophyses in the middle caudal vertebrae extend anterior to the anterior edge of the centrum, and the neural arches are shifted anteriorly. Therefore, although 'wing'-like transverse processes are lost, NMMNH 3690, as well as DMNS 1494 (referred to *D. hallorum* by Tschopp et al., (2015a) retain distinct CPRLs. *Supersaurus lourinhanensis* only preserves a single caudal centrum (Mannion et al., 2012), *Galeamopus pabsti* does not preserve caudal vertebrae, and the preservation of the anterior caudal vertebrae of *G. hayi* is inadequate, such that these specimens cannot be compared to MAB011899. *Supersaurus vivianae* only preserves a single anterior caudal vertebra, previously part of *Ultrasauros macintoshi* (formerly BYU 725-5002, currently BYU 725-9045; Jensen, 1985; Lovelace et al., 2007). Although the serial position is unknown, the vertebra possesses 'wing'-like transverse processes and has distinct CPRLs. *Tornieria* MB.R.2956.1, a seventh caudal vertebra, has robust, very wide CPRLs, in combination with 'wing'-like transverse processes (Remes, 2006). As discussed before, *Leinkupal* is diagnosed based on the extreme development of the 'wing'-like transverse processes, as well as the extremely robust CPRLs, which are also present in the paratype caudal vertebra MMCH-Pv 63-6. Finally, the holotype of *Barosaurus* preserves five anterior caudal vertebrae (Lull, 1919), which in Lull (1919) were determined to be caudal vertebrae two to six. McIntosh (2005), however, comparing to AMNH FARB 6341, concluded that they were the first five caudal vertebrae. We herein follow McIntosh (2005). The first vertebra of YPM VP.000429 does not preserve the CPRLs or the transverse processes. The second vertebra contains robust CPRLs and a robust TPRL with the accompanying 'wing'-like transverse processes. Although not specifically mentioned or figured, the third vertebra is stated to be anteriorly indistinguishable from the second. Caudal vertebra four lacks most of the arch, and the fifth vertebra, although preserving a portion of the arch, is not described in detail or figured. The caudal vertebrae of AMNH FARB 6341 have 'wing'-like transverse processes up to Cd9, and all anterior caudal vertebrae have distinct CPRLs. All aforementioned specimens have in common that distinct CPRLs are present in caudal vertebrae with or without 'wing'-like transverse processes, but that in most cases these laminae disappear when the trans-

verse processes become less 'wing'-like. In MAB011899, however, in both Cd?4-6 and Cd?5-8, no CPRLs are present, but based on the trajectory of the dorsal edge of the transverse processes, they were still distinctly touching the neural arch, and thus appear to be 'wing'-like, although no longer as extreme as SV5. The only vertebra that does preserve CPRLs, albeit faintly and not connecting to the centrum, is Cd3. Reduced to absent CPRLs in anterior-most caudal vertebrae (i.e., caudal vertebrae that retain 'wing'-like transverse processes extending onto the neural arch) is unique in MAB011899 compared to other diplodocid specimens.

Autapomorphies or Individual Variation?

There is a number of features which are uncommon in diplodocid specimens, but are present in MAB011899 and could be interpreted as potentially autapomorphic. However, these features are herein not considered to represent autapomorphies for *Ardetosaurus viator* for several reasons. MAB011899 possesses a ventral bifurcation of the PRPL in DV5 on the left side. This is not present in rebbachisaurids (Torcida Fernández-Baldor et al., 2011; Carballido et al., 2012b; Wilson and Allain, 2015; Bellardini et al., 2022), dicraeosaurids (Janensch, 1929a; Rauhut et al., 2005; Coria et al., 2019), apatosaurines (Gilmore, 1936; Ostrom and McIntosh, 1966; Upchurch et al., 2004b) and diplodocines (Hatcher, 1901; Lull, 1919; McIntosh, 2005; Herne and Lucas, 2006; Tschopp and Mateus, 2017), and appears to be only present in the macronarian *Eucamerotus* (Blows, 1995), wherein it is potentially recognized as an autapomorphy (Campbell et al., 2017). Therefore, this feature could appear as potentially autapomorphic in *Ardetosaurus viator* amongst diplodocids. However, often, these laminae are described in limited detail, simply stated as present and often delimiting a fossa between landmarks. The bifurcation as in DV5 of MAB011899 is minor, and similar 'small' bifurcations can easily be missed in vertebral series. Additionally, the bifurcation occurs only on the left side of the vertebra; the right PRPL does not bifurcate, although preservation may affect the ventral portion of the lamina. As this feature appears to be asymmetrical and is only present in a single vertebra, we refrain from adding this relatively unique feature to the diagnosis of *Ardetosaurus viator*.

DV10 of MAB011899 possesses anterolaterally bifurcating PODLs. This bifurcation is absent in DV6 and DV7, and cannot be assessed in DV8 and DV9, as these parts of the laminae, or the laminae in their entirety, are not preserved. This laminar bifurcation is absent in *Amphicoelias* (Mannion et al., 2021), although part of the PODL is reconstructed, *Apatosaurus* (Gilmore, 1936; Upchurch et al., 2004b), *Brontosaurus excelsus* (Ostrom and McIntosh, 1966), *Galeamopus pabsti* (Tschopp and Mateus, 2017), *Haplocanthosaurus* (Hatcher, 1903) and *Supersaurus* (Jensen, 1985). In *Barosaurus*, both in YPM VP.000429 and AMNH FARB 6341, the transverse processes of the posterior dorsal vertebrae are not preserved to the extent that the PODLs can show their bifurcation. If these adult specimens, see Waskow (2019), possess a similar condition as juvenile/sub-adult *Barosaurus*, then, like CM 79038, the PODLs were likely single (Hanik et al., 2017). These bifurcations do appear in DV5-9 of *D. carnegii* (Hatcher, 1901, plate VIII), as well as DV8 and DV9 of *D. hallorum* (Herne and Lucas, 2006, figure 2) and DV5 of *Supersaurus lourinhanensis* (Mannion et al., 2012, figure 3). In CM 36041, two articulated neural arches referred to *Galeamopus* sp., a bifurcation of the PODL occurs on the right side (Tschopp et al., 2019). Outside of Diplodocinae, these bifurcations appear in DV7-9 of *Brontosaurus parvus* UW 15556 (formerly CM 563; Gilmore, 1936). Due to their presence in these taxa, its use as an autapomorphy is excluded for MAB011899. However, its use is not limited to taxon-specific diagnoses. Bifurcated PODLs are absent in rebbachisaurids (Calvo and Salgado, 1995; Mannion, 2010; Torcida Fernández-Baldor et al., 2011; Carballido et al., 2012b; Ibiricu et al., 2013; Wilson and Allain, 2015) and dicraeosaurids (Janensch, 1929a; Harris, 2006; Xu et al., 2018; Coria et al., 2019), such that the distribution of this anatomical feature is limited to diplodocid sauropods within Diplodocoidea, and can be used as a potentially phylogenetic character.

A third characteristic that is often not described in detail, and may therefore appear as unique, is the unusual first chevron of MAB011899. MAB011899 preserves the first chevron, a relatively rare occurrence in sauropods, with an anteriorly flat blade bearing a number of distinct ridges functioning as a large muscle scar. A flattened anterior surface of the blade is present in several different sauropods. Flattened chevron blades not related to taphonomic compression are present in, e.g., *Demandasaurus* MDS-RVII,590 (Torcida Fernández-Baldor et al., 2011), *Europatitan* MDS-OTII,27 (Torcida Fernández-Baldor et al. 2017), *Cetiosaurus* LCM G468.1968 (Upchurch and Martin, 2002) and *Giraffatitan* MB.R.2921. However,

none of these chevrons bear similar ridges as those in MAB011899, or are necessarily the first chevron. In the case of diplodocines,*'Dinheirosaurus', Kaatedocus, Leinkupal,* and *Tornieria* do not preserve chevrons. *Galeamopus hayi* HMNS 175 does preserve chevrons (McIntosh, 1981), among which are several anterior chevrons, but these are not part of the mount and have not been described. One of the anterior chevrons of *Supersaurus vivianae* WDC DMJ-021 shows a flattened anterior surface of the blade, albeit restricted to the dorsal portion of the blade, but this chevron appears to lack similar striations as those in MAB011899, although this could be due to taphonomy and the added reconstructions to this chevron. Both YPM VP.000429 and AMNH FARB 6341 preserve chevrons, however, neither specimen preserves the first in the sequence nor any with a similar morphology as that in MAB011899. In the case of *Diplodocus*, NMMNH 3690 preserves two chevrons (Lucas et al., 2006), which follow the basic blueprint of diplodocid anterior chevrons. This hampers direct comparison with MAB011899, as well as possible reasons for the presence/absence of certain features. CM 84 does preserve the first chevron, which shows muscle scars on the lateral sides of the blades, which in MAB011899 are restricted to the anterior portion of the blade. This may be due to the differences between both genera, individual variation of caudal musculature amongst diplodocines, or possibly sexual dimorphism.

Recognizing sexual dimorphism in sauropod dinosaurs has previously been stated to be 'hopeless' (Chapman et al., 1997), due to their incompleteness and the low number of specimens allocated to a particular species. Mallon (2017) summarized reports on elucidating sexual dimorphism in non-avian dinosaurs and recorded only a single case studying sexual dimorphism in neosauropods. Rothschild and Berman (1991) report on caudal vertebral fusion as a possible measure of sexual dimorphism in *Apatosaurus, Camarasaurus,* and *Diplodocus*, however, the fusion of these vertebra was later explained as diffuse idiopathic skeletal hyperstosis (Rothschild and Martin, 2006). Ikejiri (2004) discusses sexual dimorphism in *Camarasaurus*, describing several characteristics as possible indicators of sex in *Camarasaurus*, however, as research is still ongoing regarding Camarasauridae (Tschopp et al., 2014), some of the studied specimens of Ikejiri (2004) might not pertain to the same species. Therefore, studies investigating sexual dimorphism in neosauropods are lacking. This is further aggravated by the lack

of sexual display structures in Sauropoda as a whole, with a couple of possible exceptions, e.g., *Amargasaurus* (Salgado and Bonaparte, 1991; Cerda et al., 2022), *Bajadasaurus* (Gallina et al., 2019) and *Pilmatueia* (Coria et al., 2019). The function of the sails/highly elongated neural spines in dicraeosaurids is, however, still an ongoing debate. In other non-avian dinosaurs, cranial characteristics such as crests or frills have been reported as indicating sexual dimorphism (Mallon 2017). Sauropods lack any form of crests or frills; the raised nasal bars in macronarians *Giraffatitan* and *Europasaurus* were considered potentially sexually dimorphic, but these structures can also be related to signaling/vocalization (Hone et al. 2012).

One of the characters proposed to sexually identify non-avian dinosaurs, and which could be tested in sauropods such as MAB011899, is the use of the morphology and placement of the first chevron(s) (Larson, 1998 and references therein). Erickson et al. (2005) have shown that there is no statistical support for connecting sex to either the position or the size of the first chevron based on a large number of *Alligator* specimens and comparisons with *Tyrannosaurus*. However, micromorphological characters, such as muscle scar size, have yet to be tested. Identifying sex in the oviraptorosaur *Khaan mckennai* was investigated by looking at the larger muscle insertion areas in the anterior chevrons, as well as other factors, which were proposed to be indicative for males (Persons IV et al., 2015). Saitta et al. (2020) state that the number of specimens used by Persons IV et al. (2015) is statistically too low (n=2). A larger sample size is thus needed to further test this hypothesis.

Regarding the placement of the chevron, Erickson et al. (2005) show that in *Alligator mississippiensis*, the placement of the first chevron is always in between the second and third caudal vertebra. This is further confirmed by Wilhite (2023; unpublished data). In other crocodilians, the position of the first chevron varies only in some taxa, which Erickson et al. (2005) attribute to individual variation. In these cases, the first chevron is often deformed or severely reduced. However, this is not the case in sauropods, where, like most regular *Alligator* specimens, the first chevron is simply smaller and wider compared to posterior elements (Riggs, 1903; Osborn and Mook, 1921; Sereno et al., 1999; Torcida Fernández-Baldor et al., 2017; Royo-Torres et al., 2021). In sauropods, the placement of the first chevron varies: in *Apatosaurus louisae* CM 3018, the first chevron is placed in

between the first and second caudal vertebrae (Gilmore, 1936), similar to MAB011899, whereas in *Diplodocus carnegii* CM 84, the first chevron is placed between the second and third caudal vertebrae (Hatcher 1901). In other sauropods, such as the macronarian sauropods *Europatitan* and *Tastavinsaurus*, the first chevron articulates with the third and fourth caudal vertebrae (Canudo et al., 2008; Torcida Fernández-Baldor et al., 2017). The position of the first chevron may not have implications for detecting sexual dimorphism, but might be phylogenetically relevant among a highly diverse group of animals such as sauropods.

Unfortunately, chevrons are often only briefly described and rarely figured in detail, which hampers comparisons. More importantly, the first chevron, which, as outlined above, has a unique morphology in both *Alligator* and sauropods, is often not preserved, which makes testing its importance difficult. Considering variation in crocodilians and the preliminary evidence in the oviraptorosaur *Khaan mckennai*, we suggest that either sexual dimorphism or individual variation is the most convincing interpretation for the unique shape of the chevron, and that the little information available on sauropod chevrons (and of first chevrons in general) currently hampers detailed comparative study. We exclude the possible autapomorphic nature of the morphology. A more detailed study investigating the variability of anterior chevrons, especially the first, is needed to confirm whether there is any evidence for recognizing sauropod sexual dimorphism from chevrons, or if this variability is simply individual variation.

CONCLUSION

We describe a new specimen of diplodocine sauropod dinosaur from the Howe-Stephens Quarry, Wyoming (MAB011899). Detailed comparison of this material with all other diplodocine sauropods, including putative members such as *Amphicoelias*, leads to the erection of a new genus and species, *Ardetosaurus viator*. Five distinct autapomorphies were found: accessory laminae in the SPRF of the posterior cervical vertebrae; anteriorly bifurcating ACDLs in the anterior dorsal vertebrae; the presence of CPOL-f in the second dorsal vertebra; low vertebral height/centrum length ratio of the posterior dorsal vertebrae; and lack of distinct CPRLs in the anterior caudal vertebrae. This specimen sheds light on the variability of morphological features in diplodocine sauropods such as laminar capture in the cervico-dorsal transition and laminar transitions in caudal vertebrae. Additionally, the specimen preserves a relatively rare first chevron with a peculiar morphology, which in comparison with other sauropods and other non-avian dinosaurs, highlights the need to further investigate the possible recognition of sexual dimorphism in sauropod dinosaurs through micromorphological characteristics in chevrons.

ACKNOWLEDGEMENTS

REFERENCES

Apesteguía, S. 2005. Evolution of the hyposphene-hypantrum complex within Sauropoda, p. 248–267. In Tidwell, V. and Carpenter, K. (eds.), Thunder-lizards: the sauropodomorph dinosaurs. Indiana University Press, Bloomington.

Ayer, J. 2000. The Howe Ranch Dinosaurs. Aathal: Sauriermuseum Aathal, Switzerland.

Baron, M.G. 2021. Tactile tails: a new hypothesis for the function of the elongate tails of diplodocid sauropods. Historical Biology, 33:2057–2066. https://doi.org/10.1080/08912963.2020.1769092

Bellardini, F., Filippi, L., Garrido, A., Carballido, J., and Baiano, M. 2022. New rebbachisaurid remains from the Huincul Formation (Middle Cenomanian-Early Turonian) of the Central Neuquén Basin, Patagonia, Argentina. Publicación Electrónica de la Asociación Paleontológica Argentina, 2:1–24. https://doi.org/10.5710/PEAPA.22.04.2022.419

Bird, R.T. 1985. Bones for Barnum Brown: adventures of a dinosaur hunter. Texas Christian University Press, Fort Worth.

Blows, W.T. 1995. The early Cretaceous brachiosaurid dinosaurs *Ornithopsis* and *Eucamerotus* from the Isle of Wight, England. Palaeontology, 38:187–198.

Bonaparte, J.F. 1986. The early radiation and phylogenetic relationships of the Jurassic Sauropod dinosaurs, based on vertebral anatomy, p. 247–258. In Padian, K. (ed.), The beginning of the age of dinosaurs. Cambridge University Press, Cambridge.

Bonaparte, J.F. and Mateus, O. 1999. A new diplodocid, *Dinheirosaurus lourinhanensis* gen. et sp. nov, from the Late Jurassic beds of Portugal. Revista Del Museo Argentino de Ciencias Naturales, 5:13–29.

Bonaparte, J.F., Heinrich, W.-D., and Wild, R. 2000. Review of *Janenschia* Wild, with the description of a new sauropod from the Tendaguru beds of Tanzania and a discussion on the systematic value of procoelous caudal vertebrae in the Sauropoda. Palaeontographica Abteilung A, 256:25–76. https://doi.org/10.1127/pala/256/2000/25

Brown, B. 1935. Sinclair dinosaur expedition, 1934. Natural History, 36:2–15.

Button, D.J., Rayfield, E.J., and Barrett, P.M. 2014. Cranial biomechanics underpins high sauropod diversity in resource-poor environments. Proceedings of the Royal Society B, Biological Sciences, 281:20142114. https://doi.org/10.1098/rspb.2014.2114

Calvo, J.O. and Salgado, L. 1995. *Rebbachisaurus tessonei* sp. nov. a new Sauropoda from the Albian-Cenomanian of Argentina; new evidence on the origin of the Diplodocidae. Gaia, 11:13–33.

Campbell, A., Upchurch, P., and Mannion, P.D. 2017. The anatomy and relationships of *Eucamerotus foxi* (Dinosauria, Sauropoda) from the Early Cretaceous of England. PeerJ PrePrints. https://doi.org/10.7287/peerj.preprints.3247v1

Canudo, J.I., Royo-Torres, R., and Cuenca-Bescós, G. 2008. A new sauropod: *Tastavinsaurus sanzi* gen. et sp. nov. from the Early Cretaceous (Aptian) of Spain. Journal of Vertebrate Paleontology, 28:712–731. https://doi.org/10.1671/0272-4634(2008)28[712:anstsg]2.0.co;2

Carballido, J.L. and Sander, P.M. 2014. Postcranial axial skeleton of *Europasaurus holgeri* (Dinosauria, Sauropoda) from the Upper Jurassic of Germany: implications for sauropod ontogeny and phylogenetic relationships of basal Macronaria. Journal of Systematic Palaeontology, 12:335–387. https://doi.org/10.1080/14772019.2013.764935

Carballido, J.L., Marpmann, J.S., Schwarz-Wings, D., and Pabst, B. 2012a. New information on a juvenile sauropod specimen from the Morrison Formation and the reassessment of its systematic position. Palaeontology, 55:567–582. https://doi.org/10.1111/j.1475-4983.2012.01139.x

Carballido, J.L., Salgado, L., Pol, D., Canudo, J.I., and Garrido, A. 2012b. A new basal rebbachisaurid (Sauropoda, Diplodocoidea) from the Early Cretaceous of the Neuquén Basin; evolution and biogeography of the group. Historical Biology, 24:631–654. https://doi.org/10.1080/08912963.2012.672416

Cerda, I.A., Paulina Carabajal, A., Salgado, L., Coria, R.A., Reguero, M.A., Tambussi, C.P., and Moly, J.J. 2012. The first record of a sauropod dinosaur from Antarctica. Naturwissenschaften, 99:83–87. https://doi.org/10.1007/s00114-011-0869-x

Cerda, I.A., Novas, F.E., Carballido, J.L., and Salgado, L. 2022. Osteohistology of the hyperelongate hemispinous processes of *Amargasaurus cazaui* (Dinosauria: Sauropoda): Implications for soft tissue reconstruction and functional significance. Journal of Anatomy, 240:1005–1019.
https://doi.org/10.1111/joa.13659

Chapman, R., Weishampel, D.B., Hunt, G., and Rasskin-Gutman, D. 1997. Sexual dimorphism in dinosaurs, p. 83–93. In Wolberg, D.L., Stump, E., and Rosenberg, G.D. (eds.), Philadelphia: Academy of Natural Sciences, Dinofest International: proceedings of a symposium held at Arizona State University.

Christiansen, P. 2000. Feeding mechanisms of the sauropod dinosaurs *Brachiosaurus, Camarasaurus, Diplodocus* and *Dicraeosaurus*. Historical Biology, 14:137–152.
https://doi.org/10.1080/10292380009380563

Christiansen, N.A. and Tschopp, E. 2010. Exceptional stegosaur integument impressions from the Upper Jurassic Morrison Formation of Wyoming. Swiss Journal of Geosciences, 103:163–171.
https://doi.org/10.1007/s00015-010-0026-0

Conti, S., Tschopp, E., Mateus, O., Zanoni, A., Masarati, P., and Sala, G. 2022. Multibody analysis and soft tissue strength refute supersonic dinosaur tail. Scientific Reports, 12:19245.
https://doi.org/10.1038/s41598-022-21633-2

Cope, E.D. 1877. On *Amphicoelias*, a genus of Saurians from the Dakota epoch of Colorado. Paleontology Bulletin, 27:1–5.

Coria, R.A., Windholz, G.J., Ortega, F., and Currie, P.J. 2019. A new dicraeosaurid sauropod from the Lower Cretaceous (Mulichinco Formation, Valanginian, Neuquén Basin) of Argentina. Cretaceous Research, 93:33–48.
https://doi.org/10.1016/j.cretres.2018.08.019

Damke, L.V.S., Bem, F.P., Doering, M., Piovesan, T.R., and Müller, R.T. 2022. The elongated neck of sauropodomorph dinosaurs evolved gradually. The Anatomical Record:ar.25107.
https://doi.org/10.1002/ar.25107

D'Emic, M.D., Whitlock, J.A., Smith, K.M., Fisher, D.C., and Wilson, J.A. 2013. Evolution of High Tooth Replacement Rates in Sauropod Dinosaurs. PLoS ONE, 8:e69235.
https://doi.org/10.1371/journal.pone.0069235

Demuth, O.E., Benito, J., Tschopp, E., Lautenschlager, S., Mallison, H., Heeb, N., and Field, D.J. 2022. Topology-Based Three-Dimensional Reconstruction of Delicate Skeletal Fossil Remains and the Quantification of Their Taphonomic Deformation. Frontiers in Ecology and Evolution, 10:828006.
https://doi.org/10.3389/fevo.2022.828006

Erickson, G.M., Kristopher Lappin, A., and Larson, P. 2005. Androgynous rex – The utility of chevrons for determining the sex of crocodilians and non-avian dinosaurs. Zoology, 108:277–286.
https://doi.org/10.1016/j.zool.2005.08.001

Filippini, F.S., Otero, A., and Gasparini, Z. 2017. The phylogenetic relevance of the sacrum among macronarian sauropods: insights from a pelvis from the Upper Cretaceous of Patagonia, Argentina. Alcheringa: An Australasian Journal of Palaeontology, 41:69–78.
https://doi.org/10.1080/03115518.2016.1180806

Filla, B.J. and Redman, P.D. 1994. *Apatosaurus yahnahpin*: a preliminary description of a new species of diplodocid dinosaur from the Late Jurassic Morrison Formation of Southern Wyoming, the first sauropod dinosaur found with a complete set of "belly ribs", p. 159–178. In Nelson, G.E. (ed), The dinosaurs of Wyoming. Wyoming Geological Association 44th annual field conference guidebook. Wyoming Geological Association, Casper.

Foster, J.R. 2003. Paleoecological Analysis of the Vertebrate Fauna of the Morrison Formation (Upper Jurassic), Rocky Mountain Region, U.S.A., New Mexico Museum of Natural History and Science, 23:2–100.

Foth, C., Evers, S.W., Pabst, B., Mateus, O., Flisch, A., Patthey, M., and Rauhut, O.W.M. 2015. New insights into the lifestyle of *Allosaurus* (Dinosauria: Theropoda) based on another specimen with multiple pathologies. PeerJ, 3:e940.
https://doi.org/10.7717/peerj.940

Fraas, E. 1908. Ostafrikanische Dinosaurier. Palaeontographica, 15:105–144.

Gallagher, T., Poole, J., and Schein, J.P. 2021. Evidence of integumentary scale diversity in the late Jurassic Sauropod *Diplodocus* sp. from the Mother's Day Quarry, Montana. PeerJ, 9:e11202.
https://doi.org/10.7717/peerj.11202

Gallina, P.A., Apesteguía, S., Haluza, A., and Canale, J.I. 2014. A Diplodocid Sauropod Survivor from the Early Cretaceous of South America. PLoS ONE, 9:e97128.
https://doi.org/10.1371/journal.pone.0097128

Gallina, P.A., Canale, J.I., and Apesteguía, S. 2018. New materials of the diplodocid sauropod *Leinkupal laticauda* from the Bajada Colorada Formation (Berriasian-Valanginian), Neuquén Province. Publicación Electrónica de la Asociación Paleontológica Argentina, 18:R29.

Gallina, P.A., Apesteguía, S., Canale, J.I., and Haluza, A. 2019. A new long-spined dinosaur from Patagonia sheds light on sauropod defense system. Scientific Reports, 9:1392.
https://doi.org/10.1038/s41598-018-37943-3

Gallina, P.A., Canale, J.I., and Carballido, J.L. 2021. The Earliest Known Titanosaur Sauropod Dinosaur. Ameghiniana, 58:35–51.
https://doi.org/10.5710/amgh.20.08.2020.3376

Garderes, J.P., Gallina, P.A., Whitlock, J.A., and Toledo, N. 2022. Neuroanatomy of a diplodocid sauropod dinosaur from the Lower Cretaceous of Patagonia, Argentina. Cretaceous Research, 129:105024.
https://doi.org/10.1016/j.cretres.2021.105024

Gillette, D.D. 1991. *Seismosaurus halli*, gen. et sp. nov., a new sauropod dinosaur from the Morrison Formation (Upper Jurassic/Lower Cretaceous) of New Mexico, USA. Journal of Vertebrate Paleontology, 11:417–433.
https://doi.org/10.1080/02724634.1991.10011413

Gilmore, C.W. 1936. Osteology of *Apatosaurus*: with special reference to specimens in the Carnegie Museum. Memoirs of the Carnegie Museum, 11:175–300.

González Riga, B.J., Previtera, E., and Pirrone, C.A. 2009. *Malarguesaurus florenciae* gen. et sp. nov., a new titanosauriform (Dinosauria, Sauropoda) from the Upper Cretaceous of Mendoza, Argentina. Cretaceous Research, 30:135–148.
https://doi.org/10.1016/j.cretres.2008.06.006

Gross, O. 1993. The bighorn mountain dinosaur project. Aathal: Sauriermuseum Aathal, Switzerland Bulletin nr. 5.

Hanik, G.M., Lamanna, M.C., and Whitlock, J.A. 2017. A Juvenile Specimen of *Barosaurus* Marsh, 1890 (Sauropoda: Diplodocidae) from the Upper Jurassic Morrison Formation of Dinosaur National Monument, Utah, USA. Annals of Carnegie Museum, 84:253–263.
https://doi.org/10.2992/007.084.0301

Harris, J.D. 2006. The axial skeleton of the dinosaur *Suuwassea emilieae* (Sauropoda: Flagellicaudata) from the Upper Jurassic Morrison Formation of Montana, USA. Palaeontology, 49:1091–1121.
https://doi.org/10.1111/j.1475-4983.2006.00577.x

Harris, J.D. and Dodson, P. 2004. A new diplodocoid sauropod dinosaur from the Upper Jurassic Morrison Formation of Montana, USA. Acta Palaeontologica Polonica, 49:197–210.

Hatcher, J.B. 1901. *Diplodocus* (Marsh): its osteology, taxonomy, and probable habits, with a restoration of the skeleton. Memoirs of the Carnegie Museum, 1:1–63.

Hatcher, J.B. 1903. Osteology of *Haplocanthosaurus*, with description of a new species and remarks on the probable habits of the Sauropoda and the age and origin of the *Atlantosaurus* beds: additional remarks on *Diplodocus*. Memoirs of the Carnegie Museum, 2:1–72.

Herne, M.C. and Lucas, S.G. 2006. *Seismosaurus hallorum*: osteological reconstruction from the holotype. Bulletin of the New Mexico Museum of Natural History and Science, 36:139–148.

Holland, W.J. 1906. The osteology of *Diplodocus* Marsh. Memoirs of the Carnegie Museum, 2:225–264.

Holland, W.J. 1924. The skull of *Diplodocus*. Memoirs of the Carnegie Museum, 9:378–403.

Holwerda, F.M., Rauhut, O.W.M., and Pol, D. 2021. Osteological revision of the holotype of the Middle Jurassic sauropod dinosaur *Patagosaurus fariasi* Bonaparte, 1979 (Sauropoda: Cetiosauridae). Geodiversitas, 43:575–643.
https://doi.org/10.5252/geodiversitas2021v43a16

Hone, D.W.E. and Chure, D.J. 2018. Difficulties in assigning trace makers from theropodan bite marks: an example from a young diplodocoid sauropod. Lethaia, 51:456–466.
https://doi.org/10.1111/let.12267

Hone, D.W.E., Naish, D., and Cuthill, I.C. 2012. Does mutual sexual selection explain the evolution of head crests in pterosaurs and dinosaurs?: Ornithodiran mutual sexual selection. Lethaia, 45:139–156.
https://doi.org/10.1111/j.1502-3931.2011.00300.x

Huene, F. 1929. Los Saurisquios y Ornithisquios de Cretaceo Argentine. Annales de Museo de La Plata, 3:1–196.

Hummel, J., Gee, C.T., Südekum, K.-H., Sander, P.M., Nogge, G., and Clauss, M. 2008. In vitro digestibility of fern and gymnosperm foliage: implications for sauropod feeding ecology and diet selection. Proceedings of the Royal Society B, 275:1015–1021.
https://doi.org/10.1098/rspb.2007.1728

Ibiricu, L.M., Casal, G.A., Martínez, R.D., Lamanna, M.C., Luna, M., and Salgado, L. 2013. *Katepensaurus goicoecheai* , gen. et sp. nov., a Late Cretaceous rebbachisaurid (Sauropoda, Diplodocoidea) from central Patagonia, Argentina. Journal of Vertebrate Paleontology, 33:1351–1366.
https://doi.org/10.1080/02724634.2013.776562

Ikejiri, T. 2004. Anatomy of *Camarasaurus lentus* (Dinosauria: Sauropoda) from the Morrison Formation (Late Jurassic), Thermopolis, central Wyoming, with determination and interpretation of ontogenetic, sexual dimorphic, and individual variation in the genus. Unpublished Master Thesis, Fort Hays State University, Kansas.

Janensch, W. 1929a. Die Wirbelsäule der Gattung *Dicraeosaurus*. Palaeontographica Supplement, 7:38–133.

Janensch, W. 1929b. Material und Formengehalt der Sauropoden in der Ausbeute der Tendaguru-expedition. Palaeontographica-Supplementbände:1–34.

Janensch, W. 1929c. Magensteine bei Sauropoden der Tendaguruschichten. Palaeontographica Supplement, 7:137–143.

Janensch, W. 1950. Die Wirbelsäule von *Brachiosaurus brancai*. Palaeontographica Supplement, 7:27–93.

Janensch, W. 1961. Die gliedmaßen und gliedmaßengürtel der Sauropoden der Tendaguru-Schichten. Palaeontographica-Supplementbände:177–235.

Jensen, J.A. 1985. Three new sauropod dinosaurs from the Upper Jurassic of Colorado. Western North American Naturalist, 45:697–709.

Kanayama, Y. and Iwasa, Y. 2021. Why did sauropod dinosaurs grow so big? – A possible answer from the life history theory. Journal of Theoretical Biology, 508:110485.
https://doi.org/10.1016/j.jtbi.2020.110485

Klinkhamer, A.J., Mallison, H., Poropat, S.F., Sinapius, G.H., and Wroe, S. 2018. Three-dimensional musculoskeletal modeling of the sauropodomorph hind limb: the effect of postural change on muscle leverage. The Anatomical Record, 301:2145–2163.
https://doi.org/10.1002/ar.23950

Knötschke, N., Mastroianni, M., and Wings, O. 2014. A song of blasting and fire: *Europasaurus holgeri*. 74th Annual Meeting of the Society of Vertebrate Paleontology: Program and Abstracts:160–161.

Kvale, E.P., Johnson, G.D., Mickelson, D.L., Keller, K., Furer, L.C., and Archer, A.W. 2001. Middle Jurassic (Bajocian and Bathonian) Dinosaur Megatracksites, Bighorn Basin, Wyoming, U.S.A. Palaios, 16:233–254.

Larson, P.L. 1998. The theropod reproductive system. Gaia, 15:389–397.

Lovelace, D.M., Hartman, S.A., and Wahl, W.R. 2007. Morphology of a specimen of *Supersaurus* (Dinosauria, Sauropoda) from the Morrison Formation of Wyoming, and a re-evaluation of diplodocid phylogeny. Arquivos Do Museu Nacional, 65:527–544.

Lucas, S.G., Spielmann, J.A., Rinehart, L.F., Heckert, A.B., Herne, M.C., Hunt, A.P., Foster, J.R., and Sullivan, R.M. 2006. Taxonomic status of *Seismosaurus hallorum*, a Late Jurassic sauropod dinosaur from New Mexico. New Mexico Museum of Natural History and Science Bulletin, 36:149–162.

Lull, R.S. 1919. The sauropodous dinosaur Barosaurus Marsh. Memoirs of the Connecticut Academy of Arts and Sciences, 6:1–42.

Maidment, S.C.R. and Muxworthy, A. 2019. A chronostratigraphic framework for the Upper Jurassic Morrison Formation, western U.S.A. Journal of Sedimentary Research, 89:1017–1038.
https://doi.org/10.2110/jsr.2019.54

Mallon, J.C. 2017. Recognizing sexual dimorphism in the fossil record: lessons from nonavian dinosaurs. Paleobiology, 43:495–507.
https://doi.org/10.1017/pab.2016.51

Mannion, P.D. 2010. A revision of the sauropod dinosaur genus *'Bothriospondylus'* with a redescription of the type material of the Middle Jurassic form *'B. madagascariensis'*. Palaeontology, 53:277–296.
https://doi.org/10.1111/j.1475-4983.2009.00919.x

Mannion, P.D., Upchurch, P., Mateus, O., Barnes, R.N., and Jones, M.E.H. 2012. New information on the anatomy and systematic position of *Dinheirosaurus lourinhanensis* (Sauropoda: Diplodocoidea) from the Late Jurassic of Portugal, with a review of European diplodocoids. Journal of Systematic Palaeontology, 10:521–551.
https://doi.org/10.1080/14772019.2011.595432

Mannion, P.D., Tschopp, E., and Whitlock, J.A. 2021. Anatomy and systematics of the diplodocoid *Amphicoelias altus* supports high sauropod dinosaur diversity in the Upper Jurassic Morrison Formation of the USA. Royal Society Open Science, 8:210377.
https://doi.org/10.1098/rsos.210377

Marsh, O.C. 1877. Notice of some new dinosaurian reptiles from the Jurassic Formation. American Journal of Science, 3:514–516.

Marsh, O.C. 1878. Principal characters of American Jurassic dinosaurs, Part I. American Journal of Science, 3:160–168.

Marsh, O.C. 1884. Principal characters of American Jurassic dinosaurs. Part VII. American Journal of Science, 3:160–168.

Marsh, O.C. 1890. Description of new dinosaurian reptiles. American Journal of Science, 3:81–86.

McHugh, J.B. 2018. Evidence for niche partitioning among ground-height browsing sauropods from the Upper Jurassic Morrison Formation of North America. Geology of the Intermountain West, 5:95–105.
https://doi.org/10.31711/giw.v5.pp95-103

McIntosh, J.S. 1981. Annotated catalogue of the dinosaurs (Reptilia, Archosauria) in the collections of Carnegie Museum of Natural History. Bulletin of Carnegie Museum of Natural History, 18:1–67.

McIntosh, J.S. 2005. The genus *Barosaurus* Marsh (Sauropoda, Diplodocidae), p. 38–77. In Tidwell, V. and Carpenter, K. (eds.), Thunder-lizards: the sauropodomorph dinosaurs. Indiana University Press, Bloomington.

Mikhailov, K.E. 1997. Fossil and recent eggshell in amniotic vertebrates: fine structure, comparative morphology and classification. Special Papers in Palaeontology, 56:1–80.

Moore, A.J., Barrett, P.M., Upchurch, P., Liao, C.-C., Ye, Y., Hao, B., and Xu, X. 2023. Re-assessment of the Late Jurassic eusauropod *Mamenchisaurus sinocanadorum* Russell and Zheng, 1993, and the evolution of exceptionally long necks in mamenchisaurids. Journal of Systematic Palaeontology, 21:2171818.
https://doi.org/10.1080/14772019.2023.2171818

Moretti, J., Tschopp, E., Barta, D., Waskow, K., and Norell, M.A. 2018. Histological study of sauropod dinosaur bones from the historic Upper Jurassic Howe Quarry (Wyoming, USA): determination of an age range for every specimen. Fossilia, 2018:23–25.
https://doi.org/10.32774/fosreppal.20.1810.092325

Osborn, H.F. 1904. Manus, sacrum and caudals of Sauropoda. Bulletin of the American Museum of Natural History, 20:181–190.

Osborn, H.F. and Mook, C.C. 1921. *Camarasaurus*, *Amphicoelias*, and other sauropods of Cope. Memoirs of the American Museum of Natural History, New series, 3:249–387.

Ostrom, J.H. and McIntosh, J.S. 1966. Marsh's Dinosaurs: the collection from Como Bluff. Vol. 1. Yale University Press, New Haven.

Otero, A., Gallina, P.A., Canale, J.I., and Haluza, A. 2012. Sauropod haemal arches: morphotypes, new classification and phylogenetic aspects. Historical Biology, 24:243–256.
https://doi.org/10.1080/08912963.2011.618269

Owen, R. 1842. Report on British fossil reptiles, part II. Report for the British Association for the Advancement of Science, Plymouth, 1841:60–294.

Parrish, J.T., Peterson, F., and Turner, C.E. 2004. Jurassic "savannah"-plant taphonomy and climate of the Morrison Formation (Upper Jurassic, Western USA). Sedimentary Geology, 167:137–162.
https://doi.org/10.1016/j.sedgeo.2004.01.004

Persons IV, W.S., Funston, G.F., Currie, P.J., and Norell, M.A. 2015. A possible instance of sexual dimorphism in the tails of two oviraptorosaur dinosaurs. Scientific Reports, 5:9472.
https://doi.org/10.1038/srep09472

Peterson, O.A. and Gilmore, C.W. 1902. *Elosaurus parvus*; a new genus and species of the Sauropoda. Annals of the Carnegie Museum, 1:490–499.

Peterson, J., Lovelace, D., Connely, M., and McHugh, J. 2022. A novel feeding mechanism of diplodocid sauropods revealed in an Apatosaurine skull from the Upper Jurassic Nail Quarry (Morrison Formation) at Como Bluff, Wyoming, USA. Palaeontologica Electronica, 25, 2:1–23.
https://doi.org/10.26879/1216

Price, J.R. and Whitlock, J.A. 2022. Dental histology of *Diplodocus* (Sauropoda, Diplodocoidea). Journal of Vertebrate Paleontology, 42:e2099745.
https://doi.org/10.1080/02724634.2022.2099745

Rauhut, O.W.M., Remes, K., Fechner, R., Cladera, G., and Puerta, P. 2005. Discovery of a short-necked sauropod dinosaur from the Late Jurassic period of Patagonia. Nature, 435:670–672.
https://doi.org/10.1038/nature03623

Rauhut, O.W.M., Fechner, R., Remes, K., and Reis, K. 2011. How to get big in the Mesozoic: the evolution of the sauropodomorph body plan, p. 119–149. In Klein, N., Remes, K., Gee, C.T., and Sander, P.M. (eds.), Biology of the Sauropod Dinosaurs: Understanding the Life of Giants, Indiana University Press, Bloomsburg.

Remes, K. 2006. Revision of the Tendaguru Sauropod dinosaur *Tornieria africana* (Fraas) and its relevance for sauropod paleobiogeography. Journal of Vertebrate Paleontology, 26:651–669.
https://doi.org/10.1671/0272-4634(2006)26[651:rottsd]2.0.co;2

Remes, K. 2007. A second Gondwanan diplodocid dinosaur from the Upper Jurassic Tendaguru beds of Tanzania, East Africa. Palaeontology, 50:653–667.
https://doi.org/10.1111/j.1475-4983.2007.00652.x

Riggs, E.S. 1903. Structure and relationships of opisthocoelian dinosaurs: *Apatosaurus* Marsh. Field Columbian Museum, Geological Series, 2:165–196.

Rogers, K.C. 2009. The postcranial osteology of *Rapetosaurus krausei* (Sauropoda: Titanosauria) from the Late Cretaceous of Madagascar. Journal of Vertebrate Paleontology, 29:1046–1086.
https://doi.org/10.1671/039.029.0432

Rothschild, B.M. and Berman, D.S. 1991. Fusion of Caudal Vertebrae in Late Jurassic Sauropods. Journal of Vertebrate Paleontology, 11:29–36.
https://doi.org/10.1080/02724634.1991.10011373

Rothschild, B.M. and Martin, L.D. 2006. Skeletal impact of disease. New Mexico Museum of Natural History and Science Bulletin, 33:1–226.

Rothschild, B.M. and Witzmann, F. 2021. Identification of growth cessation in dinosaurs based on microscopy of long bone articular surfaces: preliminary results. Alcheringa: An Australasian Journal of Palaeontology, 45:260–273.
https://doi.org/10.1080/03115518.2021.1921273

Royo-Torres, R., Cobos, A., Mocho, P., and Alcalá, L. 2021. Origin and evolution of turiasaur dinosaurs set by means of a new 'rosetta' specimen from Spain. Zoological Journal of the Linnean Society, 191:201–227.
https://doi.org/10.1093/zoolinnean/zlaa091

Saitta, E.T., Stockdale, M.T., Longrich, N.R., Bonhomme, V., Benton, M.J., Cuthill, I.C., and Makovicky, P.J. 2020. An effect size statistical framework for investigating sexual dimorphism in non-avian dinosaurs and other extinct taxa. Biological Journal of the Linnean Society, 131:231–273.
https://doi.org/10.1093/biolinnean/blaa105

Salgado, L. and Bonaparte, J.F. 1991. Un nuevo saupodo Dicraeosauridae, *Amargasaurus cazaui* gen et sp. nov., de la Formación La Amarga, Neocomiano de la provincia del Neuquén, Argentina. Ameghiniana, 28:333–346.

Sander, P.M., Christian, A., Clauss, M., Fechner, R., Gee, C.T., Griebeler, E.-M., Gunga, H.-C., Hummel, J., Mallison, H., Perry, S.F., Preuschoft, H., Rauhut, O.W.M., Remes, K., Tütken, T., Wings, O., and Witzel, U. 2011. Biology of the sauropod dinosaurs: the evolution of gigantism. Biological Reviews, 86:117–155.
https://doi.org/10.1111/j.1469-185x.2010.00137.x

Schwarz, D., Ikejiri, T., Breithaupt, B.H., Sander, P.M., and Klein, N. 2007. A nearly complete skeleton of an early juvenile diplodocid (Dinosauria: Sauropoda) from the Lower Morrison Formation (Late Jurassic) of north central Wyoming and its implications for early ontogeny and pneumaticity in sauropods. Historical Biology, 19:225–253.
https://doi.org/10.1080/08912960601118651

Sereno, P.C. 1998. A rationale for phylogenetic definitions, with application to the higher-level taxonomy of Dinosauria. Neues Jahrbuch für Geologie und Paläontologie Abhandlungen, 210:41–83.

Sereno, P.C., Beck, A.L., Dutheil, D.B., Larsson, H.C.E., Lyon, G.H., Moussa, B., Sadleir, R.W., Sidor, C.A., Varricchio, D.J., Wilson, G.P., and Wilson, J.A. 1999. Cretaceous Sauropods from the Sahara and the Uneven Rate of Skeletal Evolution Among Dinosaurs. Science, 286:1342–1347.
https://doi.org/10.1126/science.286.5443.1342

Siber, H.J. 1994. The bighorn mountain dinosaur project. Aathal: Sauriermuseum Aathal, Switzerland Bulletin nr. 6.

Siber, H.J. and Möckli, U. 2009. The stegosaurs of the Sauriermuseum Aathal. Aathal: Sauriermuseum Aathal, Switzerland:1–56.

Tatehata, J.-I., Mukunoki, T., and Tanoue, K. 2023. Description of a Titanosauriform (Sauropoda, Dinosauria) Cervical Vertebra from the Lower Cretaceous Kanmon Group, Southwestern Japan. Paleontological Research, 27:350–358.
https://doi.org/10.2517/pr220009

Taylor, M.P. 2009. A re-evaluation of *Brachiosaurus altithorax* Riggs 1903 (Dinosauria, Sauropoda) and its generic separation from *Giraffatitan brancai* (Janensch 1914). Journal of Vertebrate Paleontology, 29:787–806.
https://doi.org/10.1671/039.029.0309

Taylor, M.P. 2022. Almost all known sauropod necks are incomplete and distorted. PeerJ, 10:e12810.
https://doi.org/10.7717/peerj.12810

Taylor, M.P. and Naish, D. 2005. The phylogenetic taxonomy of Diplodocoidea (Dinosauria: Sauropoda). PaleoBios, 25:1–7.

Taylor, M.P. and Wedel, M.J. 2013a. Why sauropods had long necks; and why giraffes have short necks. PeerJ, 1:e36.
https://doi.org/10.7717/peerj.36

Taylor, M.P. and Wedel, M.J. 2013b. The Effect of Intervertebral Cartilage on Neutral Posture and Range of Motion in the Necks of Sauropod Dinosaurs. PLoS ONE, 8:e78214.
https://doi.org/10.1371/journal.pone.0078214

Taylor, M.P. and Wedel, M.J. 2016. How big did *Barosaurus* get? SVPCA 2016 abstracts.

Taylor, M.P. and Wedel M.J. 2021. Why is vertebral pneumaticity in sauropod dinosaurs so variable? Qeios:1G6J3Q.4.
https://doi.org/10.32388/1g6j3q.5

Tidwell, V., Carpenter, K., and Meyer, S. 2001. New Titanosauriform (Sauropoda) from the Poison Strip Member of the Cedar Mountain Formation (Lower Cretaceous), Utah, p. 139–165. In Tanke, D.H. and Carpenter, K. (eds.), Mesozoic Vertebrate Life: New Research Inspired by the Paleontology of Philip J. Currie, Indiana University Press, Bloomington.

Torcida Fernández-Baldor, F., Canudo, J.I., Huerta, P., Montero, D., Suberbiola, X.P., and Salgado, L. 2011. *Demandasaurus darwini* , a New Rebbachisaurid Sauropod from the Early Cretaceous of the Iberian Peninsula. Acta Palaeontologica Polonica, 56:535–552.
https://doi.org/10.4202/app.2010.0003

Torcida Fernández-Baldor, F., Canudo, J.I., Huerta, P., Moreno-Azanza, M., and Montero, D. 2017. *Europatitan eastwoodi*, a new sauropod from the lower Cretaceous of Iberia in the initial radiation of somphospondylans in Laurasia. PeerJ, 5:e3409.
https://doi.org/10.7717/peerj.3409

Tschopp, E. and Mateus, O. 2013. The skull and neck of a new flagellicaudatan sauropod from the Morrison Formation and its implication for the evolution and ontogeny of diplodocid dinosaurs. Journal of Systematic Palaeontology, 11:853–888. https://doi.org/10.1080/14772019.2012.746589

Tschopp, E., Mateus, O., Kosma, R., Sander, P.M., Joger, U., and Wings, O. 2014. A specimen-level cladistic analysis of *Camarasaurus* (Dinosauria, Sauropoda) and a revision of camarasaurid taxonomy. Journal of Vertebrate Paleontology. Program and Abstracts: 241–242.

Tschopp, E., Mateus, O., and Benson, R.B.J. 2015a. A specimen-level phylogenetic analysis and taxonomic revision of Diplodocidae (Dinosauria, Sauropoda). PeerJ 3:e857. https://doi.org/10.7717/peerj.857

Tschopp, E., Wings, O., Frauenfelder, T., and Brinkmann, W. 2015b. Articulated bone sets of manus and pedes of *Camarasaurus* (Sauropoda, Dinosauria). Palaeontologia Electronica, 18:1–65. https://doi.org/10.26879/559

Tschopp, E. and Mateus, O. 2017. Osteology of *Galeamopus pabsti* sp. nov. (Sauropoda: Diplodocidae), with implications for neurocentral closure timing, and the cervico-dorsal transition in diplodocids. PeerJ, 5:e3179. https://doi.org/10.7717/peerj.3179

Tschopp, E., Mateus, O., and Norell, M. 2018. Complex Overlapping Joints between Facial Bones Allowing Limited Anterior Sliding Movements of the Snout in Diplodocid Sauropods. American Museum Novitates, 3911:1–16. https://doi.org/10.1206/3911.1

Tschopp, E., Maidment, S.C.R., Lamanna, M.C., and Norell, M.A. 2019. Reassessment of a Historical Collection of Sauropod Dinosaurs from the Northern Morrison Formation of Wyoming, with Implications for Sauropod Biogeography. Bulletin of the American Museum of Natural History, 437:1–79. https://doi.org/10.1206/0003-0090.437.1.1

Tschopp, E., Mehling, C., and Norell, M.A. 2020. Reconstructing the Specimens and History of Howe Quarry (Upper Jurassic Morrison Formation; Wyoming). American Museum Novitates, 3956:1–56. https://doi.org/10.1206/3956.1

Upchurch, P. 1995. The evolutionary history of sauropod dinosaurs. Philosophical Transactions of the Royal Society of London Series B, 349:365–390.

Upchurch, P. 1998. The phylogenetic relationships of sauropod dinosaurs. Zoological Journal of the Linnean Society, 124:43–103.

Upchurch, P. and Martin, J. 2002. The Rutland *Cetiosaurus*: the anatomy and relationships of a Middle Jurassic British sauropod dinosaur. Palaeontology, 45:1049–1074. https://doi.org/10.1111/1475-4983.00275

Upchurch, P. and Martin, J. 2003. The anatomy and taxonomy of *Cetiosaurus* (Saurischia, Sauropoda) from the Middle Jurassic of England. Journal of Vertebrate Paleontology, 23:208–231. https://doi.org/10.1671/0272-4634(2003)23[208:taatoc]2.0.co;2

Upchurch, P., Barrett, P.M., and Dodson, P. 2004. Sauropoda, p. 259–322. In Weishampel, D.B., Dodson, P., and Osmólska, H. (eds.), The Dinosauria (2nd edition). University of California Press, Berkeley.

Upchurch, P., Tomida, Y., and Barrett, P.M. 2004. A new specimen of *Apatosaurus ajax* (Sauropoda: Diplodocidae) from the Morrison formation (Upper Jurassic) of Wyoming, USA. National Science Museum Monographs, 26:1–118.

Vidal Calés, D. 2019. Evolution of sauropod dinosaur postcranial biomechanics: A virtual paleontology approach. Unpublished PhD Thesis. Universidad Nacional de Educación a Distancia (España).

Waskow, K. 2019. Patterns of life history recorded in the dorsal rib histology of amniotes. Unpublished PhD Thesis, Rheinische Friedrich-Wilhelms-Universität Bonn.

Wedel, M.J. 2003. The evolution of vertebral pneumaticity in sauropod dinosaurs. Journal of Vertebrate Paleontology, 23:344–357. https://doi.org/10.1671/0272-4634(2003)023[0344:teovpi]2.0.co;2

Wedel, M.J. 2005. Postcranial skeletal pneumaticity in sauropods and its implications for mass estimates, p. 201–228. In Curry-Rodgers, K.A. and Wilson, J.A. (eds.), The sauropods. Evolution and paleobiology, University of California Press, Berkeley.

Wedel, M.J., Cifelli, R.L., and Sanders, R.K. 2000. Osteology, paleobiology, and relationships of the sauropod dinosaur *Sauroposeidon*. Acta Palaeontologica Polonica, 45:343–388.

Wedel, M.J. and Taylor, M.P. 2013. Neural spine bifurcation in sauropod dinosaurs of the Morrison Formation: ontogenetic and phylogenetic implications. PalArch's Journal of Vertebrate Palaeontology, 10:1–34.

Whitlock, J.A. 2011. A phylogenetic analysis of Diplodocoidea (Saurischia: Sauropoda). Zoological Journal of the Linnean Society, 161:872–915.
https://doi.org/10.1111/j.1096-3642.2010.00665.x

Whitlock, J.A., and Wilson Mantilla, J.A. 2020. The Late Jurassic sauropod dinosaur *'Morosaurus' agilis* Marsh, 1889 reexamined and reinterpreted as a dicraeosaurid. Journal of Vertebrate Paleontology, 40:e1780600.
https://doi.org/10.1080/02724634.2020.1780600

Whitlock, J.A., Trujillo, K., and Hanik, G. 2018. Assemblage-level structure in Morrison Formation dinosaurs, Western Interior, USA. Geology of the Intermountain West, 5:9–22.
https://doi.org/10.31711/giw.v5.pp9-22

Wiersma-Weyand, K., Canoville, A., Siber, H.-J., and Sander, P.M. 2021. Testing hypothesis of skeletal unity using bone histology: The case of the sauropod remains from the Howe-Stephens and Howe Scott quarries (Morrison Formation, Wyoming, USA). Palaeontologia Electronica 24, 1:a10.
https://doi.org/10.26879/766

Wilhite, D.R. 2003. Biomechanical reconstruction of the appendicular skeleton in three North American Jurassic sauropods. PhD dissertation, Graduate Faculty of the Louisiana State University and Agricultural and Mechanical College.

Wilson, J.A. 1999. A nomenclature for vertebral laminae in sauropods and other saurischian dinosaurs. Journal of Vertebrate Paleontology, 19:639–653.
https://doi.org/10.1080/02724634.1999.10011178

Wilson, J.A. 2002. Sauropod dinosaur phylogeny: critique and cladistic analysis. Zoological Journal of the Linnean Society, 136:215–275.
https://doi.org/10.1046/j.1096-3642.2002.00029.x

Wilson, J.A. 2011. Anatomical terminology for the sacrum of sauropod dinosaurs. Contributions from the Museum of Paleontology, University of Michigan, 32:59–69.

Wilson, J.A. 2012. New vertebral laminae and patterns of serial variation in vertebral laminae of sauropod dinosaurs. Contributions from the Museum of Paleontology, University of Michigan, 32:91–110.

Wilson, J.A. and Sereno, P.C. 1998. Early evolution and higher-level phylogeny of sauropod dinosaurs. Journal of Vertebrate Paleontology, 18:1–79.
https://doi.org/10.1080/02724634.1998.10011115

Wilson, J.A. and Upchurch, P. 2003. A revision of *Titanosaurus* Lydekker (Dinosauria-Sauropoda), the first dinosaur genus with a 'Gondwanan' distribution. Journal of Systematic Palaeontology, 1:125–160.
https://doi.org/10.1017/s1477201903001044

Wilson, J.A., D'Emic, M.D., Ikejiri, T., Moacdieh, E.M., and Whitlock, J.A. 2011. A Nomenclature for Vertebral Fossae in Sauropods and Other Saurischian Dinosaurs. PLoS ONE, 6:e17114.
https://doi.org/10.1371/journal.pone.0017114

Wilson, J.A. and Allain, R. 2015. Osteology of *Rebbachisaurus garasbae* Lavocat, 1954, a diplodocoid (Dinosauria, Sauropoda) from the early Late Cretaceous–aged Kem Kem beds of southeastern Morocco. Journal of Vertebrate Paleontology, 35:e1000701.
https://doi.org/10.1080/02724634.2014.1000701

Woodruff, D.C. 2017. Nuchal ligament reconstructions in diplodocid sauropods support horizontal neck feeding postures. Historical Biology, 29:308–319.
https://doi.org/10.1080/08912963.2016.1158257

Woodruff, D.C. 2019. What factors influence our reconstructions of Morrison Formation sauropod diversity? Geology of the Intermountain West, 6:93–112.
https://doi.org/10.31711/giw.v6.pp93-112

Woodruff, D.C., Fowler, D., and Horner, J. 2017. A new multi-faceted framework for deciphering diplodocid ontogeny. Palaeontologia Electronica, 20:1–53. https://doi.org/10.26879/674

Woodruff, D.C., Carr, T.D., Storrs, G.W., Waskow, K., Scannella, J.B., Nordén, K.K., and Wilson, J.P. 2018. The Smallest Diplodocid Skull Reveals Cranial Ontogeny and Growth-Related Dietary Changes in the Largest Dinosaurs. Scientific Reports, 8:14341. https://doi.org/10.7934/p3281

Woodruff, D.C., Wolff, E.D.S., Wedel, M.J., Dennison, S., and Witmer, L.M. 2022. The first occurrence of an avian-style respiratory infection in a non-avian dinosaur. Scientific Reports, 12:1954. https://doi.org/10.1038/s41598-022-05761-3

Xu, X., Upchurch, P., Mannion, P.D., Barrett, P.M., Regalado-Fernandez, O.R., Mo, J., Ma, J., and Liu, H. 2018. A new Middle Jurassic diplodocoid suggests an earlier dispersal and diversification of sauropod dinosaurs. Nature Communications, 9:2700. https://doi.org/10.1038/s41467-018-05128-1